Modification of Water Uptake Capacity of Wood Using Colloidal Solution by Impregnation Technique

By

Amir Davoodi

Thesis Submitted to the University of Ottawa

In partial Fulfilment of the requirements for the

Master of Applied Science

In Civil Engineering

Under the auspices of the Ottawa-Carleton Institute for Civil Engineering

uOttawa

Department of Civil Engineering

University of Ottawa

ABSTRACT

Hygroscopic properties are important characteristics of a material that is used in building construction. Wood is an anisotropic, heterogeneous and hygroscopic material. Given the cellular structure of wood as well as capillary action in the Lumina, the level of water uptake in wood is significant.

Such amount of water uptake makes the wood susceptible to dimensional instabilities, causes alterations in the mechanical properties, and potential for degradation of the material. Various approaches have been investigated to modify the hydrophilic nature of lignocellulosic materials, including surface modifications using silane treatments, acetylation, wax etc. Although these surface modifications can decrease the rate of water uptake by the materials, the amount of water uptake at saturation remains unchanged. In fact, the lumen diameter is so small that the rise of liquid, even with a hydrophobic surface, can still occur. Therefore, the only way to halt the water uptake driven by capillary action in lignocellulosic materials is to apply a uniform cover on the material surface in addition to filling the lumen with dense material.

In the current research project, the vascular structure of softwood (Spruce) is obstructed by silica nanoparticles using the impregnation technique as one of the advanced methods to reduce the water absorption capacity in wood. This process can form a thin film of nanoparticles on solid objects with complex geometries. In addition, the technique can fill up the cavities and voids of porous materials and prevent the capillary action inside the Lumina. In this method, the wood specimen is dipped into the solution, silica 40 (wt. %) colloidal solution. Then the solvent is evaporated which results in the formation of nanoparticles in the form of thin films or particulates. The former may change the moisture absorption on the surface and the later reduces the capillarity of the vascular system. This project aims to find the optimal impregnation condition to minimize the water uptake capacity of wood in order to increase wood physical and mechanical stabilities.

Three immersing times (i.e. short, medium, and long) were used to coat wooden samples with the silica colloidal solution. The samples were conditioned in wet environments with specific

relative time and then their weight as percentage change were examined. To investigate the capability of the method to obstruct the vascular structure of the wood samples, the characteristic process was done in the next step by some common tests such as X-ray Diffraction (XRD), Scanning Electron Microscope (SEM), Water Contact Angle (WCA), etc.

The results from the experiments show that dip-coating the wood samples with silica nanoparticle colloidal solution had effect on the amount of water absorption, but significant levels of reduction in water attraction was achieved with considering the other effective parameters such as duration of each set, the number of sets that are conducted, and impregnation in vacuumed condition. More research is needed to quantify the benefits of using nanoparticle in these applications.

ACKNOWLEDGMENTS

I would like to express my deepest gratitude to my supervisor Dr. Ghasan Doudak for his advice, patience, guidance, help, and support. His guidance helped me in all time of my research and writing the thesis.

I would also like to express my sincere appreciation to my co-supervisor Dr. Mohammad Reza Foruzanmehr. The door to his office was always open to me whenever I had a question about my research.

I would like to thank my thesis committee Dr. Leandro F.M. Sanchez and Dr. Julio Angel Infante Sedano for serving as my committee members, and for their constructive comments and suggestions.

This thesis is dedicated to my beloved parents that I will never be able to appreciate their continuous encouragement and support through my life. Without their financial and spiritual support, none of my accomplishments could have been possible. I would also like to thank my dear sister for her motivation and support.

Table of Contents

LIST OF TABLES

LIST OF FIGURES

1 INTRODUCTION

1.1 Motivation

The development of human societies has resulted in an overproduction of synthetic materials, which have shown to be adversely affecting the environment, and causing depletion of resources. Changes in the environment as well as pollution are few examples that demonstrate the need to change the status quo in terms of material selection.

The building industry is responsible for more than 10% of CO_2 emission (Lee et al. 2018). Population growth along with more demand for dwelling and the growing scarcity of non-renewable resources is expected to create a shortage of building materials and hence increase the construction cost. The use of renewable materials may be one feasible solution to address this problem.

Wood has long been used in construction in Europe and North America, especially in Canada, mainly to the abundance of forests (Figure 1.1). Wood has numerous advantages in comparison with other commonly used construction materials such as steel and concrete. These attributes include renewability, low cost, lightweight, acoustic and thermal insulation, as well as, the intrinsic high compression strength of wood (Brunner 2000), and shorter construction time, which make wood an attractive material for the construction industry (Icc et al.2015).

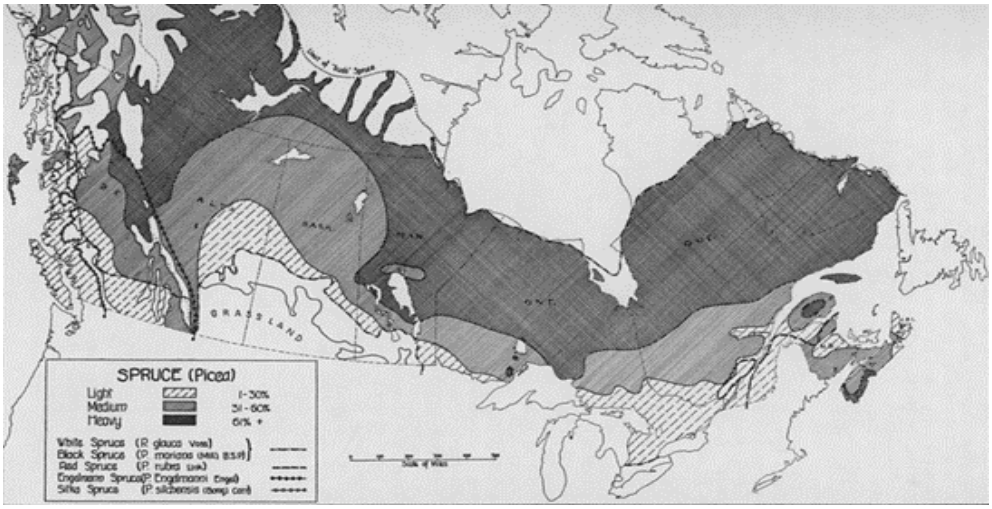

Figure 1.1: Spruce Forest Canada Map (Halliday et al. 1943)

Despite its advantages, wood has some drawbacks including low dimensional stability and durability in alkaline environments (Di Blasi et al. 2009). The hydrophilic nature of wood and its high capacity to absorb water are the main reasons for those deficiencies. The high level of water sorption in wood is mainly due to the presence of a hollow lumen which creates a path for water to penetrate by capillarity.

Several methods, such as surface modifications using water repellents and physio-chemical treatments have been suggested to modify the hydrophilic nature of wood, however, none of these solutions have been able to significantly decrease the water uptake capacity of wood. In fact, these surface modifications simply produce a hydrophobic surface on wood and only reduce the rate of water uptake. However, they are unable to reduce the level of water absorption at saturation as a rise of the liquid through the fiber lumen can still occur (Denes et al. 1999). Therefore, in order to stop the rise of water driven by capillary pressure in wood (Choong and Tesoro 1989), it has to be homogenously impregnated and its vascular system must be impregnated with a dense material. Metal oxides ceramics are dense enough to obstruct the vascular system of wood (Boulos et al. 2017). The textile industry has long used these ceramics to create new properties such as antibacterial and self-cleaning properties (Li et al. 2010), super hydrophobicity (Shupe et al. 2012), UV radiation protection (Zhi et al. 2017), and fire retardancy (Evans et al. 2009). Silicon dioxide (SiO_2) is a dense ceramic with a good chemical inertness (Shi et al. 1989; da Silva et al. 2017), and with good compatibility with cementitious materials such as composite (concrete and fibers or concrete and wood) . Many methods have been developed to synthesize SiO_2, including the sol-gel technique, which is a simple, economic and effective method to produce ceramic coatings on objects with irregular geometries (Gao et al. 2015). This method can be also used to impregnate the vascular system of natural fibers and wood (Boulos et al. 2017).

1.2 Research Contribution

The available knowledge on the topic of hygroscopic effects on wooden materials is primarily focused on surface protection of the samples using water resistant and hydrophobic materials (i.e. wax, and oil), with limited studies that explicitly address the reducing wood capacity in water absorption in saturation. The studies' lack is in investigating the individual contribution

of the vascular system to the level of water uptake due to the capillary action in them. Capillary action is owing to the pressure of adhesion and cohesion which cause the water to rise against gravity. Furthermore, no experimental research has been done, in which available and cheap hydrophilic materials were used to reduce the water absorption capacity of the wood specimens. The current study attempts to provide a better technique in which, the colloidal nanoparticle solution is used to form homogenously impregnated surface as well as impregnated lumen pores with a dense material. The approach involving experimental studies at different conditions (i.e. pretreating, time and vacuum).

1.3 Objective

In this research a great deal of attention has been paid to develop low-cost and scalable coating methods to reduce hydrophilicity characteristics of the wood material. The coating is optimized to minimize the level of water absorption at saturation in order to prevent them from degradation in the alkaline environment for construction purposes such as facades and roofing applications. More specifically, the targets are as follows:

1. Develop simple techniques to reduce the amount of water absorption in wood.
2. Investigation of the effects of immersion time on the water absorption ability of the samples.
3. Evaluation of influence of immersion times in the dip coating process on the level of water uptake.
4. Evaluation of the effect of dip coating under the vacuum conditions on the total amount of water absorption in the samples.
5. Characterizing the physical properties of the wood samples in micro-scale before and after the coating process to check for any possible changes.

1.4 Scope

The current research project applied the homogeneous nature of coatings based on silicon dioxide nanoparticles to further improve wood materials to water exposure. Scalable fabrication techniques based on dip coating are adapted to meet the requirements for minimal

water absorption. This is attained by blocking the vascular network within the wood structure which assist capillary impregnation of water deep inside the material. Pretreatment processes are also introduced for obtaining better result for the samples produced from the wood specimens. A parametric study is conducted during the fabrication process. This involves (i) the effect of the vacuumed condition on quality of impregnation of the vascular system in the wood specimens, (ii) testing the hydrophilicity of the impregnated wood by Tensiometer, and (iii) correlating the experimental observations with the microscopic features of the wood samples before and after exposing to the colloidal solution obtained by the Scanning Electron Microscope (SEM) images. On the basis of the findings in this study, improved material is provided for practical application in the proposed fabrication process.

The aforementioned research objectives will be attained through the following steps:

• Detailed literature review on the behavior of wood, especially when exposed to the wet environment, and review existing hydrophobization techniques.

• Producing the required wood samples and trying to obtain better output by the pretreatment process.

• Using the Nanoparticle colloidal solution and dip-coating technique in order to create homogenous coat and blocking the vascular system of the wooden specimens.

• Investigating the effect of the vacuumed condition on quality of impregnation of the vascular system in the wood specimens.

• Testing the hydrophilicity of the impregnated wood by Tensiometer.

• Investigating the microscopic features of the wood samples before and after exposing to the colloidal solution by utilizing the characterization methods (XRD and SEM).

• Discussing the results by comparing the experimental outputs and proposing potential recommendations.

1.5 Thesis Structure

The current thesis is divided into six chapters.

- Chapter 1 provides a general introduction and outlines the motivations, key objectives and scope.
- Chapter 2 presents a detailed literature review on the topic.
- Chapter 3 discusses the experimental methodology, including the experimental procedures, characterization, and provides details regarding the preparation of samples.
- Chapter 4 presents the experimental results for all tests performed, including the Non-treated samples, pre-treated samples, pre-treated impregnated samples, and pre-treated impregnated vacuumed samples. The outputs from characterization methods are also provided in this chapter.
- Chapter 5 includes detailed discussion on the results and presents comparisons between various methods.
- Chapter 6 presents the key findings and provides some suggestions for future research.

2 LITREATURE REVIEW

2.1 General

The need to develop water-resistant wood-based construction materials has and initiated a great deal of research directed towards enhancing the wood surface characteristics as the first barrier against environmental threats. Given the ease of application and fabrication process, coating wood with protective layers has been the most favorable way to tackle this issue. However, this surface protection does not contribute to the protection of the inner layers of wood. For this reason, the current research seeks to develop low-cost and scalable coating methods to reduce hydrophilicity characteristics of the wood material. The coating is optimized to reduce the level of water absorption at saturation in order to prevent them from potential degradation in an alkaline environment and to make them suitable for facades and roofing applications. To this end, dip coating of some wood samples in a colloidal solution of silicon dioxide nanoparticles is proposed as the potential candidate for decreasing the water absorption property of the wood samples by filling up the cavities and vascular systems that intrinsically exist inside the wood. The structure property was also investigated using material characterization methods, such as Water Contact Angle (WCA), Scanning Electron Microscope (SEM) and X-ray powder diffraction (XRD).

The following sections present the material properties of wood that are relevant to the treatment process.

2.2 Wood

Wood is three phases non-homogeneous material. The history of human use of wood dates back thousands of years. Early humans gradually learned to use wood elements to build their shelters. Trees are woody plants with leaves, branches, elongated main trunk and roots(D Fengel and Wegener 1984; Malkov et al. 2003). The roots are subsurface structures for attracting water and mineral materials from the soil as well as providing biochemical storage and mechanical support to the trunk. Water and nutrients are transported from the roots to the branches by the trunk (Figure 2-1a)(Rowell 2012).

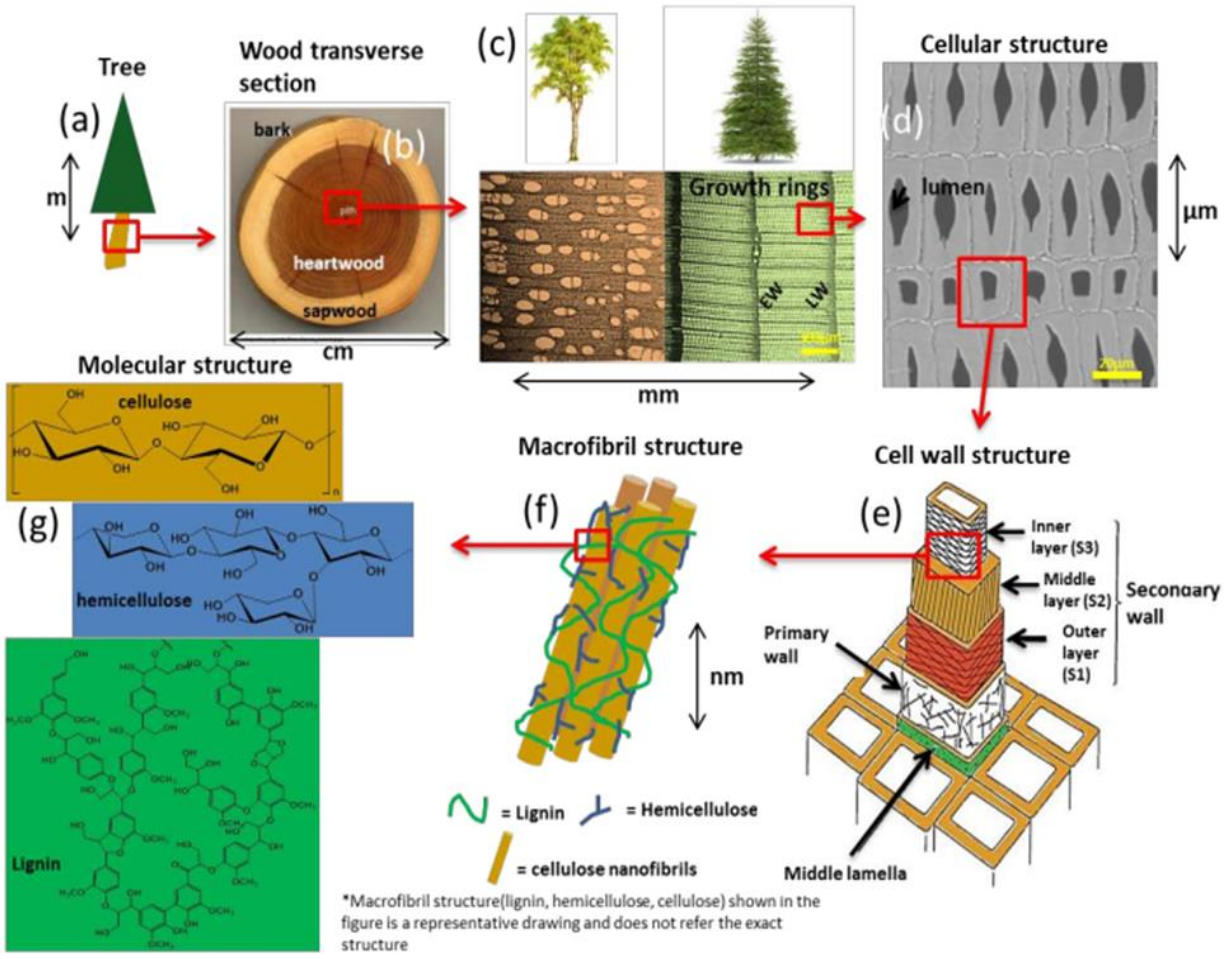

Figure 2.1: From the tree to molecular structure of its polymeric matrices (a) A tree with an elongated trunk (b) Various sections of a trunk including heartwood, sapwood and bark (c) Left: The microscope image of a birch's cellular structure. Right: The microscope image of the Spruce consisted of earlywood and latewood cells as well as growth rings, (d) SEM image of the spruce wood's latewood cell walls (e) A single cell wall composed of the primary and secondary cell wall layers (f) Lignin and hemicellulose embracing the crystalline cellulose microfibrils (g) Molecular structures of hemicellulose, cellulose, and lignin polymeric matrices (Rowell 2012)

In the almost all types of trees, the most part of the wood for industry and construction is obtained from this part of trees. Figure 2.1b shows the transverse section of a trunk. The bark is an outer covering layer of dead tissue, which protects the tree from the mechanical injury, fire, insects or weather (Schweingruber 2007). The phloem is the thin layer consist of the alive cells to transfer nutrient from one part to another part. Followed by the thin layer of vascular cambium, the living tissue that produces xylem cells to the inside and new phloem cells to the

outside. Usually, the wood (xylem) is the largest part of the trunk and for some of the trees, a distinction between heartwood and sapwood can be observed (Figure 2.1b) (Fengel and Wegener 1984; Kolleman and Cote 1984).

Sapwood, the outer part, consist of living cells, whereas in the heartwood, all the cells and tissues are dead. The sapwood, compared to the heartwood, is lighter in colour and less durable. The heartwood is less permeable due to the deposition of extractive in the wood cells during the wood formation. Thus, the heartwood contains larger amount and types of extractive compared to the sapwood (Hon and Shiraishi 2000; Kolleman and Cote 1984;). Also, the sapwood contains higher amounts of triglycerides. However, the heartwood has more resin acids, fatty acids and pinosylvin in Scots pine (Back 2000; Nuopponen et al. 2004).

Properties in wood can be considered in three main directions: along the grain direction is the longitudinal direction (L), radial direction (R), and tangential direction (T) (See Figure 2.2).

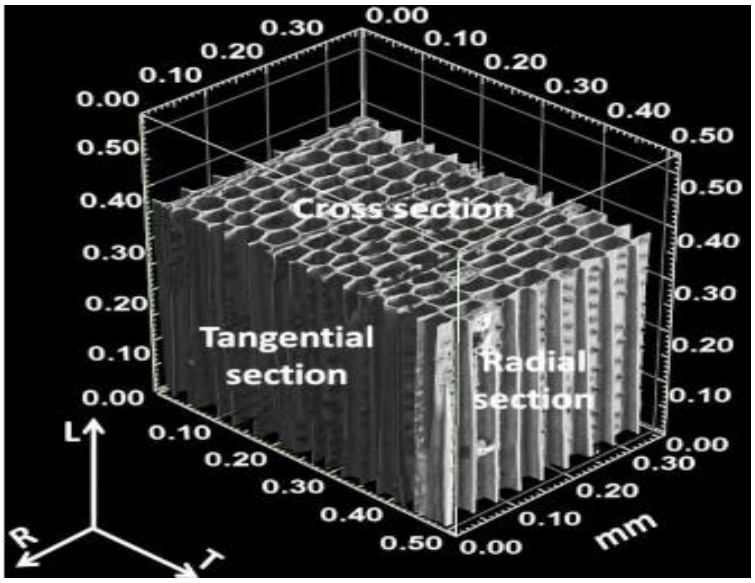

Figure 2.2: 3D photomicrograph image showing the cross-section, tangential section, and radial section of a softwood/Southern yellow pine (Rowell 2012)

Typically, there are two categories of wood, namely softwoods (gymnosperms) including pine and spruce and hardwood (angiosperms) such as maple and beech (see Figure 2.4). These two types of wood are dissimilar based on their cell group types and their xylem structure (Rowell

2012). The terms ‘softwood’ and ‘hardwood’ have nothing to do with the hardness of the wood. In fact, some softwoods are heavier and harder than hardwoods. For instance, the balsa tree is a hardwood and it is softer than any commercial softwood (Dietrich et al. 1984; Rowell 2005). Softwoods have less complicated anatomy than hardwoods and they mainly consist of axially extended tracheids (90-95%) and extended ray cell (5-10%). While tracheids are specifically responsible for the mechanical support and longitudinal water transport to the top of the tree, the ray cells are in charge of activating radical liquid transport (Ek et al. 2009).

On the contrary, the structure for hardwood is believed to be more complicated and developed, containing, vessels, fibers (libriform fibers and fiber tracheids) and parenchymas (longitudinal oriented and ray cells). Pits enable water transport between the wood cells. Those pits are known as boarded pits in softwoods, which have a relatively similar function to a valve. The highly lignified middle lamella can hold the cells together and also in addition to the primary cell walls and secondary cells walls (Figure 2.4e)(Rowell 2005, 2012). One of the building blocks of the wood cell wall is cellulose microfibril, which is made from a bunch of cellulose polymer chains in highly ordered crystalline lattices oriented with microfibril angle (MFA) which is an angle to the longitudinal cell axis (Barnett and Bonham 2004). Cellulose microfibrils, which are formed by the bonding of cellulose molecules, have both merged zones of non-crystalline and crystalline (Figure 2.3).

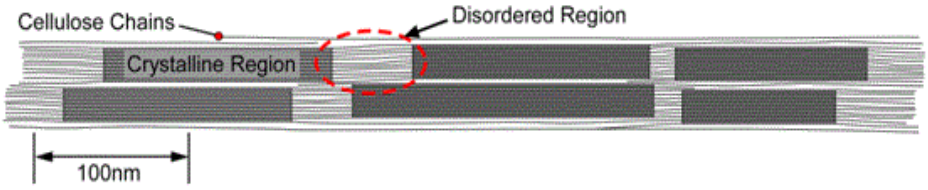

Figure 2.3: Cellulose microfibril showing ordered (crystalline) and disordered (amorphous) regions (Robert 2011)

Then the microfibrils themselves are join together to form fibril aggregates (i.e., macrofibrils), by a matrix of lignin and hemicellulose. The partly crystalline cellulose fibrils are put in amorphous lignin and hemicellulose matrix (Figure 2.4)(Gibson 2012; Robert 2011). The first layer formed after the cell division is the primary cell wall, which consists of minimum

oriented microfibrils that allow expansion of the cell (Kesten et al. 2017).

The next layer is the secondary cell wall having sub-layers showing different patterns in the orientation of microfibrils with a helical winding pattern (Figure 2.4e) (Burgert et al. 2007). The thinner layer with microfibril angles between 50 to 70 degrees called S1. The biggest volume of the microfibril angle is for S2 layer (between 5-45 degrees) which has more effect on wood properties such as mechanical and stability. The S3 layer is pretty thin and has a microfibril angle similar to the S1 layer. Micro- or nano-pores are also existing in cell walls which are reachable under certain conditions(Ek et al. 2009; Kojiro et al. 2010).

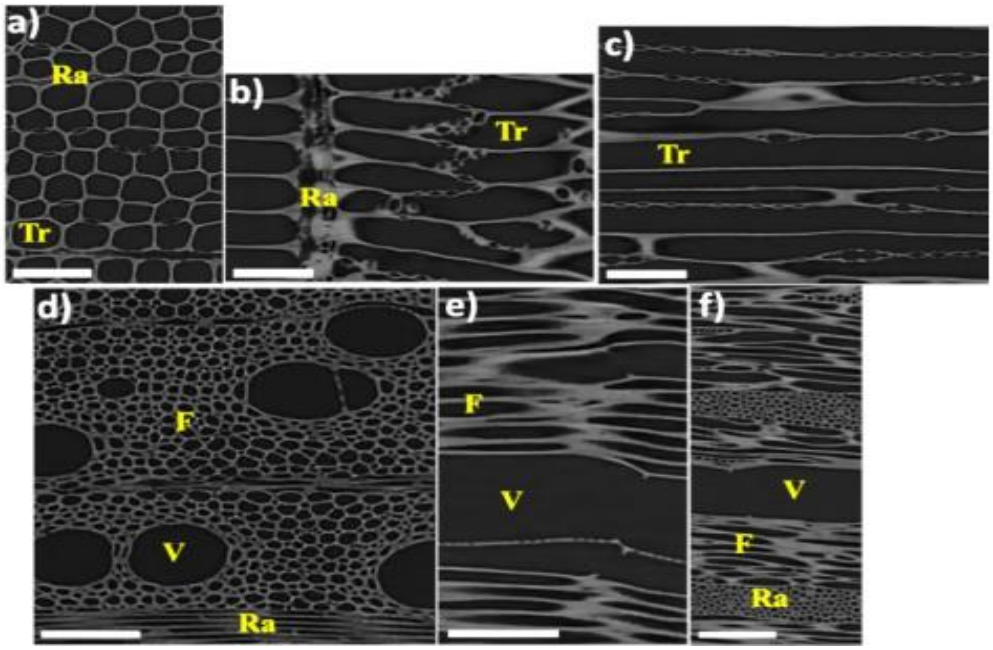

Figure 2.4: SEM images representing (a,d) transverse, (b,e) radial, (c,f) tangential sections of a softwood sample (southern yellow pine) and a hardwood sample (maple), respectively. The structure of softwood samples includes tracheids (Tr) and ray cells (Ra), while vessels (V), fibers (F) and rays (Ra) are the components of hardwood samples. The scale bars are 100 µm (Petrič and Oven 2015)

Considering the growing season as a factor in wood macroscopically structure, there are two types of wood, early wood (EW) which is lighter and late wood (LW) that is darker (Figure 2.4c). Tracheids are the elements that differentiate those two types of wood since they have relatively higher porosity in EW than in LW as there are thinner cell walls and wider lumen in EW. In other words, longitudinal tracheids in EW are mainly responsible for the

transmission of water and nutrients, whereas tracheids in LW have more mechanical and supportive function (Figure 2.4d) (Petrič and Oven 2015).

2.2.1 Cell Wall Components

The heterogeneous structure of the cell walls has consisted of cellulose, hemicellulose, and lignin which are three main polymeric materials, and the other non-structural cell wall components are called extractives (i.e. pectin) (Rowell 2012).

2.2.1.1 Cellulose

Cellulose, as a biopolymer of D-glucopyranose units, is one of many polymers found in nature. Paper, cotton, and wood all contain cellulose. Also, crystalline regions formed by several cellulose molecules link together and form the intramolecular and intermolecular hydrogen bonds which result in the formation of microfibrils. These microfibrils have been used in a large variety of living species as a reinforcement material (Kitir et al. 2018).

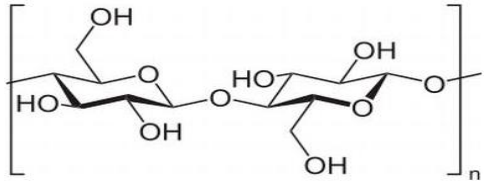

Figure 2.5: Single linear chain of cellulose (Kitir et al. 2018)

2.2.1.2 Hemicelluloses

Hemicelluloses are heterogeneous (i.e., amorphous) polymers made from C5 and C6 sugars, such as xylose, arabinose, glucose, galactose, mannose, etc. As shown in Figure 2.1g, it is one of the most common components of biomass with lower molecular weight. (Dumitriu 2004; Kollmann et al. 2012). Hemicelluloses, which have a specific structural supportive function in wood, are located in the cell wall matrix between the cellulose microfibrils. Also they can hold the cellulose together, and assumed to function as a compatibilizer, or link between cellulose and lignin (Ali 2012; Rowell 2012).

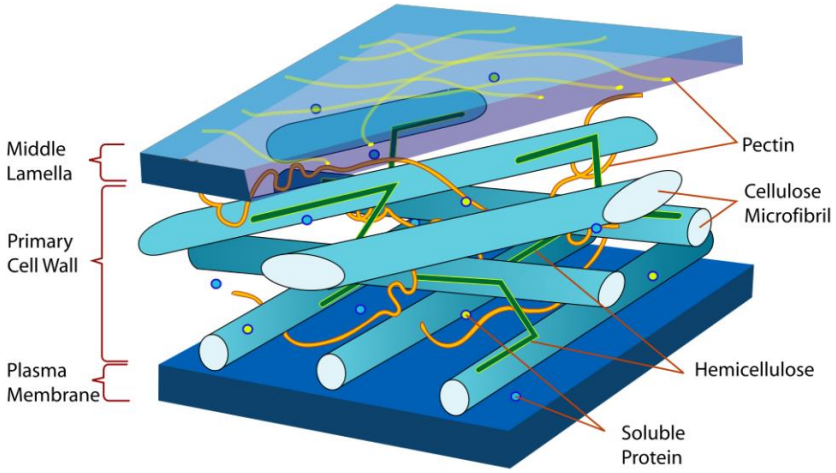

Figure 2.6: Schematic of a cell wall; green colour shows hemicellulose (Sticklen 2008)

Cellulose and hemicelluloses in wood carry huge amounts of hydroxyl groups (OH). Polar liquids such as water causing swelling of the cell walls due to the hydrogen bonding with the OH groups of the cell walls, this is the most important reason for the hygroscopic nature of wood. The amount of swelling in longitudinal direction is much less than the transverse direction which leads to the curvature in the component (Salmén and Burgert 2009; Scheller and Ulvskov 2010; Sticklen 2008).

2.2.1.3 Lignin

Lignin (i.e., plant cell adhesive) is an amorphous aromatic polymer with intermediate molecular weight and a complicated structure consisting of different phenylpropane units linked by either carbon-oxygen (C-O) or carbon-carbon (C-C) bonds in a 3-D network Figure 2.7. It is made based on the polymerization of three various monomers called coumaryl, coniferyl, and sinapyl alcohols. In contrast to cellulose, lignin does not have any single monomer[1] unit. Hardwood lignins usually are copolymers of coniferyl and synapyl alcohols (i.e., SG-lignin), while softwoods mostly consist of coniferyl alcohol (i. e., G-lignin) (Ek et al.

[1] A molecule that can be bonded to other identical molecules to form a polymer.

2009; Sjöström and Westermark 1999). Lignin is also responsible for bonding the individual cells together in the middle lamella region as well as providing more stiffness to the cell wall. The other functions of lignin in the wood structure are include connecting the cellulose and hemicellulose to each other and providing better stiffness for the cell walls (Shmulsky and Jones 2019; Sjöström and Alén 2013). In addition, lignin can provide more hydrophobicity for the cell walls and protect the cells against microbiological degradation. It also reduces the effect of water sorption on the stiffness and strength of tracheids. The lignin content of hardwoods is usually in the range of 18-25%, whereas in softwoods its content varies between 25-35%. Moreover, there is no proof that lignin is associated with cellulose, but hydrogen bonds and even covalent bonds are established with hemicelluloses (Dumitriu 2004; Mark 1967).

2.2.1.4 Extractives

Extractives (i.e. pectin) are organic materials present in wood structure, which can be extracted with neutral solvents. Some extractives have an effect on some wood natural features such as colour, durability, etc (Walker 2006). They can change the surface chemistry of wood because of their inherent mobility and movement to the surface regions. Some of the extractive materials are in the form of aromatic (phenolic) compounds (e.g. flavonoids), terpenes, aliphatic acids, alcohols, and inorganic substances (D Fengel and Wegener 1984).

2.2.2 Component Reactivity

Cellulose is able to form a compressed form due to the intermolecular hydrogen bonds which is why reactants fail to access the crystalline region of the cellulose polymer resulting in a low reactivity. The side chain in the hemicellulose causes an obstruction in the creation of intermolecular.

Hydrogen bond and the abundance of its configuration are limited. That is why cellulose is less reactive to hemicelluloses. Lignin has restricted reactivity in contrast to its feature as a branched polymer because of the aromatic group in its formations. The formation of

intermolecular hydrogen bonds leads to an increase in stability (Zhang, Yang, and Blasiak 2011).

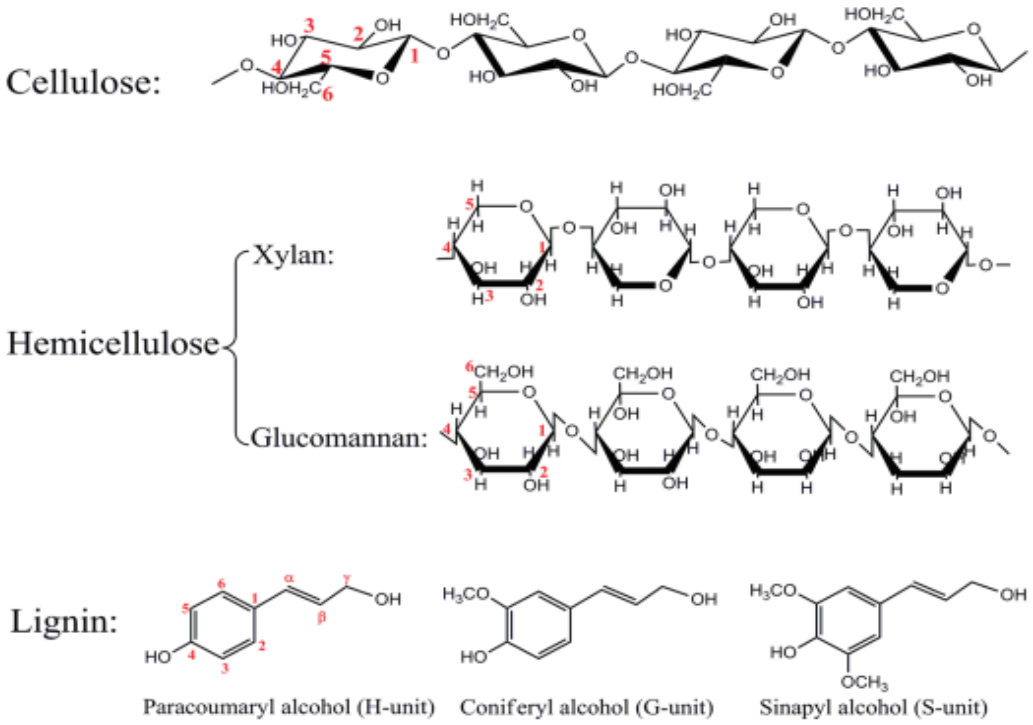

Figure 2.7: The structural compression of the cell wall's components (Zhang et al. 2011)

2.3 Wood Modification Techniques

Wood is intrinsically hydrophilic material and this property has unfortunate side effects on its strength and resistance properties especially in exposure to the moisture (e.g., properties of modulus of elasticity (E), tensile strength, shear strength, etc.)(Gerhards 2007). In additions, the natural pH of wood is normally between 4 and 6 which causes acidic property in it. This acidic property makes the wood vulnerable especially in exposure to the alkaline environment at saturation. Since, soluble alkalis are easily absorbable and damage the wood from inside(Wang et al. 2010). During the years, researchers have examined some various materials and methods to improve its week point against the moisture. These methods categorized into chemical methods (Silanization, Acetylation, etc.), and physical methods (Wax, Dip-coating,

etc.). Some of the most important of the techniques are discussed below.

2.3.1 Wood Treatment with Silanization Method

In this technique, surface of a material, which contains OH groups, is treated with organofunctional alkoxysilane molecules to form a covalent -Si-O-Si- bond and make them functional. The purpose of silanization is to form bonds between organic materials and mineral compounds (Seed 2000). Organo-Silicones have a wide variety of important applications including adhesion promoters, surface modifiers, and cross-linking agents. Mai et al. (2004) studied wide variety of organo-silicon compounds for using on wood. They did the processes by employing the tetra-alkoxysilanes as well as produced inorganic glasses consisting of pure polymeric silicic acid that have been shown in Figure 2.8.

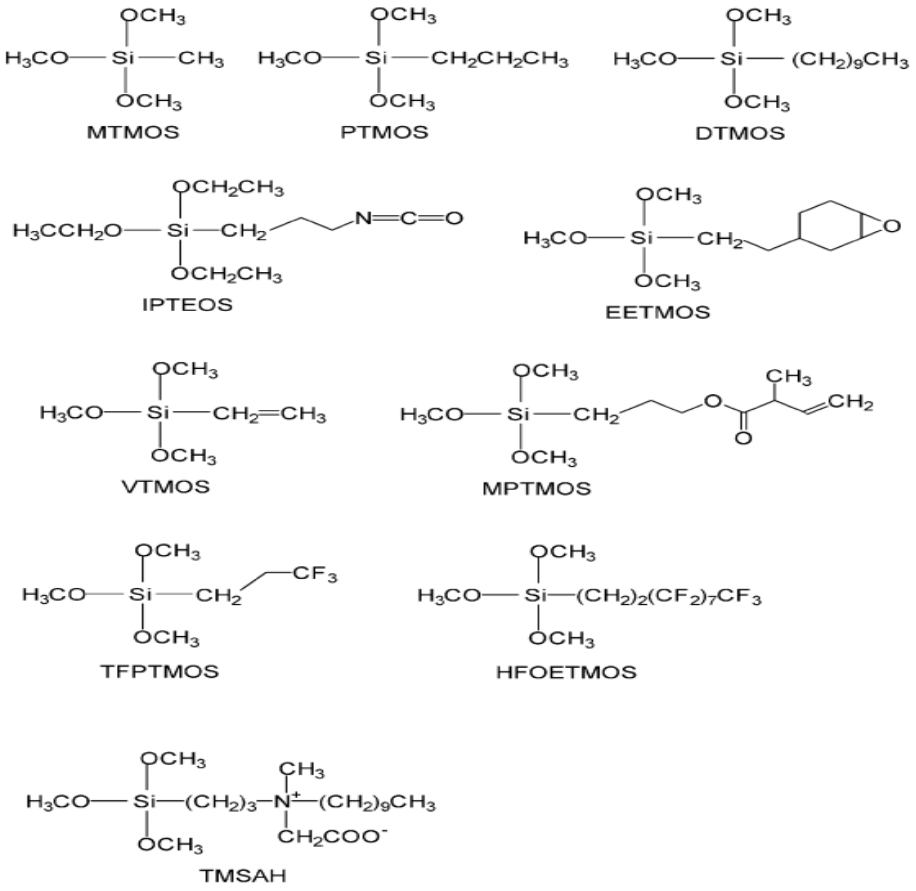

Figure 2.8: Chemical structure of diverse Organo-Silanes applied for wood modification (Mai and Militz 2004)

According to Mai, TMSAH[1] , was the most efficient combination in imparting the lowest water absorption ratio as well as the prevention of leaching among the others (Figure 2.8). Saka et al. (2004) showed the silanization with the TMSAH can improve the fire-resisting properties of the wood mainly to the presence of fluorine, and during the further researches, Miyafuji et al. (2001) also improved the decay resistance against basidiomycete [2] attack in the salinized wood by applying the amphoteric quaternary ammonium compound.

2.3.1.1 Micro-Emulsion Technology

Coating and primers based on the micro-emulsion technology that consists of different silicon polymers in the form of micro-emulsion in water with a particle size from 10 to 80 nm, have been used as surface treatment of masonry and wood (Mai and Militz 2004).

Due to the small size of the micro-emulsions, they are able to penetrate into the voids of wood which cannot be accessible by common emulsions(Hager et al.1995)

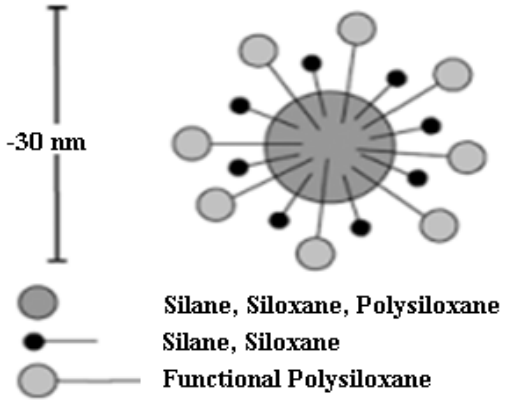

Figure 2.9: Composition of silicon micro-emulsions (Hager 1995)

[1] The amphoteric quaternary ammonium compound 3-(trimethoxysilyl) propyl (carboxymethyl) decylmethyl ammonium hydroxide inner salt (TMSAH)

[2] Higher fungi

According to Lukowsky et al. (1997) products showed high water repellence, but dimensional stability did not improve. Low bath stability in the presence of water due to hydrolysis and condensation was reportedly a disadvantage for vacuum pressure or dip treatment of products.

2.3.1.2 Surface Modification with Plasma Coating

Electrical gas discharges, called plasma, is an effective methods that make the wood surface hydrophobic (Janzen 1992). In this technique, the thin water-resistant layers are created by injection of the special gases (Argon) into a die-electric barrier gas discharge (Figure 2.10) (Avramidis et al. 2011).

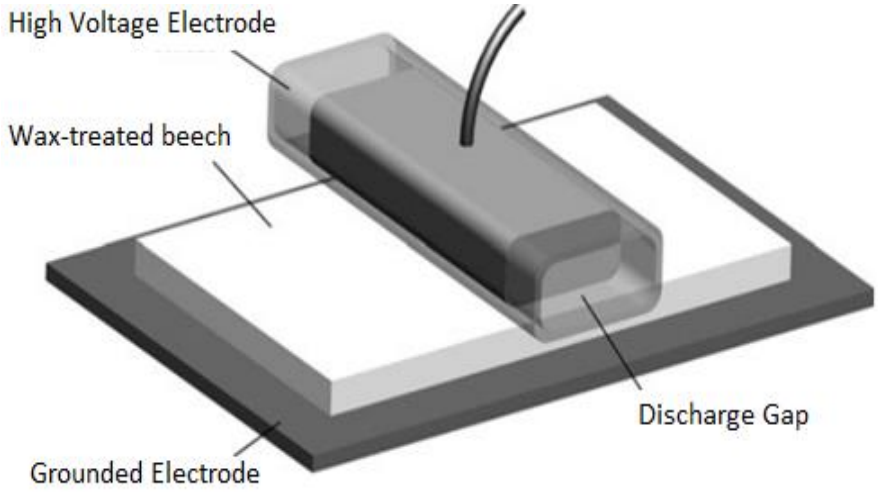

Figure 2.10: Model of Plasma treatment setup (Avramidis et al. 2011)

According to Denes et al. (1999) the plasma reactions were really intense mainly to a large number of ions which created during the discharge process. Surface modification with cold plasma[1], is a dry process that can only change the outermost layer of the wood surface. Plasma

[1] Cold plasma (Non-equilibrium plasma) is the plasma that contains individual constituents in different temperature from each other.

contains positive and negative ions, radicals, electrons, and excited and non-excited neutral particles in parallel but without electric charge.

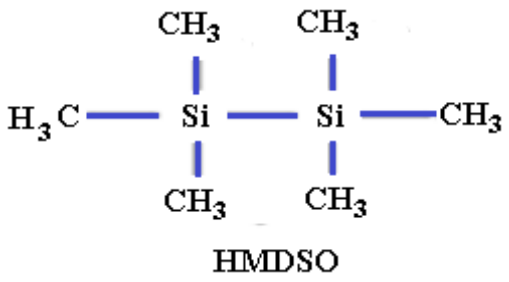

Figure 2.11: Chemical structure of hexamethyldisiloxane (Podgorski et al. 2002)

Podgorski et al. (2002) conducted impact tests on the wood plasma coating hexamethyldisiloxane (HMDSO) at room temperature (Figure 2.11). Their method was able to make the water contact angle higher than 120° while water capillarity in an immersion test was significantly declined. The coating imparted high thermal stability confirmed by thermogravimetric analysis (TGA) and differential thermal analysis (DTA). Wolkenhauer et al. (2008) conducted a same test, and according to their study, the adhesion of paints was poor due to the hydrophobic nature of the HMDSO-treated surface. But the outermost surface could be hydrophilized by acrylic acid plasma post-treatment without decrease in water penetration of the whole treated wood samples. In addition, the technique is dry process without applying poisonous or corrosive chemicals. However, the protection is limited to the outermost surface based on Bente et al. (2004).

2.3.2 Wood Modification by Acetylation

The acetylation of wood, which includes a chemical reaction where the accessible hydroxyl groups of the wood components (e.g., lignin and hemicelluloses) are esterified[1] with acetic acid derivatives, is one of the most investigated modifications and has undergone market introduction(KOZARIĆ et al. 2016). Acetylation of wood was first applied by Fuchs (1928)

[1] Conversion of carboxylic acids to esters using acid and alcohols.

on spruce wood. Acetylation is mostly carried out without catalyst while it can be catalyzed by acids or bases(Papadopoulos et al. 2019).

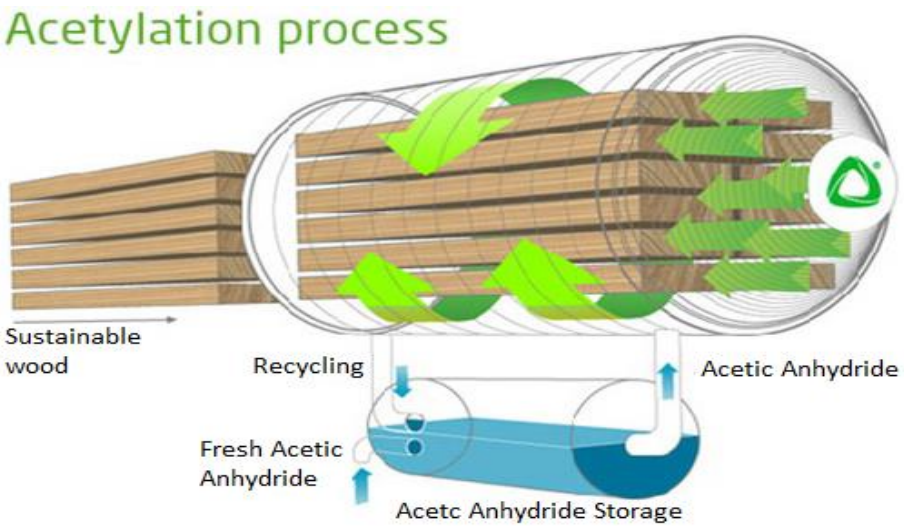

Figure 2.12: Schematic of Acetylation process(Anon n.d.)

Pries (2014) showed that it is a single site reaction, due that one acetyl group per hydroxyl group is formed. Weight Percent Gain (WPG) of the samples can be directly related to the number of blocked hydroxyl groups.

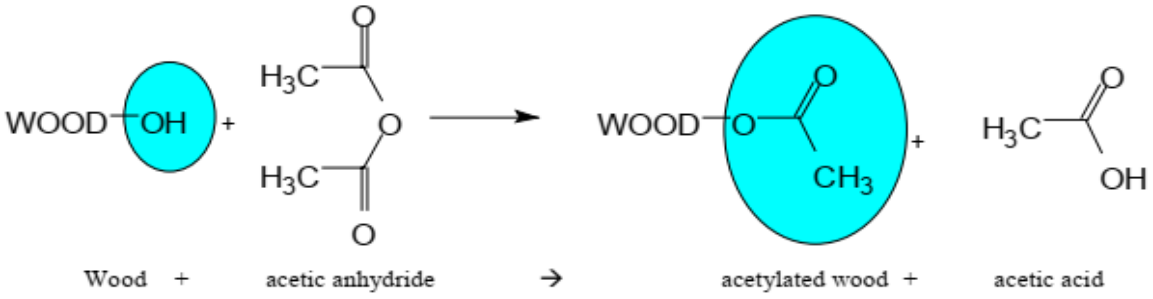

Figure 2.13: Acetylation of wood with acetic anhydride (Homan et al. 2000)

Bulking of the wood and dimensional stabilization occurs due to the introduction of acetyl groups into the cell wall. The dimensional stabilization is directly related to the WPG, since it is a function of the partial specific volume of the acetyl groups added within the cell wall (Hill 2011; Kollmann et al. 2012).

Hill et al. (2005) investigated the possible mechanisms of protection against the moisture content and the blocking of the micro-pores of the cell wall. In additions, Hill (2007) concluded that the Acetylation has no significant effect on the mechanical property of wood. Acetylation can be carried out with different chemicals, however, the most common is the acetic anhydride, which can be applied in liquid or vapor phase, as well as following to Ashori et al. (2014) not only it is a complicated and expensive process, and can lead to some environmental pollution problems.

2.3.3 Wax Impregnation

Wax have been used for protecting the wood surface against the humidity due to its weakness of penetration in wood. Particleboard productions are the most common applicant of wax. It has been shown that treated samples are more resistant against the wood decay fungi (Goethals and Stevens 1994; Lesar and Humar 2011). Based on Tjeerdsma et al. (1998) the wax methods changed the wood structure to make the durability of wood better, such that wood pests could not recognize it as food anymore. Rapp et al. (2005) reported that the, wax emulsions could improve the hardness and compression strength of the wood samples. Evans et al. (2009) added wax and oil emulsion additives into aqueous wood preservation to improve the appearance of treated exterior wood.

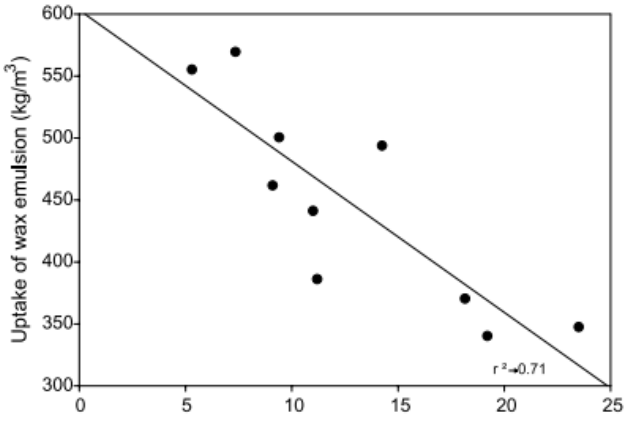

Figure 2.14: Correlation between dry contents of the emulsion and uptake of preservative solutions in spruce wood specimens (Lesar and Humar 2011)

Lesar et al.(2011), studied on the effect of wax on spruce wood, and showed there was a correlation between the ability of wax to penetrate into the wood sample and the dry content of its emulsions applied. Such that, for samples with higher concentration emulsion, less uptake of the preservative solution observed than for parallel samples preserved with emulsions with less dry content (Figure 2.14).

Several studies (e.g. Fujino et al. 1998; Lesar et al. 2008) showed that, regardless the emulsion particles are small (i.e., almost 100 nm), they are too big to penetrate the cell wall. Wood cell walls contain a nanocapillary network that is 1–10 nm in size. So, the wax is deposited in the cell lumen only. According to Lozhechnikova et al.(2015) due to the size of the particles in the emulsion they could not penetrate into the cell wall, so it assumed that during the impregnation process, wax remained on the surface while water penetrated deeper into the specimens Figure 2.15.

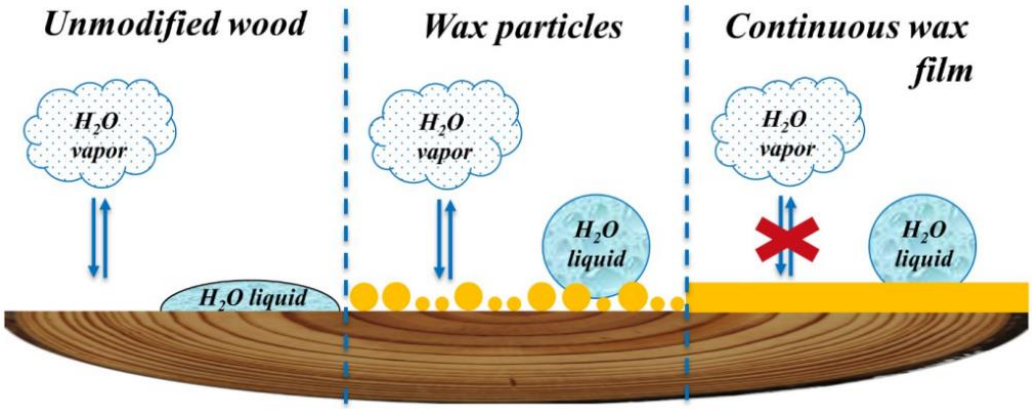

Figure 2.15: The relation between the quality of water evaporation and absorption vs Wax film condition (Lozhechnikova et al. 2015)

Several investigations (e.g., Avramidis et al. (2011); Humar et al. (2017); Petrič (2013);) have shown that wax does not have a prominent influence on the performance of the impregnated wood since the most amount of that mere remains on the surface of the specimen. In addition, using emulsions of higher concentrations will lead to better resistance against wood decay fungi. Applying the wax with some other mechanism like film barrier that formed in the cell

Lumina and on the surface of the specimen can potentially improve the performance of the wax treated wood. However, this mechanism only slows down the degradation processes and does not stop it. It is believed that wax emulsions have the potential to be used for wood protection in less hazardous outdoor applications due to the fact that, in case of a scratch or any surface damage, the wood will be endangered by humidity and moisture. Wang et al. (2007)studied the waxed wood and reported that, even though the wax was easy to formation liquid deposition on the wood surface, it damaged when the temperature increases to its melting point.

2.4 The Fick's Laws of Diffusion

The Fick's Law of diffusion, which proposed by Dr. Adolf Eugen Fick, The German physician and physiologist 1856, describe the rate of diffusion and are used to solve the problems related to the diffusion coefficient (Wadsö 1993). The amount of higher initial water absorption is mainly due to the diffusion phenomenon. In fact, the rate of water absorption depends on the moisture gradient between the water content at given time and the water content at saturation that is called the driving force (Khazaei 2008).

2.4.1 Fick's First Law

The first law of Fick examines the diffusion of mass flux rate under the constant conditions relative to the concentration (Fick 1855). Diffusion is the process that material moves from region with higher concentration to the region with lower concentration (Poirier and Geiger 2016) (Figure 2.16).

According to the First Law (i.e., equation 2-1):

$$j = -D\frac{\partial c}{\partial x} \qquad (2\text{-}1)$$

In which, j is the amount of material that pass per unit area per unit time (i.e., mass flux), D is coefficient of diffusion (i.e., diffusivity) based on area per unit time, C is the concentration and the dimension is the amount of material per unit volume, and X is position which its dimension is length (Poirier and Geiger 2016).

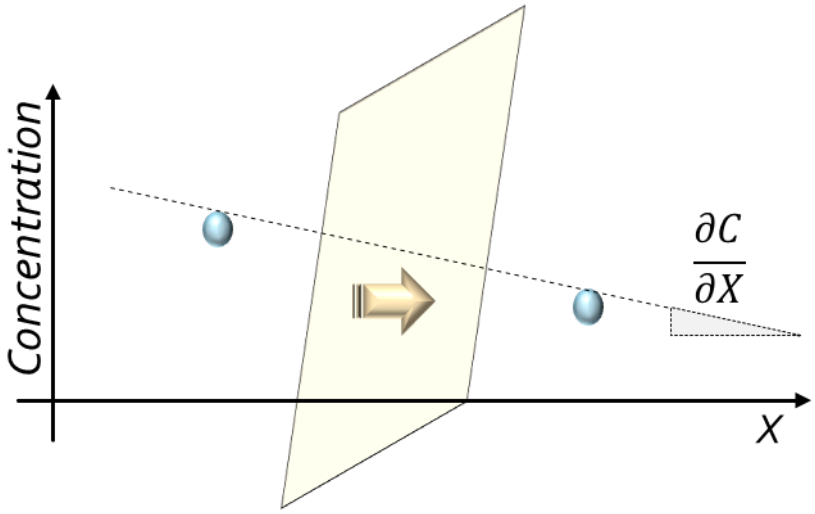

Figure 2.16: Schematic of diffusion process based on the concentration gradient $(\frac{\partial c}{\partial x})$

2.4.2 Fick's Second Law

The second law of Fick, which predict the effect of diffusion on concentration variations with respect to the time, is a one- dimensional partial differential equation (Shi 2007).

According to the Second Law (i.e., equation 2-2):

$$\frac{\partial c}{\partial t} = -\frac{\partial j}{\partial x} \tag{2-2}$$

Moreover, another form of the Fick's second law is obtainable by replacing the j from the first law (2-1), as it shown in equation (2-3) to (2-4).

$$\frac{\partial C}{\partial t} = -\frac{\partial}{\partial x}\left(-D\frac{\partial C}{\partial x}\right) \quad (2\text{-}3)$$

$$\frac{\partial C}{\partial t} = D\frac{\partial^2 C}{\partial x^2} \quad (2\text{-}4)$$

The equation (2-4) is the diffusion equation in mathematics (Philipse 2018).

Therefore, any change in concentration with time in a specific zone is proportional to the change in gradient of concentration at the point (Figure 2.17).

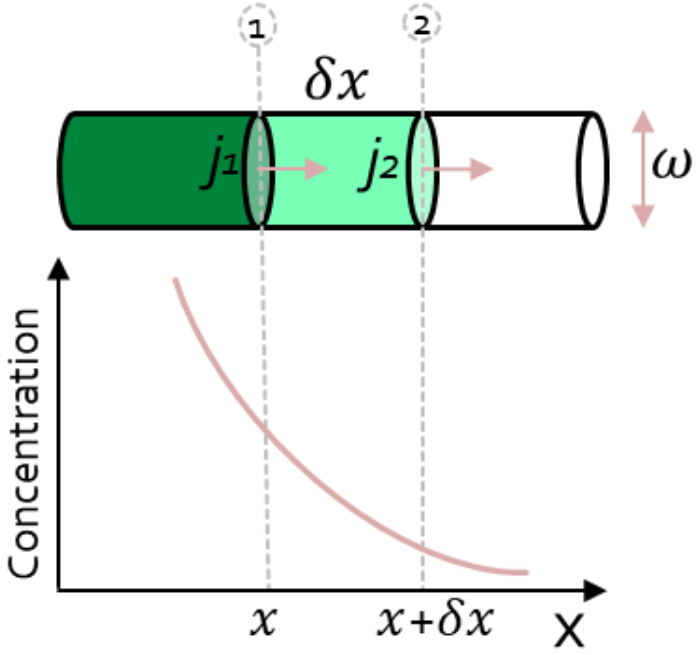

Figure 2.17: Schematic of concentration curve with respect to distance in the x direction according to the narrow banding material with width w

2.5 Research Gaps

The available knowledge on the topic of hygroscopic effects on wooden materials is primarily focused on surface protection using water resistant and hydrophobic materials (i.e. wax, and oil), with limited studies that explicitly address the reduction in the capacity of wood to absorb water at saturation. These studies lack specific information on the contribution of the vascular

system to the level of water uptake. Furthermore, no experimental research has been conducted prior to the current study, where readily available and cost-effective hydrophilic materials were used to reduce the water absorption capacity of the wood specimens. The current study contributes to the field of knowledge by presenting a technique where colloidal nanoparticle solution is used to form a homogenously impregnated surface as well as lumen pores with a dense material.

3 METHODOLOGY

3.1 General

In this chapter, the water uptake behavior of wood samples after treatments is characterized. The notations for the samples are given as follows:

1. Non-treated (N)

2. Pre-treated (P)

3. Non-treated Impregnated (NI)

4. Pre-treated Impregnated (PI)

5. Multiple Impregnated samples in which the coating process was repeated for several times (e.g., PI4, PI10), and

6. Pre-treated multi Impregnated Vacuumed (PIV)

The sample preparation and the details of the treatment procedure are discussed in the following sections. In addition, the weight of the samples before and after immersion in water is recorded. To better understand the water uptake behavior of the treated samples, the physical and chemical properties are further characterized.

3.2 Materials

3.2.1 Wood

In this study, the wood samples were fabricated from lumber belonging to species group SPF[1],

[1] Lumber made from combination of Canadian Spruces, Pines and Firs, which categorized as softwoods and commonly grown in various regions of the country, is labeled together as SPF.

graded by National Lumber Grade Authority (NLGA) as No. 2, which is the most commonly used group in Eastern Canada (Figure 3.1).

Figure 3.1: Spruces, Pines and Firs (SPF) timbers

3.2.2 Nanoparticle Solution Material

The colloidal silica nanoparticles solution (LUDOX® HS-40) was used as a coating material. The solution was produced by Millipore Sigma company (Silica 40 wt. % suspension in H_2O) and had a particle size of 12nm (Figure 3.2).

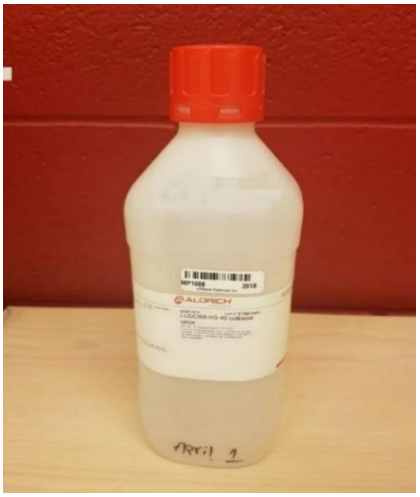

Figure 3.2: LUDOX® HS_40 Colloidal

3.3 Sample Preparation Procedure

The wood specimens were cut and sanded until a smooth surface was obtained. The cutting process was done in two steps. First, the wood was cut by a miter saw and then the cubes were fabricated from using a band saw (Figures 3.3 and 3.4). The samples were manufactured in two different sizes. Type A was prepared in accordance with the ASTM D 4761 standard and had dimensions of 5cm×1cm×0.3 cm, and Type B with dimensions of 1cm×1cm×0.3 cm, which required less time to reach a plateau during the tests due to the smaller dimension. The obtained samples were sanded using sandpaper with grits of 80, 100, 120, 220 and 600 in order to provide a smooth surface and remove any residues on the surface of the wood samples (Figure 3.5).

Figure 3.3: Cutting operation with the Miter saw

Figure 3.4: Cutting operation with the Band saw

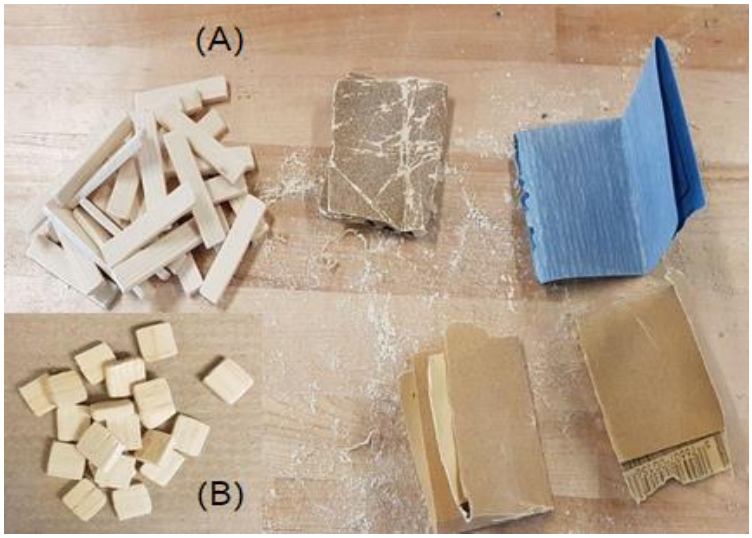

Figure 3.5: Wood samples (Type A & Type B) after the sanding process

A flow chart illustrating the sample preparation is shown in Figure 3.6. According to the flowchart, characterizations and analyses were done on both vacuumed and conventional dip-impregnated samples.

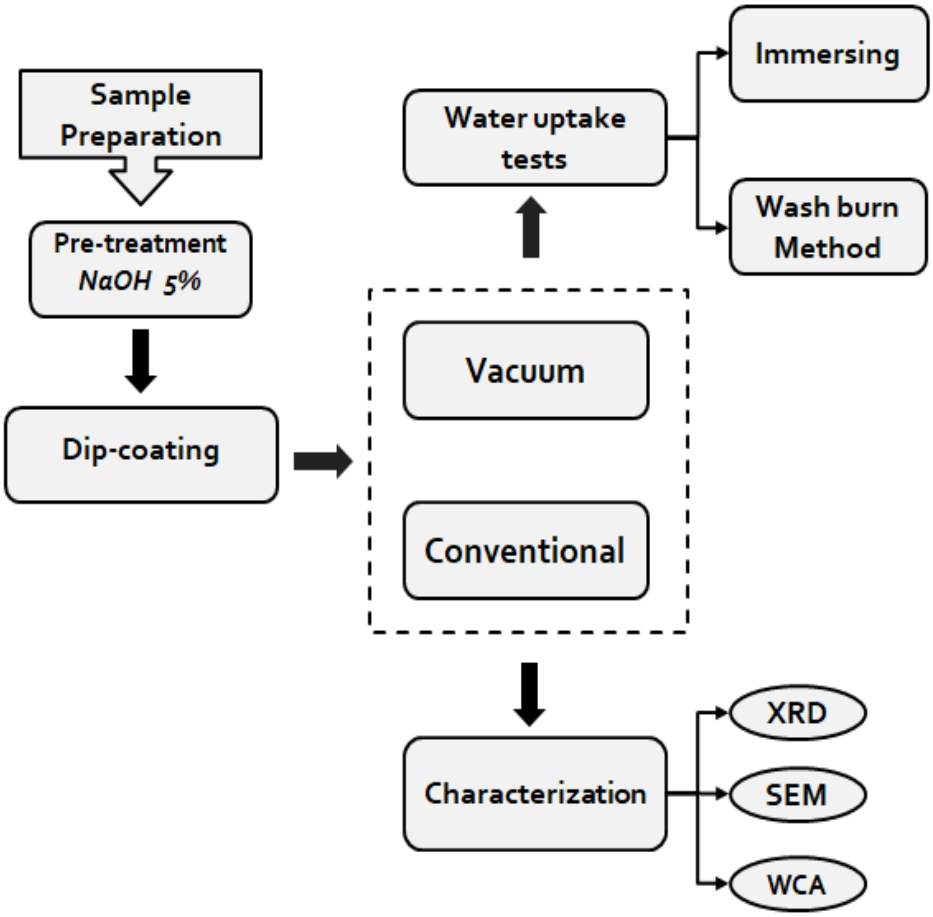

Figure 3.6: Processing flowchart of preparation of dip-coating systems and experiments

3.4 Pre-treatments

The specimens were ultrasonically rinsed with distilled water for 10 minutes to remove any dust remaining from the sanding. The samples were then placed in the oven at 80°C for five hours in order to dehydrate them. This procedure is similar to that used by Wang et al.(2014). The samples obtained at this stage are named “Non-treated” or “Reference”.

The wood material consists of Lumina that are responsible for transferring water from the roots to other parts of a tree. The internal diameter of each lumen is small enough to cause capillary pressure, and thus water can rise through it. (Figure 3.7).

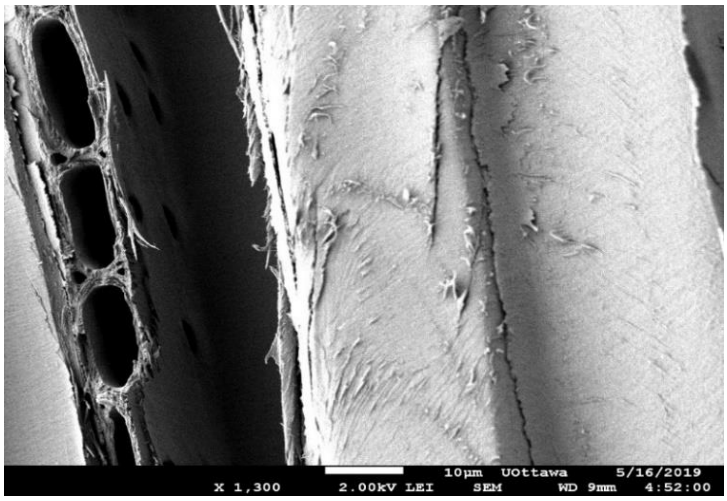

Figure 3.7: SEM micrograph of the wood sample

In order to improve the capillarity action of wood vascular system, the samples were pre-treated using the method developed by Foruzanmehr et al. (2015). In this method the samples were subjected to an alkali solution using a 5% aqueous sodium hydroxide (NaOH) (Fig. 3.8) for 45 minutes. The solution can remove organic residues such as wax and oil that may be trapped inside the Lumina and cannot be removed by simply washing with the distilled water. The samples were also washed with the aqueous citric acid (Figure 3.9), to neutralize the alkaline effect until the rinsed water reached a neutral pH. The immersing of the samples in sodium hydroxide and citric acid is shown in Figure 3.10.

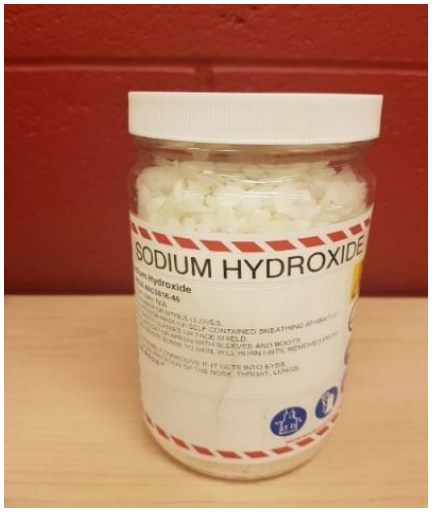

Figure 3.8: Sodium Hydroxide NaOH (caustic soda) white solid ionic compound

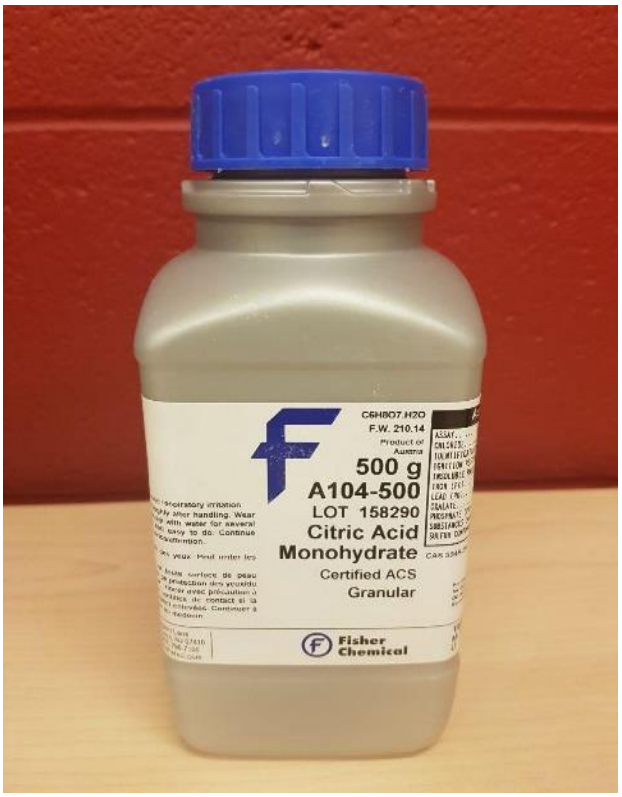

Figure 3.9: Citric Acid (C6H8O7)

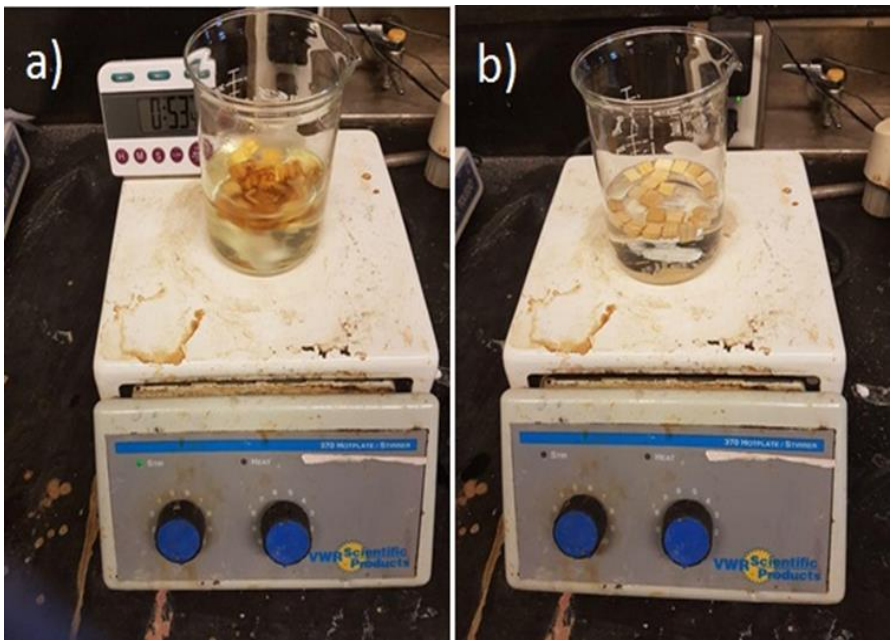

Figure 3.10: Samples (Type B) immersing inside: a) NaOH 5% b) Citric Acid

The samples were rinsed with the distilled water and the pH was controlled by a digital pH meter (Figure 3.11). Following the rinsing, the samples were placed in an oven at 80°C for five hours to dry (Wang et al. 2014). These samples are labeled “Pre-treated” (Figure 3.12).

Figure 3.11: PH measuring with the Digital PH Meter

Figure 3.12: The dried Pre-treated samples ready for the experiment

3.5 Dip Coating by Colloidal Silica Nanoparticles Solution

Dip coating by colloidal silica nanoparticles solution was done to reduce the Water Absorption Capacity (WAC) of wood. The samples were placed in glass containers with a capacity of 20ml. Glass stoppers were also used to keep the samples submerged within the liquid and to prevent them from floating to the surface (Figure 3.13). Each container was sealed with parafilm during the impregnation process to prevent evaporation and entry of any impurities. The samples were then withdrawn and dehydrated in the oven.

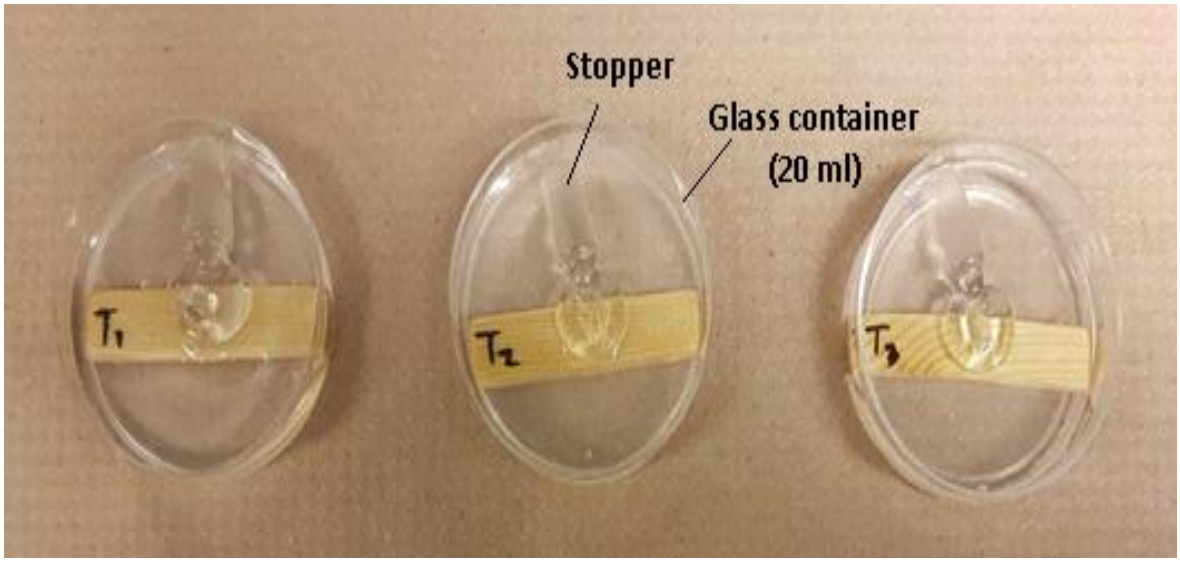

Figure 3.13: Dip-coating the samples by the LUDOX® HS_40 colloidal solution

3.5.1 Nano-SiO_2 Particles Impregnation Using a Conventional Dip-Coating Technique

The humidity that exists inside the samples may lead to the agglomeration of nanoparticles and thus non-uniform impregnation in wood. Therefore, the samples were dried in the oven at 80 °C for five hours. In this experiment, the samples were immersed in the colloidal silica nanoparticles solution. Three groups, consisting of five specimens each (Figure 3.14) were immersed for 20, 45, and 60 minutes for group 1, 2, and 3, respectively.

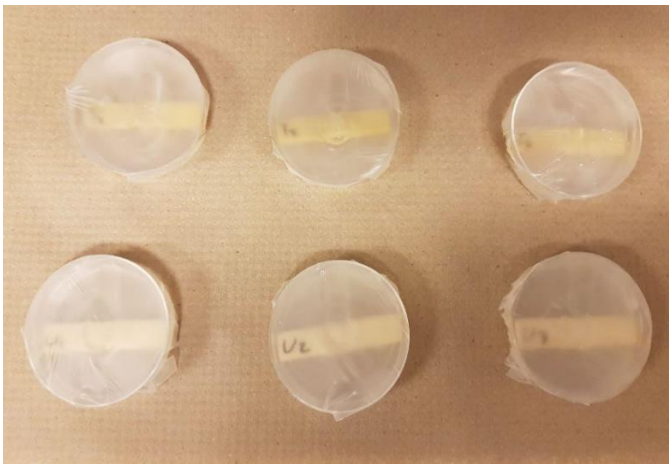

Figure 3.14: Non-treated groups immersed in the colloidal silica nanoparticles solution

The samples were then withdrawn manually at the speed of about 25 mm/min from the solution in two minutes to make sure that no spot is left uncovered on the surface. The samples were the dried in three steps. First, the samples were kept at 22 °C and 20% humidity for 20 minutes. Then, they were transferred to an oven at 50 °C for 60 minutes followed by 100 °C for 5 minutes (Figure 3.15) (Bayart et al. 2017).

Figure 3.15: Drying process inside the oven

Following the solvent evaporation, agglomerated nanoparticles are formed inside the samples while a thin layer of nanoparticles is produced. The schematic of the sample preparation procedure is illustrated in Figure 3.16.

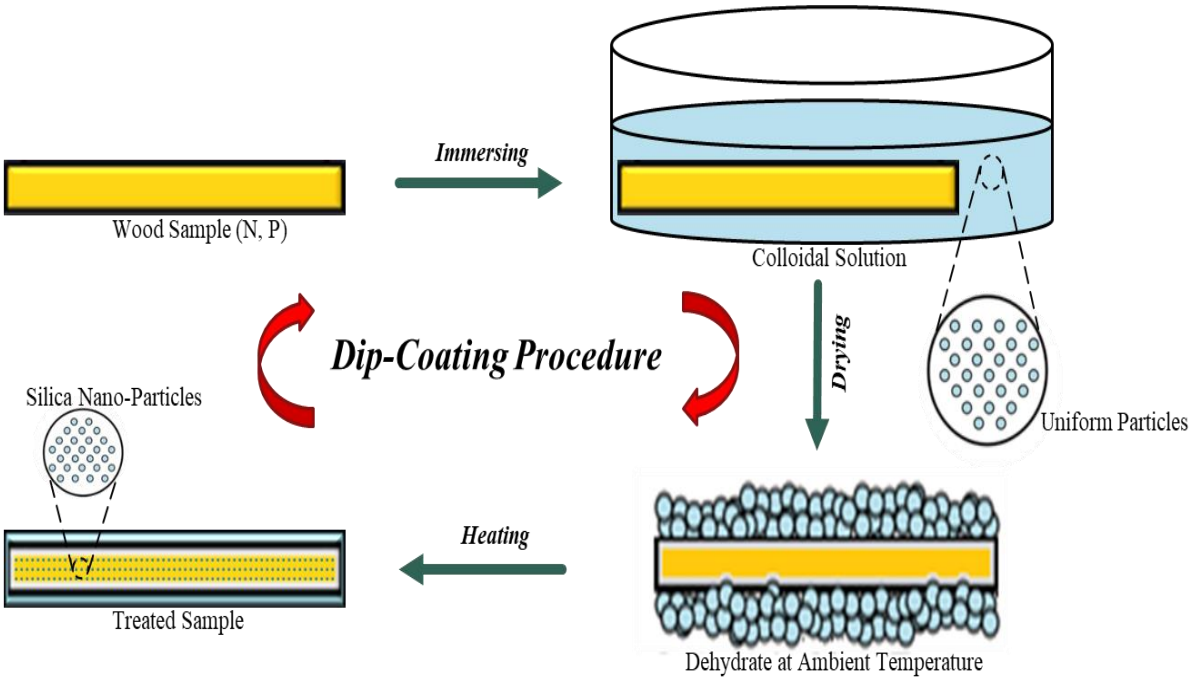

Figure 3.16: Schematic representation of the different stages and routes of the Dip-coating process

To amplify the effect of the treatment, the process is repeated multiple times. The samples were immersed in the solution for 60 minutes during the previous experiments. In this experiment, the samples that divided in to two groups, and each group was dipped and dried for 4 and 10 times, respectively.

3.5.2 Vacuum Aided Impregnation

Capillarity action causes liquids to rise inside the Lumina, hence taking entrapped air off from the samples can favor the capillary effect and thus improve the permeation of the colloidal solution into the specimens. The same procedure as that discussed in the previous section was used to impregnate the samples. However, in this case, the samples were kept in a vacuum

chamber (Figure 3.17) at −0.3 bar for four minutes to enhance the infusion of the colloidal solution through negative pressure. The samples were then dried in three consecutive steps as described in the previous section (Figure 3.17).

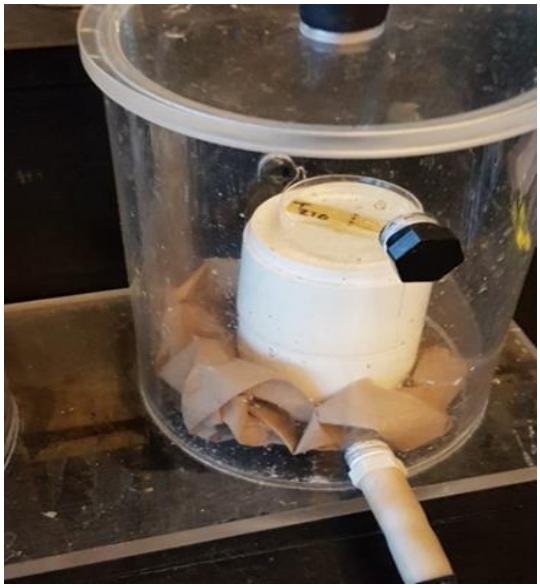

Figure 3.17: Pre-treated Impregnated sampled inside the vacuum

Figure 3.18: The drying process for Non-treated Impregnated samples (NI)

A schematic of the sample preparation procedure is illustrated in Figure 3.19.

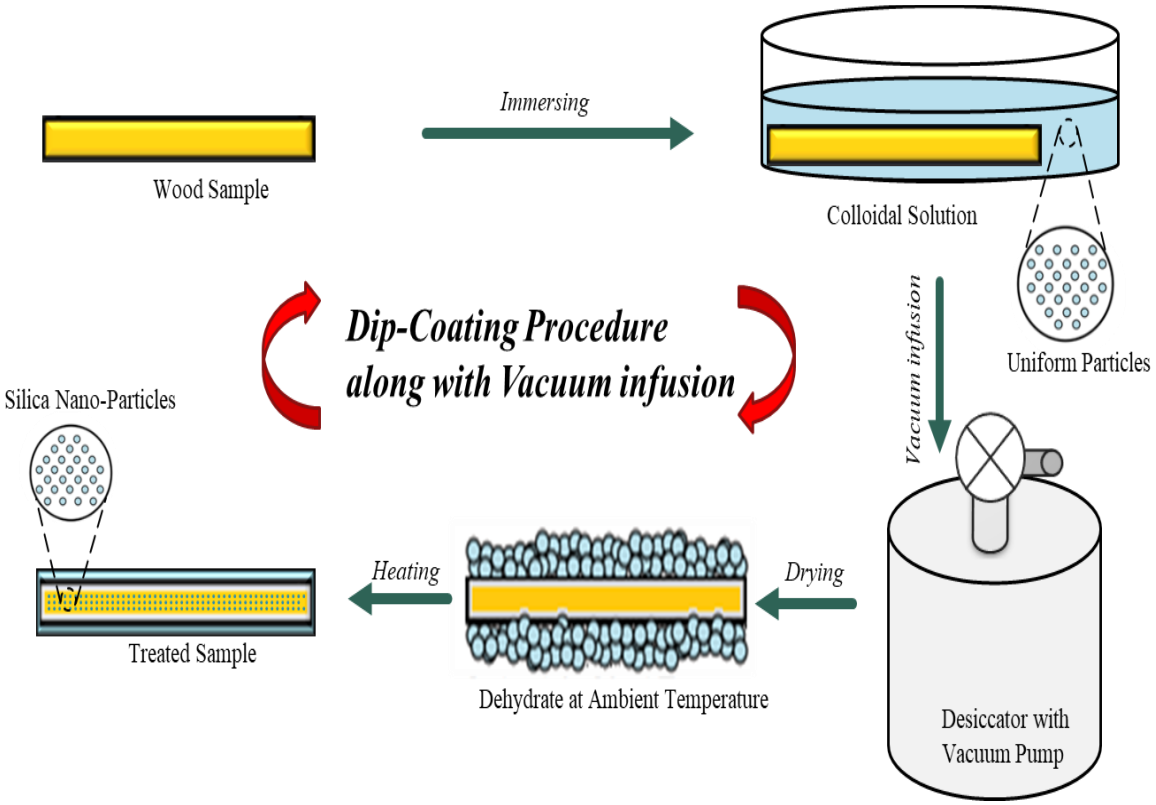

Figure 3.19: Schematic representation of the different stages and routes of the dip-coating process along with vacuum infusion process

The solution changes the water absorption on the surface and also reduces the capillarity of the vascular system as described before. The dip-coating procedure was repeated several times, as shown in Figure 3.19, in order to fabricate the multistep dip-impregnated samples.

3.6 Characterization Techniques

The wettability of solid surfaces as well as surface free energy (SFE) of the dried samples could be evaluated by Water Contact Angle test (WCA) (Żenkiewicz 2007). In addition, Scanning Electron Microscopy (SEM) was used to characterize the morphology and elemental composition of the impregnated wood samples. Also, X-ray diffraction (XRD) technique was used to provide information, such as crystal structure and crystallite size of the SiO_2 nanoparticles.

3.6.1 Water Contact Angle (WCA)

In order to evaluate the wettability of solid surfaces, the water contact angle test was done on the surface of the samples using a goniometer. The applied technique used to measure the WCA was sessile drop. In this technique, a graduated syringe dosed an accurate volume of water, precisely and slowly to drop a regular droplet on the surface of samples. The volume of each droplet put on the surface was 3 µl and the evaluations took place 10 seconds after the time that droplets were put (Figure 3.20). The procedure was previously adopted by Schuster et al. (2015).

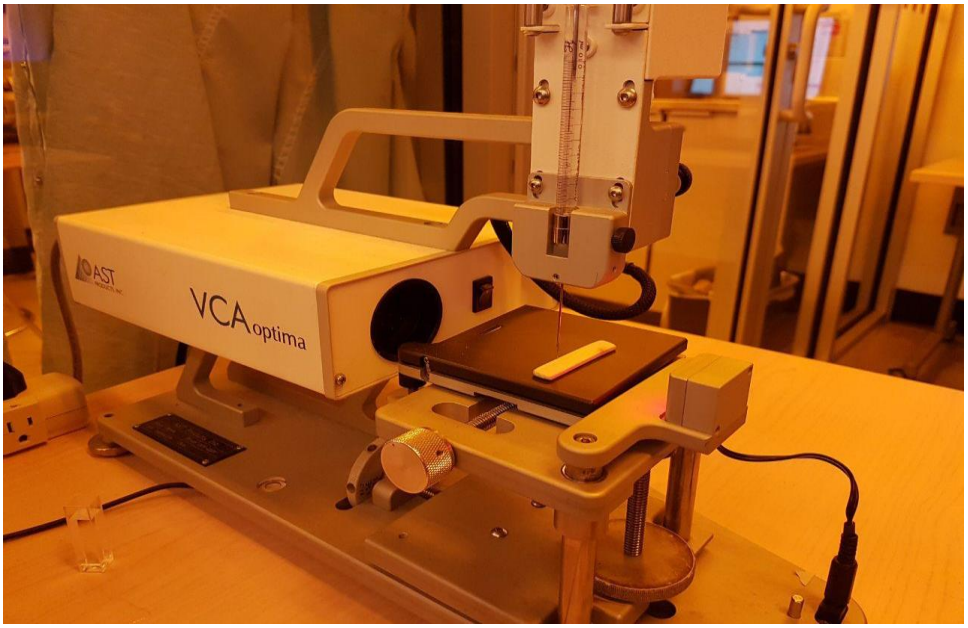

Figure 3.20: VCA Optical contact angle measuring and contour analysis systems

3.6.2 Scanning Electron Microscope (SEM)

Scanning electron microscopes (SEM) use a focused beam of electrons to scan the surface of a specimen in a vacuumed chamber (Figure 3.21).

Figure 3.21: Scanning Electron Microscope (SEM), The Centre for Advanced Materials Research (CAMaR)

3.6.2.1 General Steps for Sample Preparation

The general scheme of the sample preparation involves the following steps. The first step in this process is to dry the specimens in the oven. Once the drying is completed, the samples are removed from the oven and mounted on the metal stub covered with sticky carbon tape. The samples are then sputtered with a thin film of conductive material (e.g., gold nanoparticle). Finally, a strip of conductive metal (e.g., copper) is attached to one side of the samples, to collect the electrons remaining from the SEM.

3.6.2.2 Morphology Assessment of Impregnated Samples

One sample from each group, group A and Non-treated samples, were chosen randomly for SEM. The samples were put in the oven for 5 hours at 80 ° C to dry and they were split in half to evaluate the permeation of nanoparticles in the structure of wood. Moreover, the metal stubs were cleaned by acetone to remove any residue and to prevent any contaminations. The carbon

tapes were applied to cover the whole surface of the metal stubs, mainly because the double adhesive surface permits quick mounting of samples on the stubs. Moreover, the tapes could improve the electrical conductivity in order to boost the quality of the micrographs. Then a thin layer of gold nanoparticles was added to the surface by the machine in Figure 3.22 and a thin copper film was attached to one side of the specimens to collect the electrons during the process (Figure 3.23). Finally, the prepared specimens were put in the Electron Microscope (Figure 3.21).

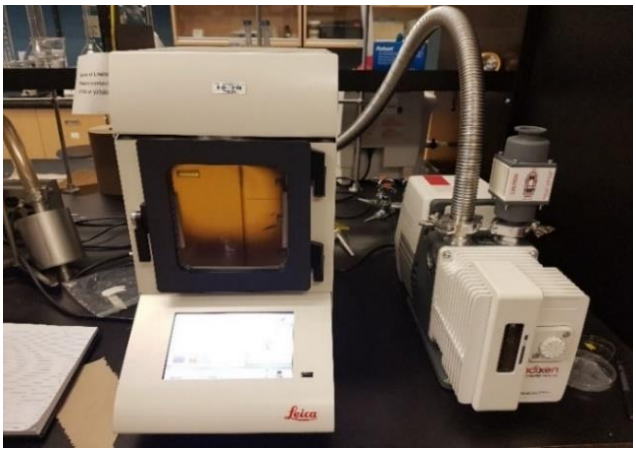

Figure 3.22: Coating the powder specimen with gold nanoparticles

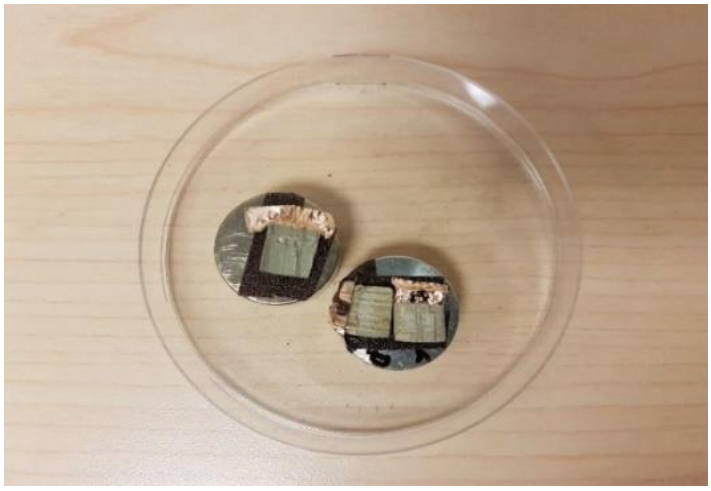

Figure 3.23: The prepared specimens for the SEM technique from Group A, and reference coverd by gold as conductor

The surface morphology of the specimens before and after the coating process was provided by the SEM.

3.6.2.3 Morphology Assessment of Silica Powder

To prove the presence of the silicon nanoparticles in the wood samples, the SEM technique was done on the solid nanoparticles, existing in the colloidal solution to study their morphological features. For this purpose, some solution was exposed to the ambient temperature to evaporate, and the remaining nanoparticles were collected and ground by a mortar to powder form (Figure 3.24).

Figure 3.24: Silica nanoparticles extracted from the colloidal solution

To prepare the specimens for SEM, the silica powder was attached to the metal stub using carbon tape and a thin layer of gold nanoparticles, as the conductor, was sputtered on the surface of the powder (Figure 3.25).

Figure 3.25: The prepared powder specimen for the SEM technique

The morphology and the topography of the powder samples were compared with the sedimentation of the nanoparticles inside the wood samples.

3.6.3 X-ray Diffraction (XRD)

X-ray powder diffraction (XRD) (i.e., a non-destructive rapid analytical technique) is primarily used for elemental analysis, chemical characterization of a sample, phase identification of a crystalline material and it provides information on unit cell dimensions.

The crystallinity index (*CrI*) of the samples is calculated from the XRD data, using the Segal's equation(Segal et al. 1959):

$$CrI = (1 - \frac{I_{am}}{I_{200}}) \times 100 \quad (3.1)$$

Where I_{200} is the peak intensity of the (200) lattice diffraction, and I_{am} is the minimum intensity of diffraction in the same units between (200) and (110) peaks regarding to the non-crystalline material in cellulose.

The inter planar spacing of crystalline structures can be obtained by the following equation

known as Bragg's law (Epp 2016):

$$n\lambda = 2d\sin\theta \quad (3.2)$$

Where *n* is order of reflection that is an integer, λ is the wavelength of x-rays, *d* is the inter planer spacing of every single crystallographic phase, and θ is the angle between the normal beam and the incident to the reflecting lattice plane.

In addition, *d*, which is the characteristic distance between the crystal planes of the sample , can be obtained by calculating the angles, θ, under which the constructive interfering x-rays leave the crystal (Taylor et al. 2004).

3.6.3.1 Sample Preparation

The most common sample holder for powder samples is aluminum (Al) and glass plate with a 20 mm hole at the center. It is important that the powder specimens are well ground with a mortar to produces the uniform fine powders with all possible crystalline orientations (Figure 3.26).

Figure 3.26: SiO_2 particles extracted from the colloidal solution

The XRD technique was conducted using Rigaku Ultima IV Diffractometer system equipped

with a Micro focus Copper Anode at 40 kV/ 44 mA. The Divergence slit was 2/3 deg, the Divergence Height Limiting slit was 10mm, the Scattering slit was 2/3 deg and the Receiving slit was 0.3mm. MONTAL OPTICS and a VANTEC 2000 2DDetector at 1086.000 mm distance from the samples calibrated with a Silver Behenate standard (Figure 3.27).

Figure 3.27: X-ray Machine

3.7 Water Uptake Measurements

The water uptake test was conducted for Non-treated samples. In these experiments, the amount of water absorption was determined by measuring water uptake in the sample over time. The samples were periodically removed from the distilled water, dried and weighed, until full saturation, according to ASTM D5795. The water uptake was obtained in terms of weight percent (wt. %), using equation (3-3).

$$M\% = \frac{100\times(M_{cond}-M_{dry})}{M_{dry}} \quad (3\text{-}3)$$

M_{cond} is the mass gain after immersing in distilled water

M_{dry} is the mass gain before immersing in distilled water

$M\,\%$ the mass gain during the water uptake

The level of water uptakes was measured using Conventional and Washburn techniques (Pucci et al. 2016).

3.7.1 Conventional Method

To determine the water uptake variation, the samples (Type A) were put in a container filled with distilled water and the weight was recorded at different times (Figure 3.28).

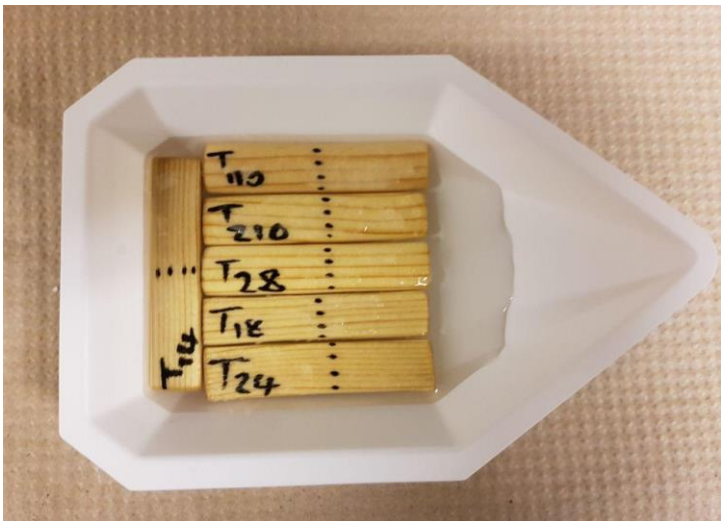

Figure 3.28: Non-treated wood samples immersed in distilled water

The measurements were performed every 30 minutes on the first day with a balance as it shows

in Figure 3.29. The recording interval was then doubled every day thereafter (i.e., 60 min on 2nd day, 120 min on 3rd day, etc.) and the process continued until the water uptake remained almost constant. In addition, the dimension of the samples was measured by the caliper before and after the dip coating process in order to evaluate the probability of swelling in the samples (at their cross-section) which may cause by the colloidal solution.

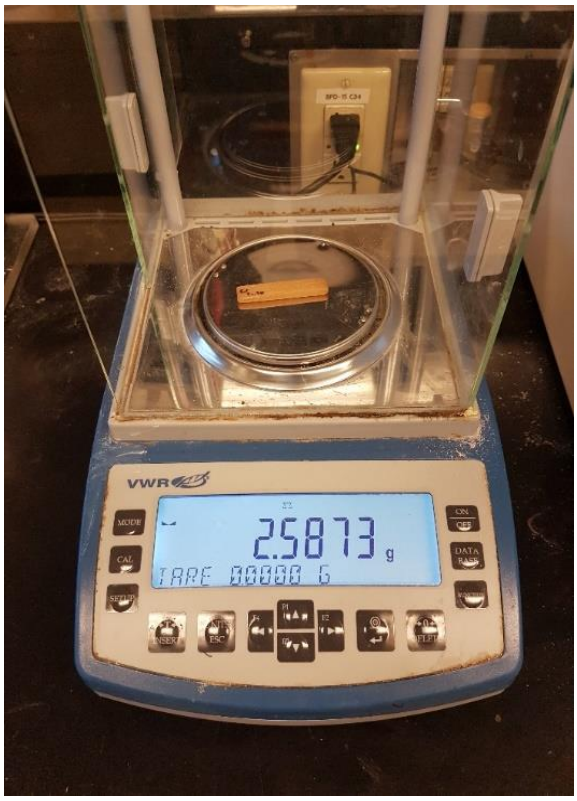

Figure 3.29: Measurement of the Non-treated Impregnated samples (NI) weight on a balance scale

3.7.2 Washburn Theory

In order to evaluate the effect of the silica colloidal solution on the level of water absorption in the samples, the Washburn theory was applied (Teipel and Mikonsaari 2004). The Washburn theory is a framework for studying the wetting of porous solids. This theory indicates that if a porous solid is touching the liquid's surface, the capillary rise of liquid into the voids of the solid will be governed by the following equations:

$$t = Am^2 \quad (3\text{-}4)$$

t, is the time after liquid and solid are in contact

m, is mass of liquid absorbed by the solid

A, is a constant which is dependent on the properties of the liquid and the solid, and can be found using equation (3-5)

$$A = \frac{\eta}{c\sigma\rho^2 \cos\theta} \quad (3\text{-}5)$$

$\eta, \sigma,$ and ρ are respectively, viscosity, surface tension, and density of the liquid. θ is contact angle between liquid and solid, and *c* is the material constant which depends on porosity of the solid, calculable using equation (3-6).

$$c = 0.5\pi^2 r^5 n^2 \quad (3\text{-}6)$$

r is the average capillary radius inside the porous solid, and n is the number of capillaries in the specimen.

In additions, the coefficient of diffusion, according to the Fick Theory at short time is based on equation (3-7) (Alghunaim et al. 2016; Espert et al. 2004).

$$D = \left(\frac{L}{2} \times \frac{M_t}{M_\infty}\right)^2 \times \frac{\pi}{t} \quad (3\text{-}7)$$

In which, *D* is coefficients of diffusion, *t* is the time, *L* is the thickness, M_t is the mass of absorbed water at the time *t*, and M_∞ is the mass at the equilibrium (Mrad et al. 2018).

3.7.2.1 Washburn Measurements Method

In this method, a Tensiometer is used to reveal the amount of water absorbed by porous samples as a function of time.

The wood samples are in suspended position from the balance in the Force Tensiometer just above the surface of water within a metal-framed sample holder as shown in Figure 3.30.

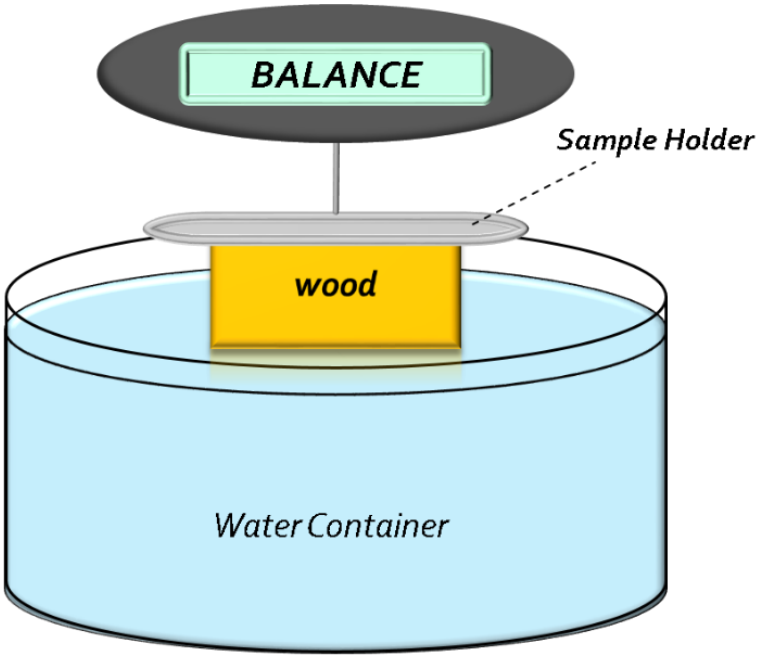

Figure 3.30: Schematic of sample holder setup

According to the schematic setup, the water uptake experiment is done using the Force Tensiometer machine, shown in Figure 3.30, simultaneously and automatically the required data is recorded in terms of water uptake percentage (wt. %) as a function of time.

3.7.2.2 Water Uptake Experiment for the N, PI10, and PIV10 Samples Using Tensiometer

The samples were divided into three groups A, B, and C. For group A, and B (pre-treated impregnated vacuumed or PIV10), and pre-treated impregnated (PI10) respectively the dip-coating process was repeated ten times. Also, for group A, the specimens were put inside the vacuum container for four minutes at all stages of the dehydration process. Group C included the reference samples, which were non-treated and non-impregnated (N). The Non-treated,

Pre-treated impregnated, and Pre-treated impregnated Vacuumed samples (after ten steps of dipping and drying), which were prepared in the previous section, were put on the water surface and the water absorption levels were measured by the Tensiometer automatically (Figure 3.31). The water level was increased until it just touched the bottom of the wood samples. Mass uptake was recorded with respect to time. In this test, the water uptake was recorded in terms of weight percent (wt. %). The data were recorded until the water uptake remained almost constant and its curve reached a plateau.

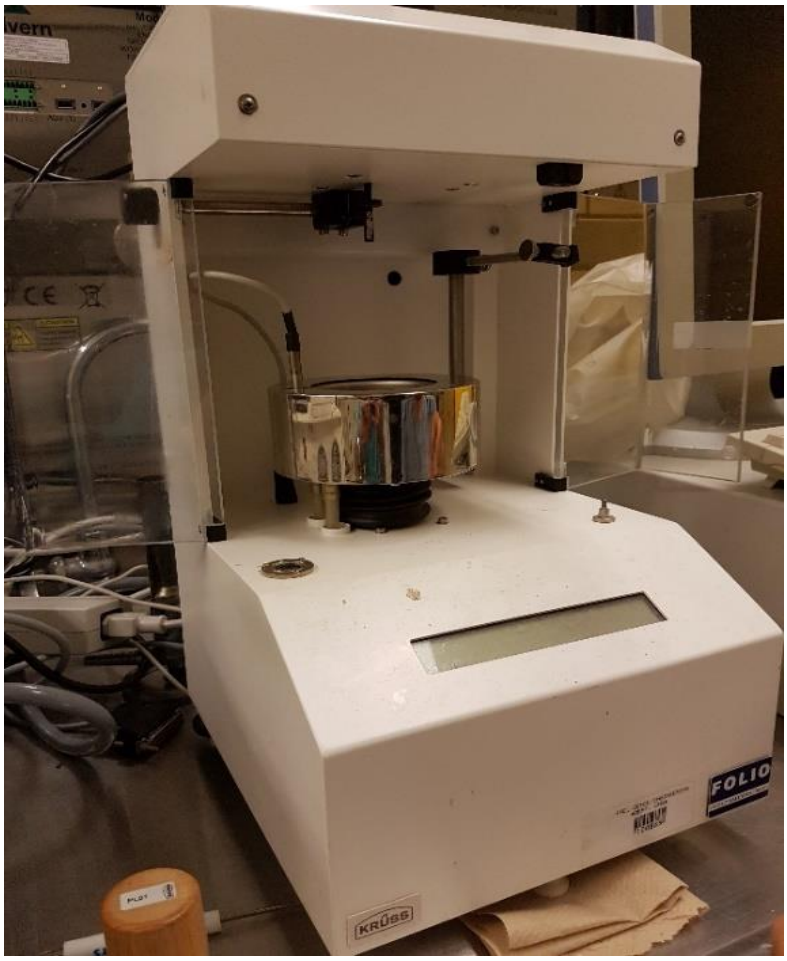

Figure 3.31: Measurement the weight % of N, PI10, and PIV10 samples by tensiometer

4 RESULTS

4.1 General

In this chapter, the results of the experimental study are presented in detail. Experimental tests have been conducted on wood samples prepared by the proposed techniques outlined in Chapter 3. The variations in the level of water uptake in the samples, which were impregnated with the colloidal silica nanoparticles solution, are studied in detail. The amount of silica nanoparticles that were impregnated in the vascular system of wood is also characterized. In order to compare the various properties investigated in this study, a statistical method (i.e. t-test) was employed (Livingston 2004).

4.2 Statistical Analysis

A statistical method of two samples (t-test) was performed to establish whether significant difference exists between the mean values of the level of water uptake. This was done by calculating the Z-scores using equation 4.1.

$$Z_{score} = \frac{A_i - A_j}{\sqrt{\frac{\sigma_i^2}{n_i} + \frac{\sigma_j^2}{n_j}}} \quad (4\text{-}1)$$

Where:

A_i: represent the level of water uptake (wt.%) tested for specimen i

σ_i: is the standard deviation considered for specimen i

n_i: the number of tested samples for sample i

A confidence interval of 95% was considered, which means that as long as the Z-score is above 1.96, the P-value (probability value) is below 0.05 (Livingston 2004).

The standard error (S_e) for the single-sample t-test is computed as shown in equation 4.2.

$$S_e = \frac{S_d}{\sqrt{N-1}} \quad (4\text{-}2)$$

Where S_d is the standard deviation for each sample, and N is the number of cases in a sample. It is well known that the sample size, N, has an inverse effect on S_e, such that as N gets smaller, the standard error of the evaluation becomes greater (Piquero and Weisburd 2010).

4.3 Loss in Mass Due to Pre-treatment

The results from the conventional tests, suggest that there is a minor increase in the level of water uptake of the samples after pretreating through the proposed methods. To evaluate the amount of extractives removed from samples after the pretreatment (i.e., alkaline treatment) process, the average weight of the samples was compared before and after the process. As it shown in Figure 4.1, there is not too much variation between the average weight of the dry specimens after the pretreatment process (i.e. almost 1% of the primary weight, and the P-value is 0.05).

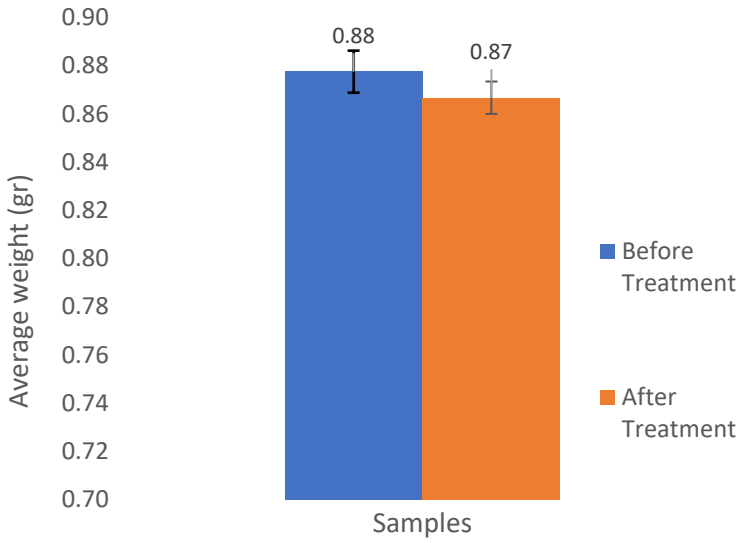

Figure 4.1: The average weight of the samples before and after Pre-treatment

4.4 Water Uptake for Non-treated Samples (N)

The reference wood samples were placed in distilled water and the amount of water uptake in terms of weight was recorded at various times. The data were collected until the weight remained almost constant, following the procedure described in Chapter 3.

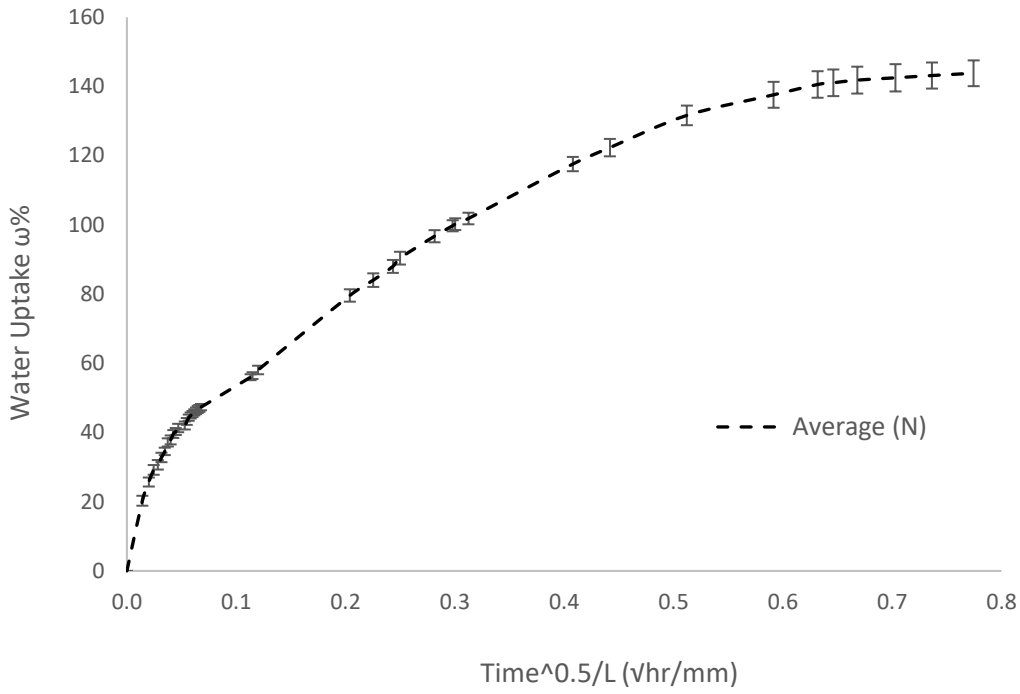

Figure 4.2: Water capillary rise of Non-treated (Reference) wood samples given as a percentage of the weight of absorbed water vs square root of time on the length of samples

The trend in Figure 4.2, represents the average amount of water uptake (wt. %) for five specimens. The slope of the curve at each point shows the rate of water absorption. The curve depicts a sharp rise at the beginning of the test, which means a quicker absorption rate in comparison with the rest of the time period. The maximum level of water uptake is 144.12 ±3.73 (wt. %), which happens at 0.77 √hr/mm.

4.5 Water Uptake for Pre-treated Samples (P)

The pre-treated wood samples were immersed in water and the weight was recorded periodically. Figure 4.3 shows the percentage of water uptake for five samples as a function of time. The process continued until the water uptake reached a steady state.

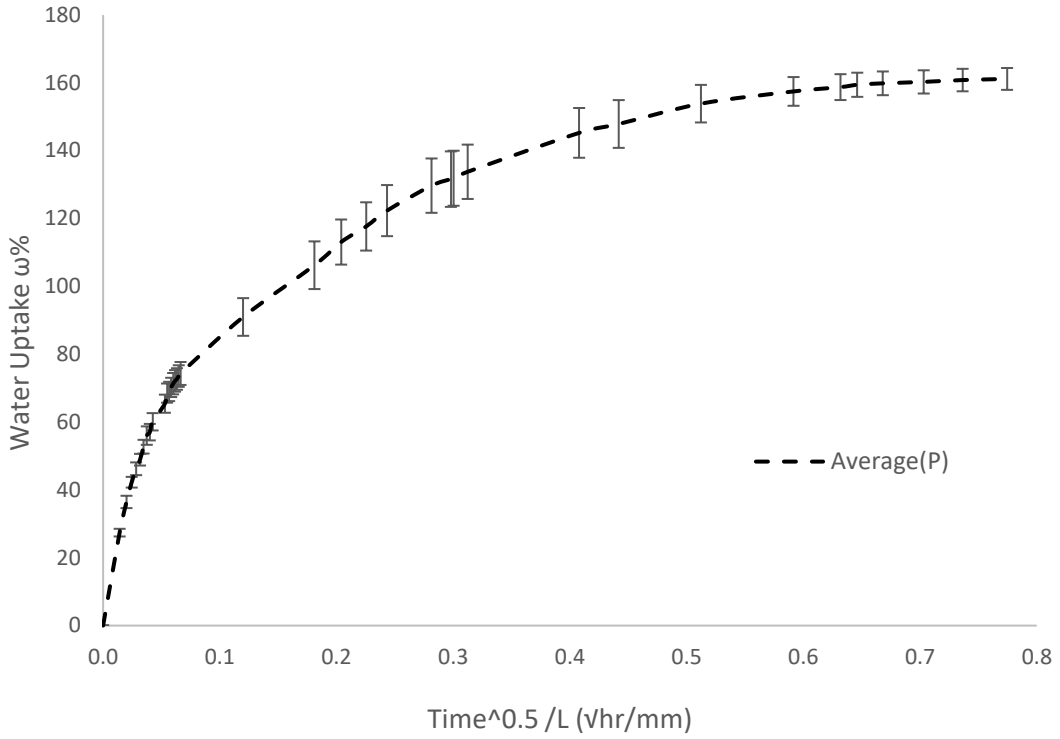

Figure 4.3: Water capillary rise of Pre-treated wood samples given as a percentage of the weight of absorbed water vs square root of time on the length of samples

Similar to the Non-treated samples, the rate of water uptake was high at first (even sharper than the slope of the Non-treated curve) but decreased over time. The plateau was reached at 0.64 (√hr/mm). The maximum percent of the water uptake for Pre-treated samples is 161.16 ±3.23 (wt. %). The curve is almost Fickian in the water uptake (wt. %) compared to the samples presented in the previous section.

4.6 Effect of Dipping Duration on the Level of Water Uptake of the Pre-treated-Impregnated and Non-treated-Impregnated Specimens

The effect of these procedures on the water absorption capacity of the samples was investigated. At least five measurements were performed to validate the statistical analyses of the data. Schematic of the average curves of the water uptake test is shown in Figure 4.4.

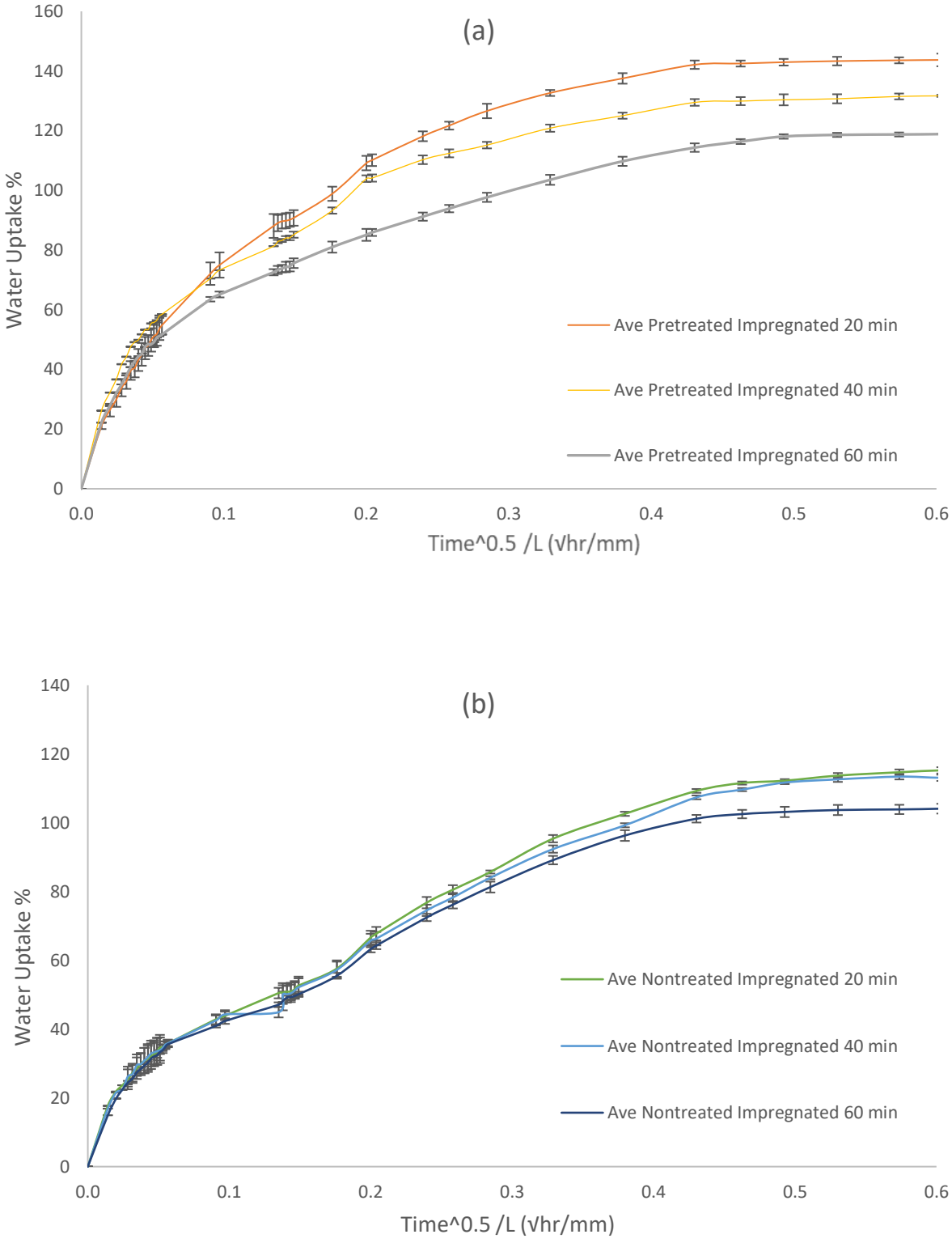

Figure 4.4: Water capillary rise of (a) Pre-treated wood samples and (b) Non-treated wood samples impregnated

The Pre-treated samples that were dipped in the colloidal solution for 20 minutes had the highest amount of water absorption at saturation (Figure 4.4 a). In addition, the rate of water absorption (i.e., the slope of the tangent line to the graph at each data point) for Pre-treated-impregnated-20 min was observed to be the highest amongst all samples. The level of water uptake was increased from 0 (wt. %) to 70 (wt. %) in the range between 0 and 0.08 (√hr/mm) with the increasing rate of 732.81±11.08(wt. % /√hr/mm). Then, in the range of 0.08-0.4 (√hr/mm), the rate of water uptake was decreased gradually until the curves reached a plateau at 0.45(√hr/mm). The maximum level of water uptake is 145.07±3.16 (wt. %). For the NI samples (Figure 4.4 b), the rate of water absorption is noticeably less than that of the PI sample. The minimum amount of water uptake is 100.12 ±2.95 (wt. %), which belongs to the Non-treated samples that were treated with the colloidal solution for 60 minutes (Non-treated-impregnated-60 min). Based on Figure 4.4, the minimum level of water uptake at saturation in both PI and NI specimens belongs to the samples which were dipped in the colloidal solution for 60 minutes. Thus, the 60 minutes immersion time was chosen for the rest of the experiments.

4.7 Effect of the Number of Impregnation on the Level of Water Uptake

The effect of the number of impregnation cycles on the water uptake properties of wood is examined on five samples in this section using statistical method to determine if repeating the cycle can reduce the level of water absorption at saturation. As noted in section 4.6, the time over which samples were submerged in the silica nanoparticle colloidal solution was 60 minutes. During the following tests, the non-treated impregnated samples, pre-treated impregnated samples, and the pre-treated impregnated vacuumed are studied.

4.7.1 Non-treated Impregnated Samples (NI)

The NI samples were divided into two groups, where the coating process was repeated four times for the first group (NI4), and ten times for the second group (NI10). The graphs of average water uptake variations (wt.%) as a function of time are shown in Figure 4.5.

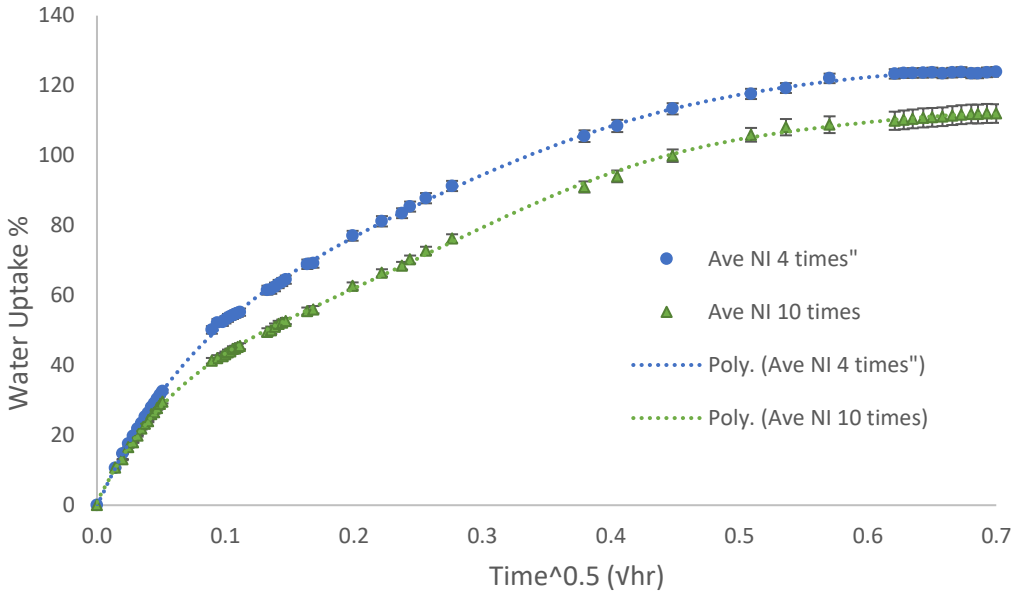

Figure 4.5: Water capillary rise of Non-treated Impregnated (NI) wood samples Impregnated in two specific times, given as a percentage of the weight of absorbed water versus square root of time on the length of samples

As shown in Figure 4.5, the rate of water absorption in the range between 0-0.1 (√hr/mm) is higher in the non-treated impregnated samples, which were impregnated 4 times, in comparison with the samples that were impregnated 10 times. The rate of water absorption for both NI4 and NI10 rose considerably between 0 (√hr/mm) and 0.15 (√hr/mm) up to 410.03±3.31 (wt. % /√hr/mm), and 313.85±2.53 (wt. % /√hr/mm), respectively. At 0.15 (√hr/mm) the average level of the water uptake for NI4 and NI10 is 65.14±1.19 (wt. %) and 50.21±1.38 (wt. %), respectively. From 0.15 to 0.6 (√hr/mm), the level was decreased gradually to 101.12±5.01 (wt. %) and 96.26±9.03 (wt. %) until the curves reached a steady state. In addition, the maximum level of water uptake at saturation for the average NI4 specimen is 124.22%±1.37 (wt. %), while the average NI10 sample shows a lower water uptake of 112.17%±3.12 (wt. %).

4.7.2 Pre-treated Impregnated Samples (PI)

The PI samples were prepared by dipping the Pre-treated specimens into the solution for 60 minutes, while recording the level of water uptake for samples that were impregnated four

times (PI4) and ten times (PI10). Figure 4.6 presents the average level of water uptake (wt.%) as a function of time (i.e. √hr/mm) for the specimens PI4 and PI10.

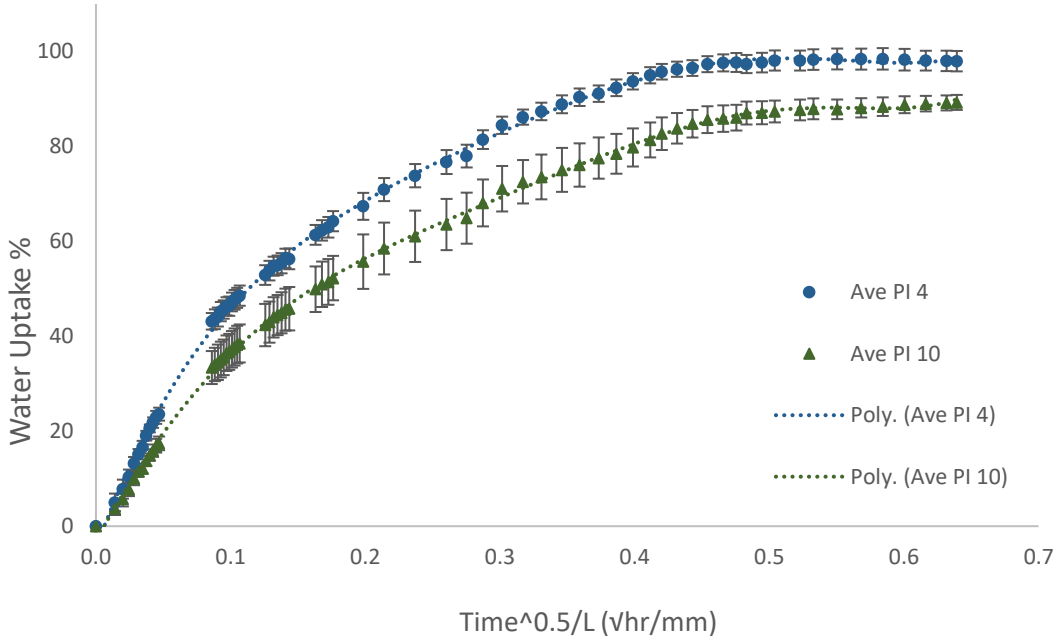

Figure 4.6: Water capillary rise of Pre-treated Impregnated (PI) wood samples Impregnated in two specific times, given as a percentage of the weight of absorbed water versus square root of time on the length of samples

The rate of water absorption between 0 to 0.1(√hr/mm) for the average of PI4 is clearly higher than the average rate of PI10. From 0.1 to 0.6 (√hr/mm), the slope of the curves gradually decreased from 494.02, and 391.06 to 98.23, and 105.93 (wt.% /√hr/mm) for PI4 and PI10, respectively. Moreover, the maximum amount of weight percent (wt. %) in Ave PI4 graph is 99.57±2.48 (wt. %) while the maximum level of water uptake in Ave PI10 curve is 87.46±1.55 (wt. %).

4.7.3 Pre-treated Impregnated Vacuumed Samples (PIV)

The pre-treated-impregnated-vacuumed samples were prepared, and the level of water uptake was recorded for specimens which were impregnated four times (PIV4) and ten times (PIV10) with the colloidal solution. The graphs of the average water uptake (wt.%) as a function of time are shown in Figure 4.7.

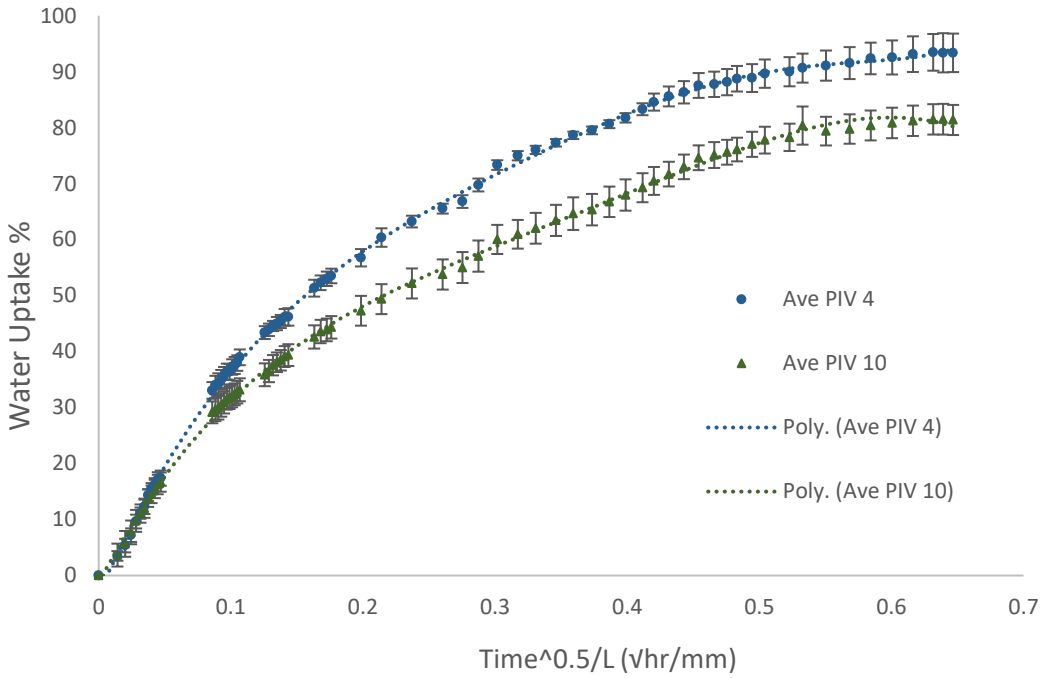

Figure 4.7: Water capillary rise of Pre-treated Impregnated Vacuumed (PIV) wood samples Impregnated in two specific times, given as a percentage of the weight of absorbed water versus square root of time on the length of samples

According to the Figure 4.7, the rate of water absorption between 0 to 0.1 (√hr/mm), for the average of PIV4 is higher than the average rate of PI10. In addition, the rate of water absorption for both PIV4 and PIV10 rose considerably between 0 and 0.2 (√hr/mm). At 0.2 (√hr/mm), the average of the water uptake for PVC4 and PIV 10 are 57.24±2.01 (wt. %) and 46.31±2.86 (wt. %), respectively. From 0.2 to 0.5 (√hr/mm), the level decreased gradually until the curves reached a steady state. Moreover, the maximum amount of weight percent in the Ave PI4 graph is 93.27±3.34 (wt. %), while the maximum value in the Ave PI10 curve is 80.56±3.29 (wt. %).

4.8 Effect of the Vacuum pressure and Number of impregnation Cycles on the Level of Water uptake of PIV4, PI4, and N Samples Measured by Tensiometer

In this experiment, the effect of number of impregnation cycles and exposure to vacuum condition on water absorption and capillary rise in the specimens is studied. To this end, the PI4, PIV4, and N samples were placed in water and the amount of water uptake was recorded

using tensiometer. The weight percentage of water uptake as a function of time is represented in Figure 4.8. According to the Figure 4.8 (a), the value of coefficient of diffusion in the PI4 and PIV4 shows dramatic decrease between 0 to 0.5 (hr), while the value for the N is almost constant.

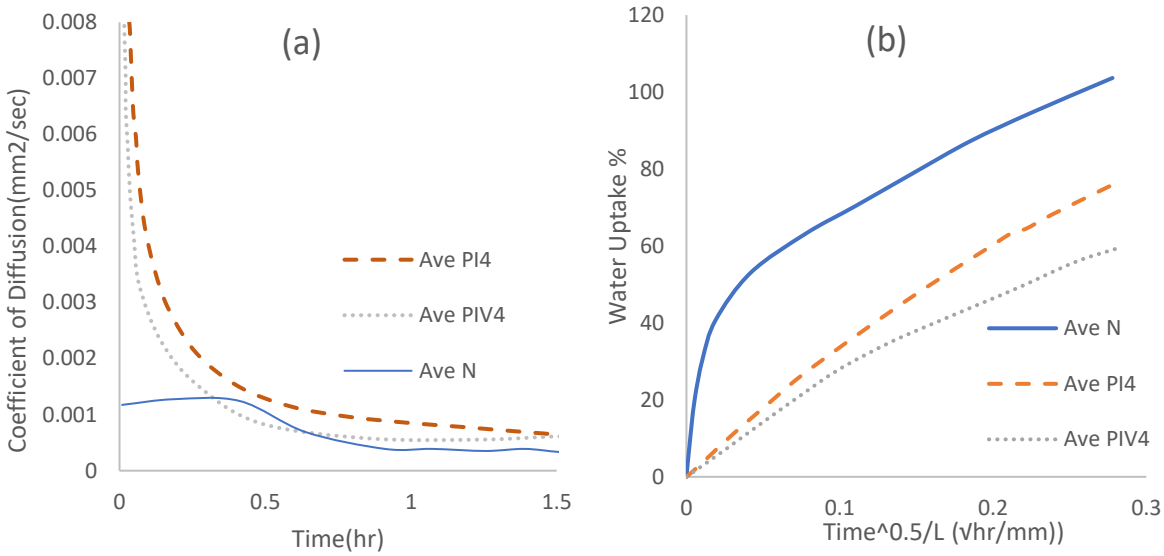

Figure 4.8: (a) Coefficient of diffusion over time for N, PI4, and PIV4, and (b) water capillary rise of N, PI4, and PIV4 given as a percentage of the weight of absorbed water vs time in (√hr/mm)

Based on Figure 4.8 (b), it can be seen that the initial rate of water absorption (slope of tangent) in AVE N is much higher compared with the AVE PIV4, and AVE PI4. Such that the rate for N, PI4, and PIV4 in the range between 0 to 0.02 (√hr/mm) are 574.21±6.05, 45.16±5.13, and 32.23±7.20 respectively. From 0.02 to 0.5 (√hr/mm), the slope of the curves gradually decreased to 76.81±4.31, 40.54±5.17, and 33.57±6.27. Moreover, the increasing rate of N, PI4, and PIV4 between 0.5 to 2.5(√hr/mm), are 23.33±3.28, 28.57±4.8, and 21.13±3.41 respectively. After about nine hours, the percentage of water uptake for N, PI4, and PIV4, were 103.65±5.64 (wt. %), 75.89±5.54 (wt. %), and 59.22±4.32 (wt. %), respectively.

4.9 Comparison Analysis Among the Experiments Results

Table 4.2 represents the amount of water uptake for the samples which have been tested by the conventional method as explained in 3.7.1. As it is shown in the table, the maximum values of the water uptake belong to the P samples in all three measured time points. However, PIV10 exhibit the least amount of water uptake.

Table 4.1: The level of Water Uptake at three specific points (wt.%)

Time (√hr/mm)	Sample	(wt. %)	S_d
0.05	Ave_Non-treated	41.29	0.99
	Ave_Pre-treated	68.55	0.89
	Ave_Non-treated Impregnated, 60 min	33.31	0.87
	Ave_Pre-treated Impregnated, 60 min	48.74	0.71
	Ave_Non-treated 10 times Impregnated, 60 min	28.86	1.12
	Ave_Pre-treated 10 times Impregnated, 60 min	19.48	1.87
	Ave_Pre-treated 10 times Impregnated, vacuumed, 60 min	17.53	1.78
0.3	Ave_Non-treated	99.74	1.61
	Ave_Pre-treated	131.89	6.87
	Ave_Non-treated Impregnated, 60 min	85.31	2.12
	Ave_Pre-treated Impregnated, 60 min	98.85	3.87
	Ave_Non-treated 10 times Impregnated, 60 min	79.74	1.52
	Ave_Pre-treated 10 times Impregnated, 60 min	73.01	6.04
	Ave_Pre-treated 10 times Impregnated, vacuumed, 60 min	60.76	2.45
0.5	Ave_Non-treated	130.61	2.43
	Ave_Pre-treated	152.24	5.23
	Ave_Non-treated Impregnated, 60 min	105.53	3.23
	Ave_Pre-treated Impregnated, 60 min	118.42	2.12
	Ave_Non-treated 10 times Impregnated, 60 min	101.74	2.02
	Ave_Pre-treated 10 times Impregnated, 60 min	89.25	2.67
	Ave_Pre-treated 10 times Impregnated, vacuumed, 60 min	77.57	3.26

The initial rate of water absorption is presented in Table 4.3. According to the table, the

maximum rate of water uptake (i.e. 1937.92 (wt. % /√hr/mm)) was observed in the pre-treated samples while the minimum was observed in sample PIV10 (i.e. 260.43 (wt. % /√hr/mm)). It can therefore be concluded that the rate of water absorption was reduced after impregnation in the vacuum condition.

Table 4.2: The initial rate of water uptake of the samples at 0.01 (√hr/mm)

Sample	Rate of water uptake (Graphing Slope(wt%)/(√hr/mm))
Ave_Non-treated	1433.83±19.21
Ave_Pre-treated	1937.91±13.81
Ave_Non-treated Impregnated, 60 min	1056.60±17.02
Ave_Pre-treated Impregnated, 60 min	1569.54±17.65
Ave_Non-treated 10 times Impregnated, 60 min	760.52±10.25
Ave_Pre-treated 10 times Impregnated, 60 min	282.64±4.32
Ave_Pre-treated 10 times Impregnated, vacuumed, 60 min	260.43±4.41

Comparing the rate of water uptake for the vacuum-impregnated and non-vacuum-impregnated samples showed that the vacuum procedure was effective in the impregnation of the samples with nanoparticles. According to Figure 4.9, the amount of weight gain before and after coating in the PIV10 samples was 96%±3.28(wt.%) and in the PIV4 samples was 66%±1.87(wt.%). The level of water uptake (wt. %) for PI10 and PI4 was 66.76±1.54 (wt. %) and 42.23±2.82 (wt. %), respectively. This suggests that more nanoparticles are absorbed by PIV10 and PIV4 samples in comparison with the PI10 and PI4 samples. The higher amounts of absorbed nanoparticles eventually reduced their water absorption capacity. In addition, the dimensional change was evaluated before and after coating process for the PIV10. According to Figure 4.10, the amount of volume gain before and after coating in the PIV10 samples was 381.01±14.47 mm^3 and 477.50±7.96 mm^3, which is due to the formation of the nanoparticle layer on the surface of the samples after the impregnation process.

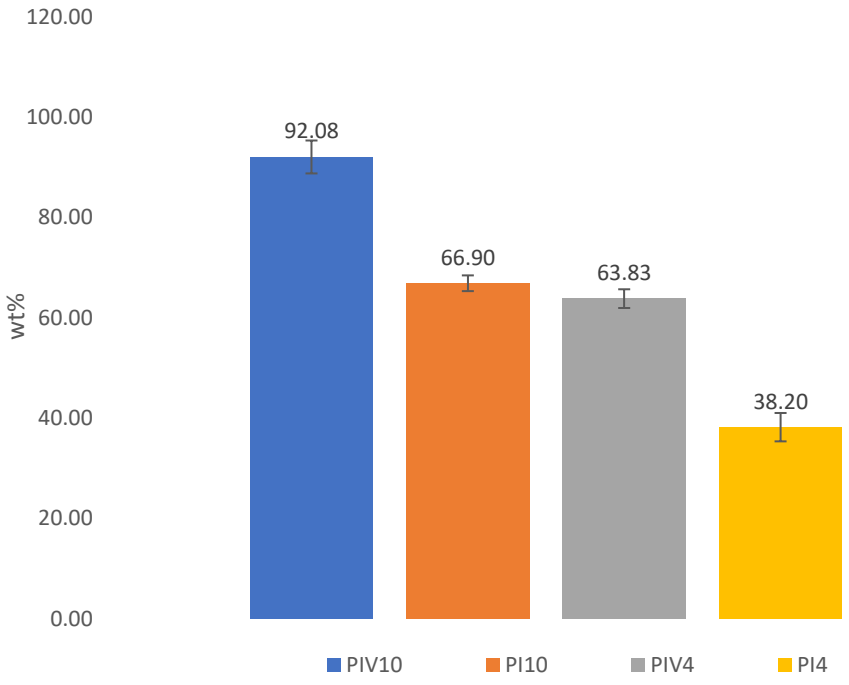

Figure 4.9: Compression of weight gain before and after the impregnation process

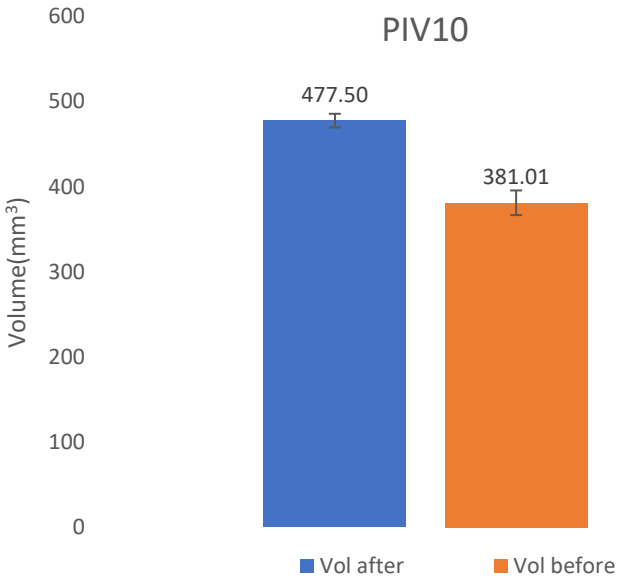

Figure 4.10: Compression of volume gain before and after the impregnation process for PIV10

4.10 The Diffusion Coefficient of N, P, PI10, and PIV10

As presented in Figure 4.11(a), the P sorption curve increases abruptly at the beginning and then decreased gradually to reach a steady state at saturation. This trend is similar to the Fickian sorption progress such that the diffusion can completely control the mass transport (Wong and Broutman 1985). In this model, the P and N samples undergo very minor changes due to the effortless transmission of water molecules through them. Therefore, the coefficient of diffusion would be constant. According to Figure 4.11 (b), the D_value for the P and N is almost constant. The D-value is correlated with the ease of permeability into sample tissues, such that as the D-value increase, the water can pass easily through the samples. On the other hand, for the PI10 and PIV10 the coefficient is dramatically decreased, which means the specimens are disrupted by the water molecules since the voids and vascular systems are blocked by the silica nanoparticles.

The cavities in PIV10 and PI10 are smaller than the reference sample, and the trapped air bubbles inside the small cavities can prevent the water from flowing freely through. As it shows in Figure 4.11(a), the level of water uptake at saturation for the N and P is higher than the one for PI10 and PIV10, which means that the PI10 and PIV10 have less capacity for water due to the lower amount of porosity. The process of water uptake stops when the specimens reach equilibrium in water content, but the maximum of water uptake is more significant than the D_value, since the required time for degradation to occur will increase with increasing the necessary time to reach full saturation. Apart from that, the potential of freezing damage (i.e., internal destruction due to expansion caused by increased volume of the frozen water) will be declined by minimizing the amount of absorbed water in the samples.

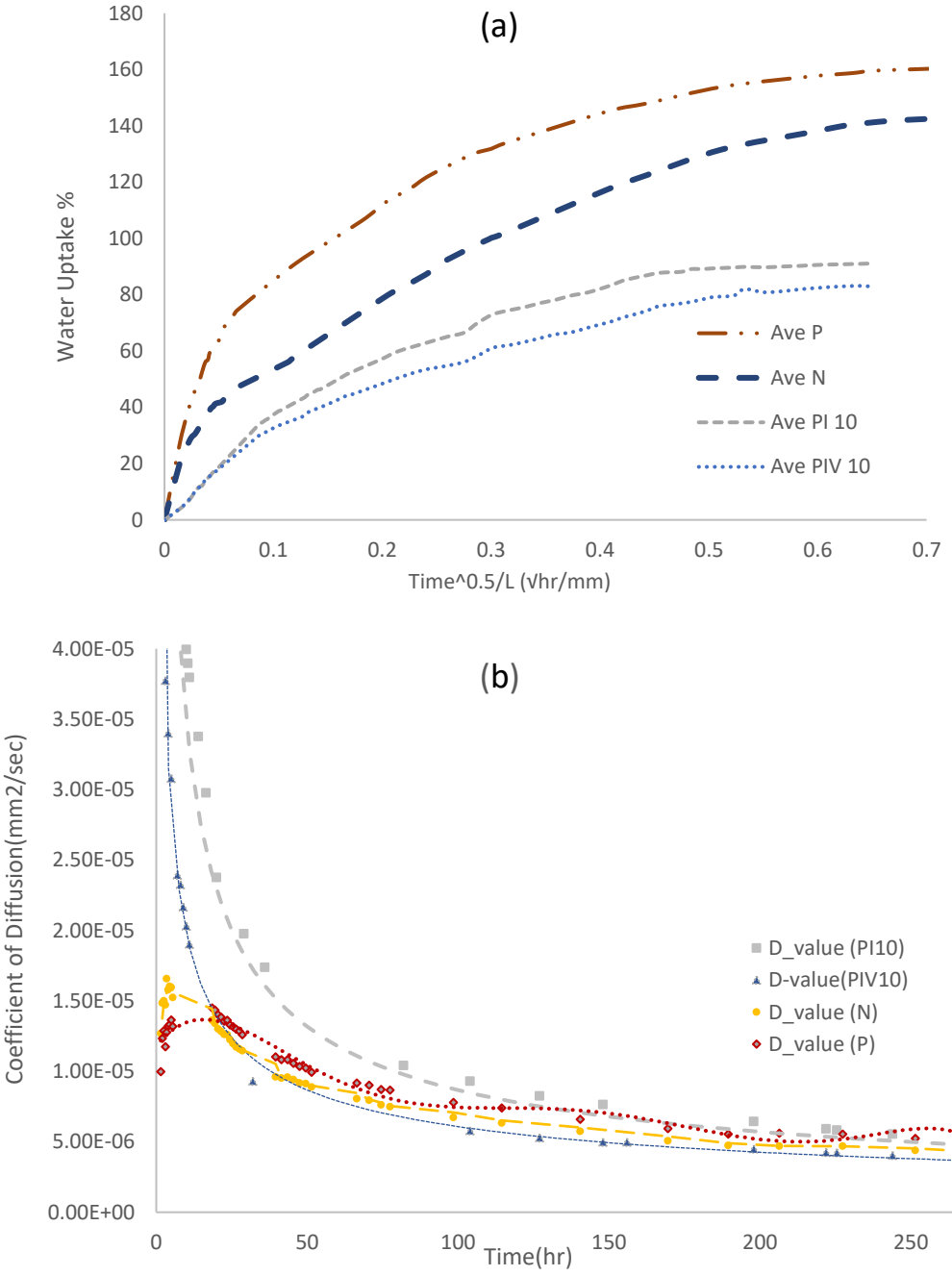

Figure 4.11: (a) the level of water uptake as a function of time and (b) coefficient of diffusion over time for P,N, PI10, and PIV10

4.11 Statistical Analyses

According to the statistical analyses (t_test), the reported changes in water absorption are statistically significant. Table 5.1 summarizes the data from statistical analyses.

Table 4.3: The amount of Zscore at saturation, due to the statistical analysis

Sample	n_i	n_j	A_i	A_j	σ_i	σ_j	Z_{score}	P-value
P-N	5	5	161.16	144.02	6.46	7.46	3.89	<<0.05
P-N4	5	5	161.16	124.21	6.46	2.74	11.78	<<0.05
P-N10	5	5	161.16	112.52	6.46	6.24	12.11	<<0.05
P-PI4	5	5	161.16	100.23	6.46	4.96	16.73	<<0.05
P-PIV4	5	5	161.16	90.23	6.46	6.68	17.07	<<0.05
P-PI10	5	5	161.16	90.13	6.46	2.90	22.43	<<0.05
P-PIV10	5	5	161.16	80.13	6.46	6.58	19.65	<<0.05
N-N4	5	5	144.02	124.21	7.46	2.74	5.57	<<0.05
N-N10	5	5	144.02	112.52	7.46	6.24	7.24	<<0.05
N-PI4	5	5	144.02	100.23	7.46	4.96	10.93	<<0.05
N-PIV4	5	5	144.02	90.23	7.46	6.68	12.01	<<0.05
N-PI10	5	5	144.02	90.13	7.46	2.90	15.05	<<0.05
N-PIV10	5	5	144.02	80.13	7.46	6.58	14.36	<<0.05
N4-N10	5	5	124.21	112.52	2.74	6.24	3.83	<<0.05
N4-PI4	5	5	124.21	100.23	2.74	4.96	9.46	<<0.05
N4-PIV4	5	5	124.21	90.23	2.74	6.68	10.52	<<0.05
N4-PI10	5	5	124.21	90.13	2.74	2.90	19.09	<<0.05
N4-PIV10	5	5	124.21	80.13	2.74	6.58	13.83	<<0.05
N10-PI4	5	5	112.52	100.23	6.24	4.96	3.45	<<0.05
N10-PIV4	5	5	112.52	90.23	6.24	6.68	5.45	<<0.05
N10-PI10	5	5	112.52	90.13	6.24	2.90	7.28	<<0.05
N10-PIV10	5	5	112.52	80.13	6.24	6.58	7.99	<<0.05
PI4-PIV4	5	5	100.23	90.23	4.96	4.96	3.19	<<0.05
PI4-PI10	5	5	100.23	90.13	4.96	6.68	2.71	<<0.05
PI4-PIV10	5	5	100.23	80.13	4.96	2.90	7.82	<<0.05
PIV4-PI10	5	5	90.23	90.13	6.68	2.90	0.03	0.49
PIV4-PIV10	5	5	90.23	80.13	6.68	6.58	2.41	0.01

5 Discussion

5.1 General

In this chapter, the water uptake capacity of spruce wood before and after the pre-treatment and impregnation with silica nanoparticles was investigated. Moreover, the effect of impregnation parameters such as the time of submersion, the number of impregnations, and the effect of vacuum on the impregnation process were studied in detail. By repeating the impregnation process on the wood sample, a dense film of silica nanoparticles deposits on the surface of the wood, filling the voids and cracks that may exist on its surface (Figure 5.1).

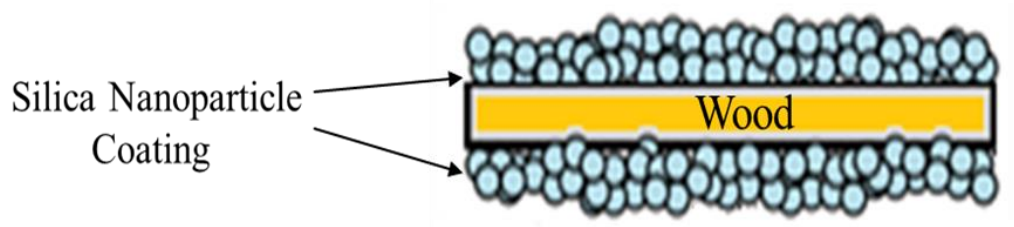

Figure 5.1: Schematic of the thin layer of silica nanoparticles deposited on the wood surface

The process of impregnation of wood samples with silica nanoparticles using colloidal solution leads to the filling of pores and cavities within the wood and may thus result in the obstruction of the Lumina, as well as voids (Figure 5.2).

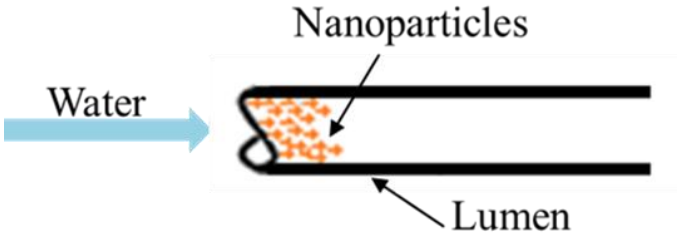

Figure 5.2: Schematic of the impregnation of nanoparticles inside the lumen

5.2 SEM and EDX Analyses

SEM micrographs of the extracted powder from the colloidal solution were provided to identify the morphology of the agglomerated particles (Figure 5.3 a). In addition, the chemical composition of the powder sample was determined using EDX micro-analysis. According to Figure 5.3 (b), the presence of silicon and oxygen, which are the main elements of the silica nanoparticles, were observed in the white powder. It should be noted that a colloidal solution (here is colloidal silica nanoparticles solution) is stable as long as the solid phase can stay in sufficient amount of the liquid phase. Any aggregation or sedimentation hinders stability. Increasing the temperature makes the liquid phase to evaporate. The evaporation of liquid phase will increase the concentration of solid phase (i.e. nanoparticles). When the concentration of nanoparticles in the colloidal solution exceeds a threshold, the nanoparticles are close enough to each other to form hydrogen bonds and nanoparticles start to agglomerate and form silicon-based particles. This can be attributed to the presence of amorphous particles of SiO2 in colloidal silica. Thus, the described process enables silicone-based particles formation. The carbon peak in the graph is related to the carbon tapes which were applied to mount the powder on the stub.

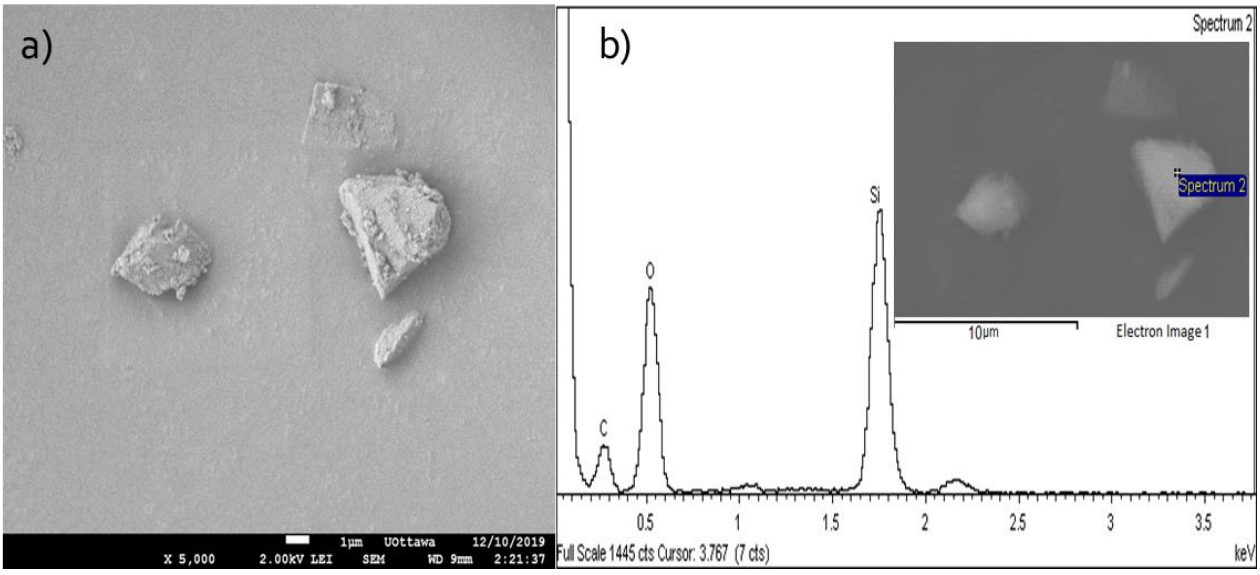

Figure 5.3: SEM micrograph (a) and EDX micro-analysis (b) of the white powder

5.3 XRD Diffractogram of White Powder Obtained from the Colloidal Solution

In order to identify the physical structure of the agglomerated particles, XRD analysis was carried out on the white powder extracted from the colloidal solution. According to Ferreira et al. (2015), the peak for biogenic silica micro-particles is located approximately at 2θ = 22.5° on the XRD diffractogram (Figure 5.4 a). The authors asserted that the peak is indicative of an amorphous characteristic of the sample which belongs to the pure biogenic SiO_2 obtained from rice husk and in accordance with the reported JCPDS[1] data. The XRD pattern of the powder extracted from the colloidal solution is presented in Figure 5.4 b, revealing a shoulder at 2θ = 21.7°, which can be attributed to amorphous SiO_2 (i.e. provided similar value of 2θ in both graphs). In addition, the crystalline materials possess long range order while amorphous materials do not. Therefore, the diffraction from amorphous materials do not show sharp Bragg peaks. It can therefore be concluded that the agglomerate from the colloidal solution is made of amorphous SiO_2.

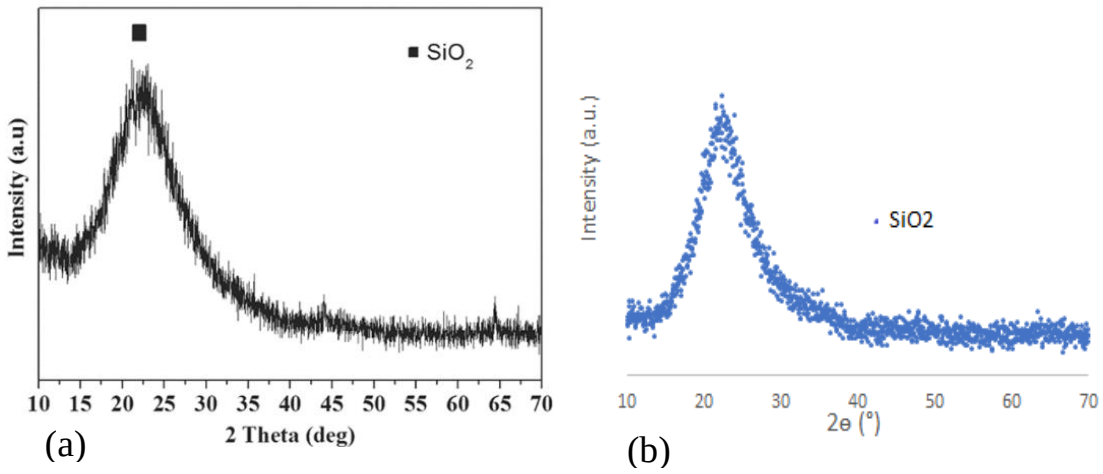

Figure 5.4: XRD obtained for (a) biogenic SiO_2 from rice husk (Ferreira et al. 2015) and (b) White powder obtained from colloidal solution.

[1] Joint Committee on Powder Diffraction Standards

5.4 Surface Characterization of the Samples

The samples in Group P (i. e., Pre-treated samples) were exposed to the pre-treatment process, including washing with the distilled water and submersion in an alkaline solution, as explained in detail in chapter 3. Following the pre-treatment process, the samples were dried in an oven at 80℃ for 5 hours. The surface hydrophilicity of the dried samples was investigated by Water Contact Angle test (WCA) (Figure. 5.5).

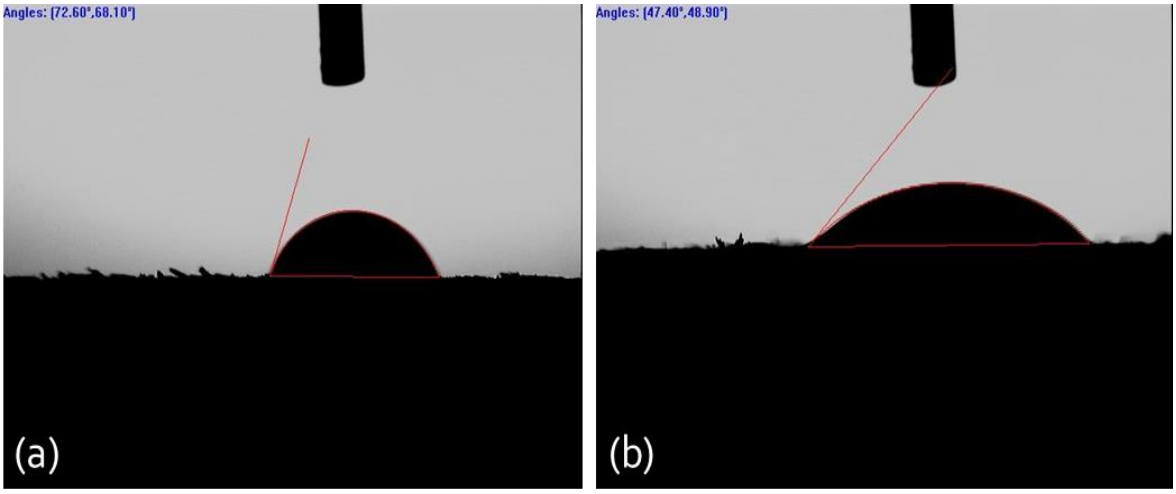

Figure 5.5: WCA value for (a) N 72.6° (i.e., Non-treated), (b) Pre-treated 48.9°

The average WCA for pre-treated and N (i. e., Non-treated) samples, based on 5 measurements at 22 ℃, were 47.8°±6.2° and 71.9°±5.4°, respectively. The angles were obtained using sessile drop method. In this method, a drop of liquid (water) is placed on the solid surface (wood). The system consists of three phases and three interfaces. The phases include solid (i.e. wood), liquid (i.e. water), and surrounding atmosphere (i.e. gas), and the interfaces include liquid-vapour (drop-atmosphere), solid-liquid (solid material-drop) and solid-vapour (solid material-atmosphere). Wettability (i. e.,

the ability of liquid to make the solid's surface wet) of the water depends on the surface energy[1] of the given interfaces (Figure 5.6) (Kwok et al. 2000; Schuster et al. 2015)..

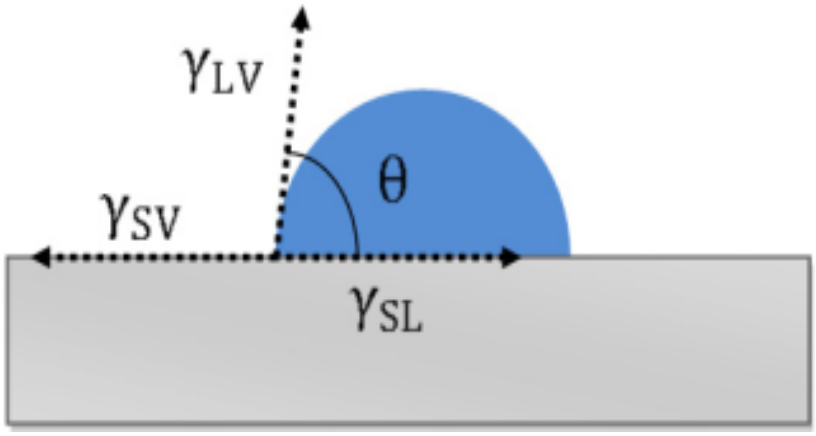

Figure 5.6: schematic of water contact angle on a solid surface (Schuster et al, 2015)

The contact angle (CA) can be obtained by Young's equation:

$$\cos\theta = \frac{\gamma^{SV} - \gamma^{SL}}{\gamma^{LV}} \quad (5\text{-}1)$$

Where γ^{LV},γ^{SV} and γ^{SL} are the liquid-vapour, solid-vapour, and solid-liquid surface tension, respectively.

The surfaces with a low CA (i.e., below 90°) are called hydrophilic but if the measured CA is above 90°, the term hydrophobic is used (Siddiqui et al. 2018). Thus, both N samples and P samples are hydrophilic, but based on Figure (5.5), the pretreated samples were more hydrophilic than the untreated ones. This is because the pre-treatment process has chemical and physical effects on the samples. The chemical treatment, including the alkaline treatment of cellulose (i.e., mercerization) using

[1] The required energy per unit area to make a new surface at the interface of liquid-vapour or solid-vapour (Vitos et al. 1998).

caustic soda, can remove hemicelluloses and lignin that both are soluble in alkali (i.e., insoluble in water) and they are hydrolyzed more easily than cellulose by both dilute acid and alkali. Therefore, the alkaline treatment could provide an outer surface area of cellulose-rich substrates, by removing hydrophobic non-structural components such as lignin (Oka et al. 2013; Jayamani et al. 2015).

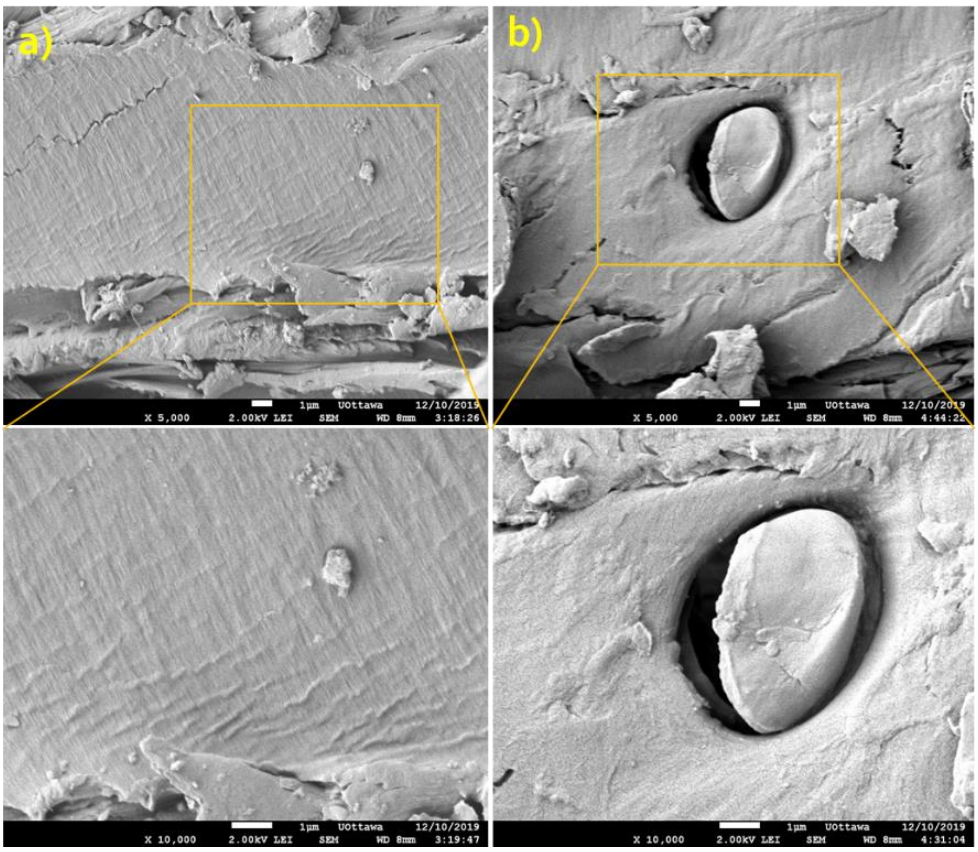

Figure 5.7: Scanning Electron Microscope (SEM) micrograph view from the external surface of (a) Pre-treated sample (b) Non-treated sample in the scale of 1µm

Comparison between crystalline index of P and N samples, which are 77.67 and 72.51 respectively, implies the progressive removal of the non-crystalline components from the samples. According to the Figure 5.7, the protrusion of the cellulose microfibrils is partially detectable in the pre-treated sample, which can be attributed to the removal of lignin during the alkaline process. According to Foruzanmehr et al. (2017), the

cellulose microfibrils can raise the potential of bonding on the samples' surface, , due to the presence of active hydroxide groups on their surfaces. This can lead to reduction in the γ^{SL}, while the γ^{SV} remains constant. Therefore, based on the Young's equation (Eq. 5.1), the WCA is decreased after the alkaline treatment, and accordingly pre-treated samples are more hydrophilic than the non-treated ones.

Similarly, PI10 and PIV10 had CA values of 27.6°±7.1°and 9.9°±4.3°, respectively. According to section 5.3, there is a direct relation between hydrophilicity and surface energy, where impregnation with the silica colloidal solution can increase the hydrophilicity of the specimens at the vicinity of the silica due to their hydrophilic characteristic (Jesionowski et al. 2002). Thus, the silica layer on the surface of the sample can reduce γ^{SL} thereby leading to a lesser contact angle for the PI10 in comparison with N sample (Figure 5.8).

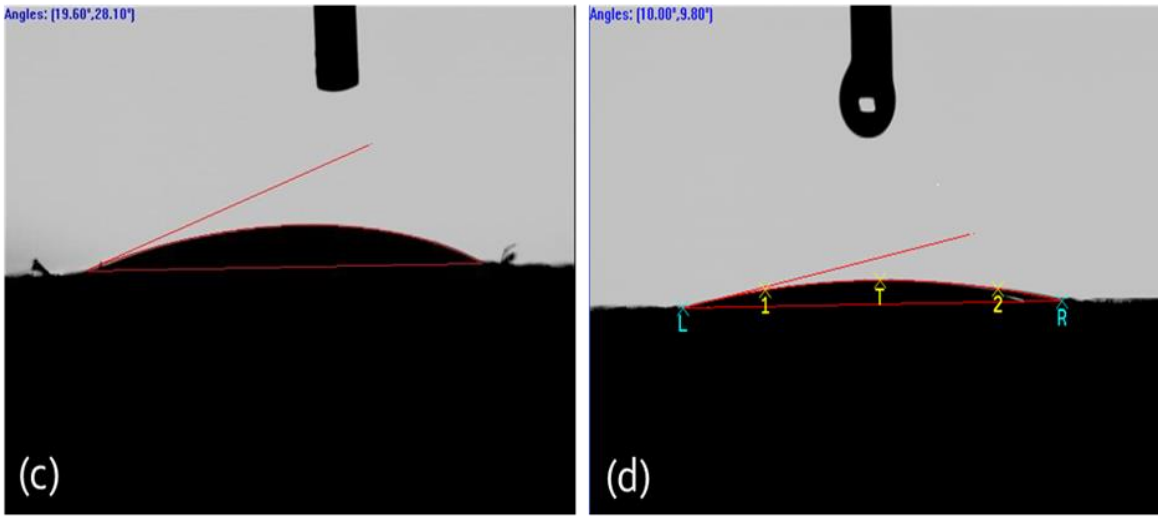

Figure 5.8: WCA value for (c) Pre-treated Impregnated ten times 28.1°, and (d) Pre-treated Impregnated Vacuumed ten times 10°.0

According to Figure 5.8, the lowest CA can be observed in PIV10, which may be attributed to the higher degree of surface roughness created during the vacuum process.

The solvent evaporates under vacuum condition much faster than normal condition, resulting in the formation of a greater number of large agglomerates in the PIV10 than PI10 (Figure 5.9).

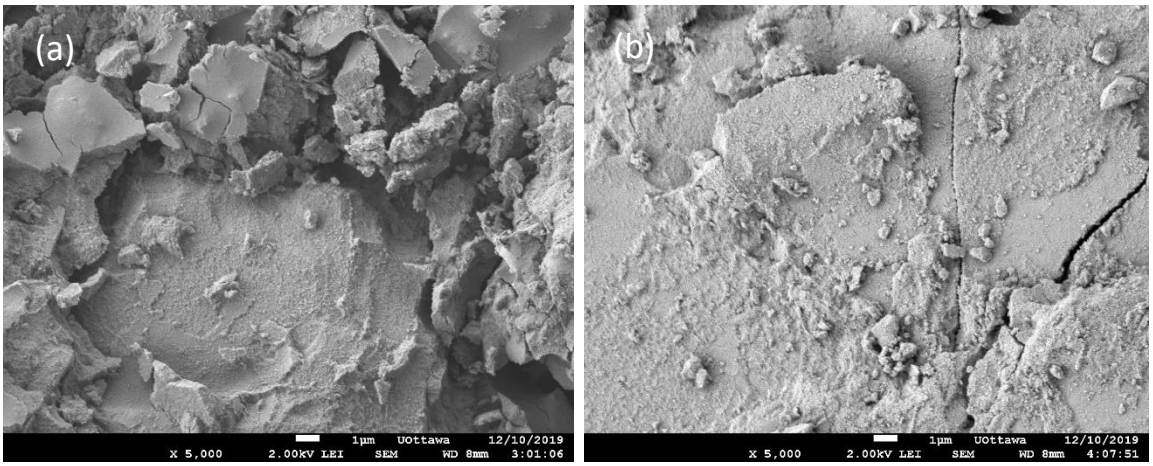

Figure 5.9: Scanning Electron Microscope (SEM) micrograph view from the external surface of (a) PIV10 (b) PI10 in the scale of 1µm

The degree of roughness on the hydrophilic materials can be computed based on equation (5-2) (Alghunaim et al. 2016).

$$\cos\theta_{app} = r_a \cos\theta_{act} \tag{5-2}$$

Where θ_{app} is the apparent contact angle on the rough surface, θ_{act} is the actual contact angle, and r_a is the roughness ratio (i. e., actual area over the apparent area, and should be greater than one). As such, the degree of roughness can decrease the CA.

5.5 The Effect of Alkaline Treatment on Water Uptake Property of Pre-treated and Non-treated Samples

The pre-treated samples and the non-treated samples were immersed in distilled water and the weight was recorded periodically until it remained almost constant. As presented in Chapter 4, the rate of primary water uptake at 0.02(√hr/mm), and the

amount of water uptake at saturation for the P samples are 1844.32±2.13 (wt. % /√hr/mm), and 160.29±3.23 (wt. %), respectively. However, the corresponding recorded values for the N samples were 1311.91±15.32 (wt. % /√hr/mm), and 142.51±3.73 (wt. %). Both graphs reached a plateau after about 51 days (Figure 5.10).

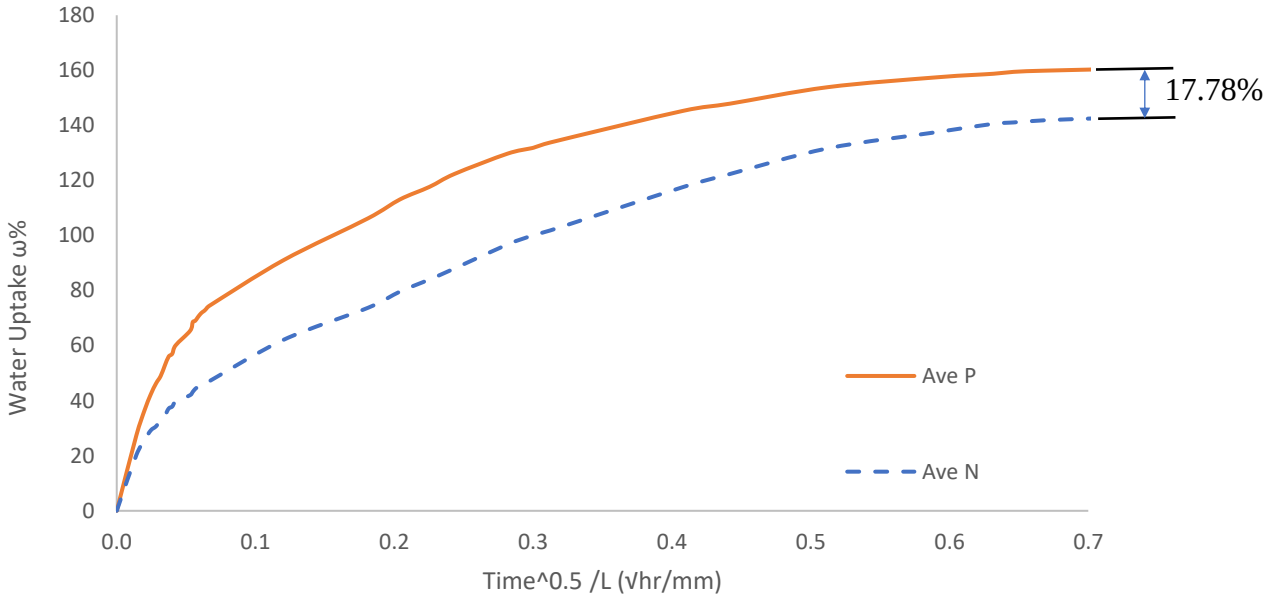

Figure 5.10: Average water capillary rise of pre-treated wood samples vs non-treated wood samples given as a percentage of the weight of absorbed water vs square root of time on the length of samples

As seen in Figure 5.10, the amount of water uptake at saturation in the P samples is higher than N ones, which can be attributed to the higher degree of porosity in the pre-treated samples. As highlighted in section 5.3, the components which have a negative effect on the hydrophilicity of wood (e.g., lignin and wax) are removed by alkali solution. Besides, based on section 2.2.1.3, the amount of lignin in softwood varies between 25-35%. Thus, losing a fraction of such material in the samples could lead to a high degree of porosity.

In addition, as shown in section 5.4, cellulose has a high tendency to absorb water due to the presence of hydroxyl groups in its molecule. Thus, there is more opportunity for water to penetrate into the samples, which could explain why the average amount of

water uptake in pre-treated samples is higher than that in the non-treated ones. Moreover, the alkaline treatment can generate some sodium ions (Na+), which have large diameter, and thus appropriate to widen the smallest pores in network planes of cellulose that may cause a swelling reaction (Figure 5.11).

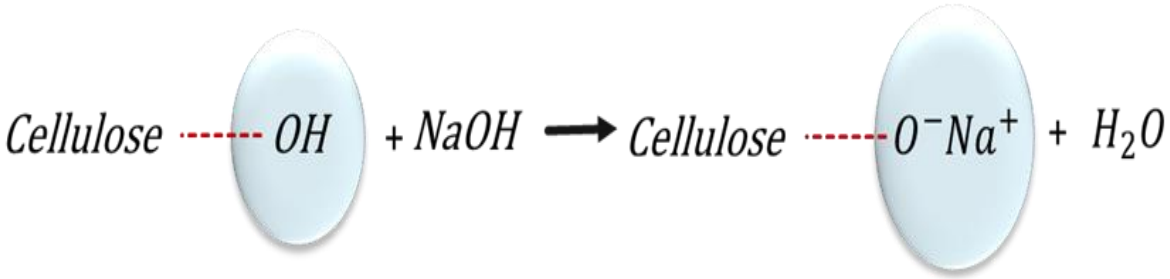

Figure 5.11: Schematic of alkaline treatment

There is a higher rate of water uptake in the pre-treated samples in comparison with the non-treated ones. This can be due to the high amount of capillary pressure inside the vascular system of the P samples. According to Sreekala et al. (2003), the water uptake rate (i.e., the slope of the water uptake graph) is the function ofthe capillary pressure. The capillarity pressure is obtainable by the Laplace equation (5.3).

$$Pc=\frac{2\gamma \cos\theta}{R} \qquad (5.3)$$

Where Pc is the capillary pressure, γ is the liquid surface tension, θ the contact angle between the liquid and inside the wall of the vascular system in wood, and R is the capillary radius.

According to the physical and chemical effect of alkaline treatment which was explained in section (5.3), and the parameters of Laplace equation, the magnitude of θ was less in the P samples in comparison with the N samples due to more hydrophilicity of the P samples, which lead to a higher capillary pressure and water uptake rate at the

beginning of the experiments. However, after a period of time, the rate is decreased owing to the reduced capillary pressure, when it reaches equilibrium inside the Lumina.

5.6 The Effect of submersion Time on the Water Uptake Property of PI and NI Samples

As presented in Section 4.4, the submersion time has a strong effect on the level of water uptake. The samples that were impregnated in the silica nanoparticle colloidal solution for a longer time (e. g., 60 min) showed lower amount of water uptake at saturation in comparison with the samples that were impregnated for a shorter time (e. g., 20 min). This difference in water uptake is due to the different amounts of nanoparticles deposited inside the samples (Figure 4.4). According to Figure 5.12, there are several hydroxyl groups around the colloidal particles, which enable them to bind to the wood samples via binding with OH groups of the cellulose, which this was also found by Azamian-Jazi et al. (2020). Therefore, the degree of porosity decreases for longer submersion time due to creation of more agglomerated particles inside the samples.

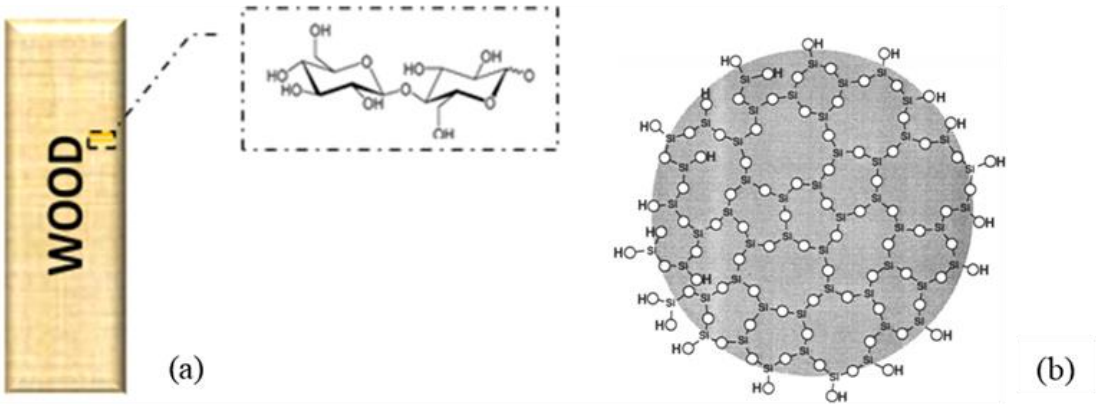

Figure 5.12: Schematic representation in two dimensions of (a) cellulose compound of wood samples, and (b) a dehydrated but fully hydroxylated colloidal silica particle (Bergna 2005)

Based on the results obtained in Chapter 4, the rate of primary water uptake at 0.02(√hr/mm), for the PI and NI samples, were 1362.95±5.13 (wt. % /√hr/mm) and 1125.34±4.45 (wt. % /√hr/mm), respectively. Thus, the primary rates for PI and NI samples are less than those measured for the P and N samples. This can be attributed to the deposited nanoparticles on the impregnated samples (Figure 5.13).

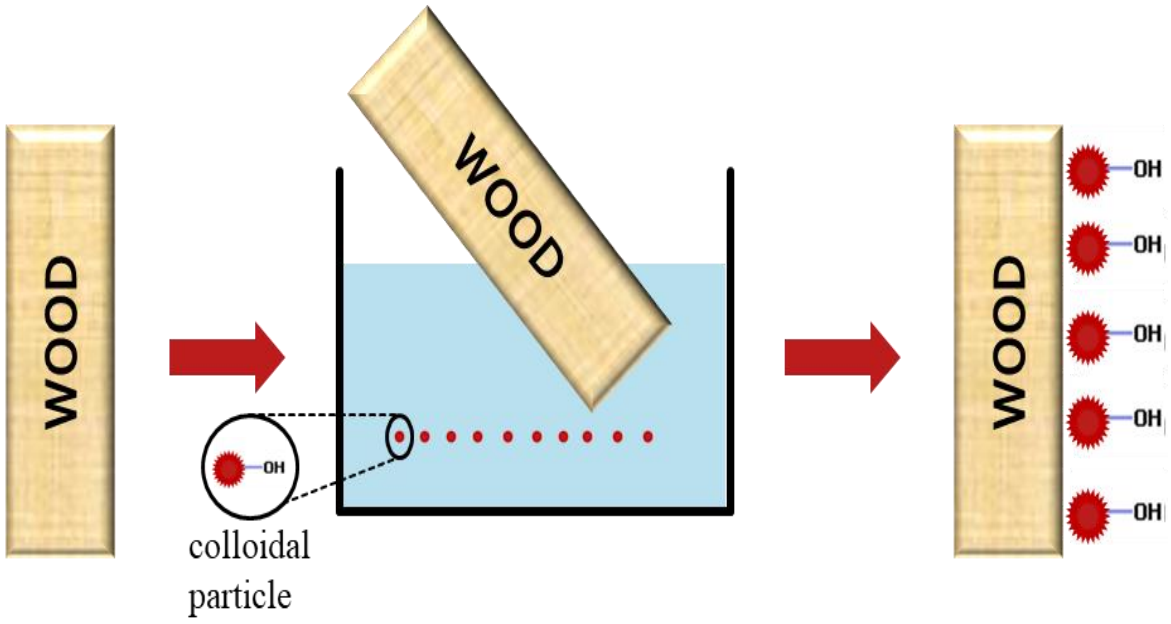

Figure 5.13: Schematic illustration of the formation of nanoparticle compound on the wood surface based on silica colloidal nanoparticle solution

According to Khazaei (2008), the presence of trapped air bubble can prevent water from flowing freely inside small cavities. Therefore, during the impregnation process, the nanoparticles that deposited on the surface can reduce the openings size of the holes and Lumina. The trapped air bubble in these smaller cavities and Lumina can restrict the ability of water to penetrate, and eventually the rate of water uptake is reduced.

In addition, the level of water uptake at saturation for the PI and NI samples were 123.71 ±5.23 (wt. %) and 106.87±4.54 (w t. %), respectively, which means that the PI

samples were still more hydrophilic than the NI samples (Figure 5.14). This can be attributed to the similar degree of porosity in both groups, and indicates that one-time impregnation for 60 minutes cannot provide sufficient condition for penetration of particles into the vascular system to completely obstruct them (i.e., only partial obstruction occurs). Therefore, impregnating the samples once did not have a strong effect on the degree of porosity as well as the capillary pressure of the samples.

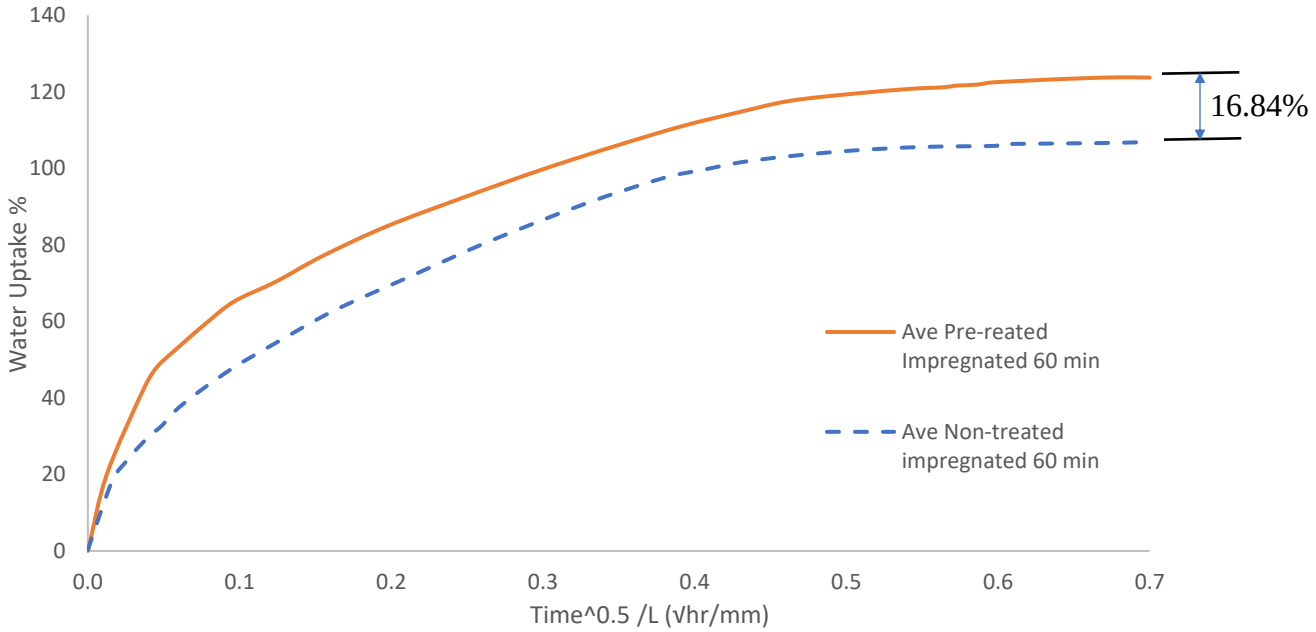

Figure 5.14: Average water capillary rise of the pre-treated wood samples and non-treated wood samples

5.7 The Effect of Vacuum and the number of impregnations on the Water Uptake capacity of NI, PI and PIV

According to Sections 4.7.1 to 4.7.3, the water uptake capacity of the samples was reduced by repeating the impregnation cycles. The PI samples experienced lower water uptake than the NI samples, because they were homogenously coated with the silica nanoparticles after the pre-treatment process owing to the cellulose-rich wood surface. Therefore, as stated by Sheykhnazari et al. (2016), pre-treatment can increase the uptake of colloidal solution forming more hydrogen bonds between cellulose and the hydroxyl groups of the colloidal silicon dioxide. The amount of active hydroxyl groups

in the PI samples were more than that in the NI ones. The cellulosic hydroxyl groups were condensed with the hydroxyl groups on the silica nanoparticles during the impregnation process. (Figure 5.15). In addition, the silica nanoparticles can agglomerate easily due to the high surface energy.

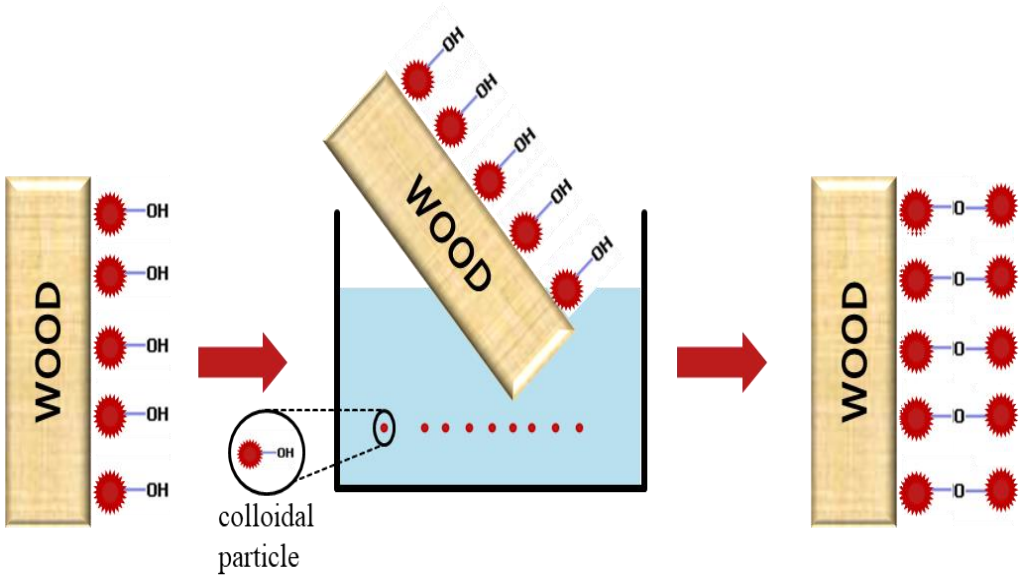

Figure 5.15: Schematic illustration of the formation of nanoparticle compound on the pre-treated covered wood surface based on silica nanoparticle colloidal solution.

Furthermore, performing the experiments in vacuum condition was effective in removing the trapped air bubbles inside the samples, due to the negative pressure that led to more uptake of colloidal solution, containing silica nanoparticles inside the voids and vascular system of wood (Siau 2012). In addition, according to Götze et al. (2008), employing the vacuum-pressure system helps in deeper penetration of the silica nanoparticles into the Lumina, obstruction of the vascular system in the samples, and ultimately decreases their degree of porosity.

5.8 Comparison of the Water Uptake Capacity of the Experiments

As shown in Figure 5.16 and Section 4.11, the lowest level of water uptake at saturation corresponds to PIV 10. In these samples the impregnation in vacuum condition

followed by dehydration process was repeated 10 times. Thus, the process created a thicker layer of particles on the surface and higher amount of agglomerated particles inside the samples. Therefore, the level of water uptake at saturation of PIV10 is almost 42% less than the N samples, while the value for the PIV4 is almost 34% less than the N. The small difference between the PIV10 and PIV4, indicates that after four times impregnation under the vacuum- pressure condition, the degree of porosity does not undergo significant change. Hence, it seems that the repetition of the process more than four times does not have a significant effect on reducing the water uptake capacity of the samples based on the statistical analysis (table 4.3).

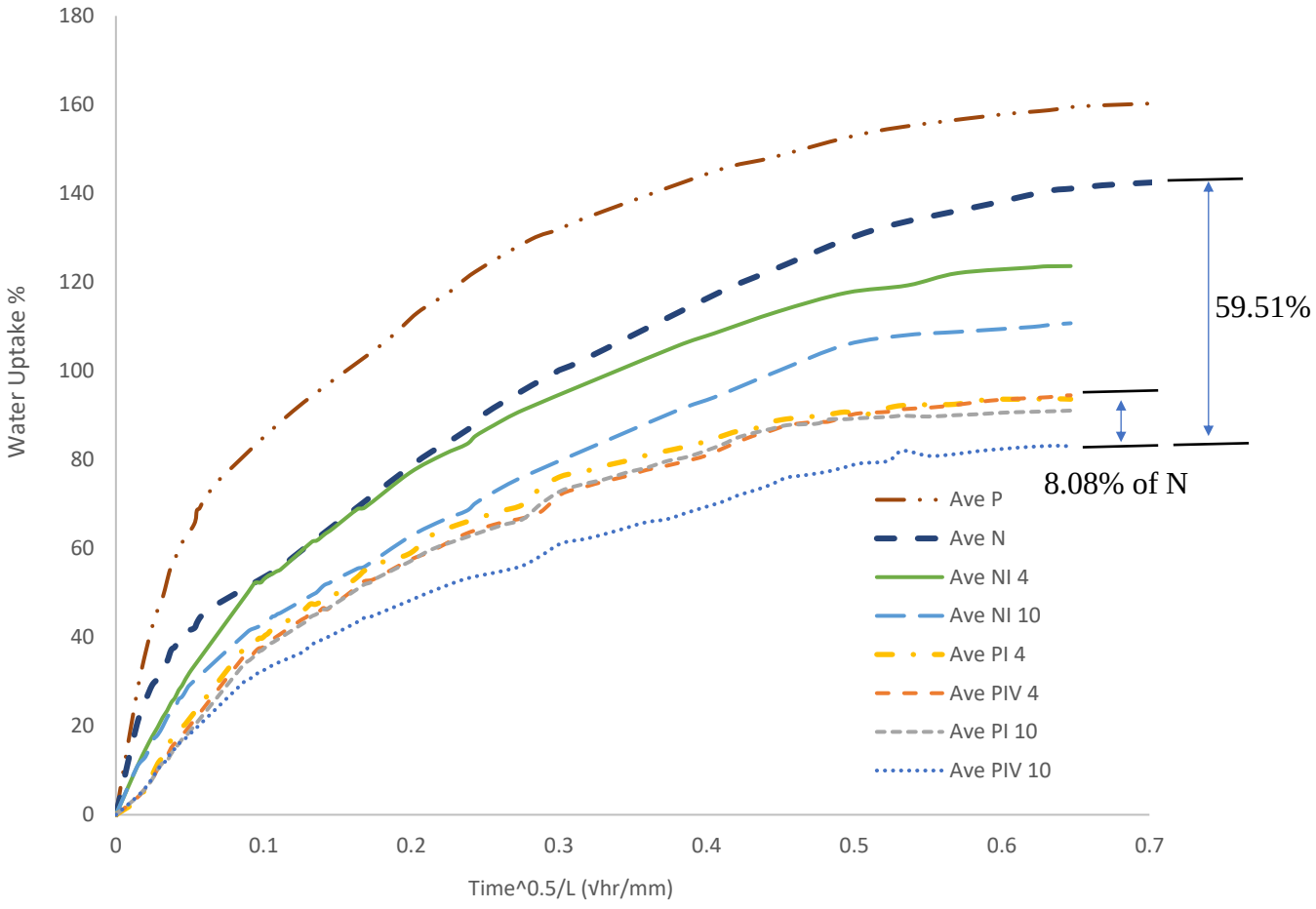

Figure 5.16: Water capillary rise of multi-impregnated PI, NI, PIV and P, N samples given as a percentage of water uptake as a function of time

5.9 Effect of the Vacuum and Number of Impregnation Cycles on the Level of Water uptake for PIV4, PI4, and N Samples Measured by Tensiometer

In order to verify the results obtained from conventional experiments, the mentioned effective parameters have been examined based on the obtained data from Washburn Measurements on the N, PI4, and PIV4 samples.

According to Figure 4.8 (a), for the N samples, the coefficient of diffusion (i.e. D-value) is practically constant due to the minor change inside the samples as the water passes through them. On the other hand, the D-value for samples PI4 and PIV4 is decreased dramatically with respect to time, which could be attributed to the mobility of nanoparticles inside the samples obstructing the pores and vascular system to prevent the water from passing effortlessly through them.

Moreover, higher value of water uptake was observed in the N samples, which can be attributed to the higher degree of porosity and capillary effect of vascular system that are blocked by the nanoparticles in the PI4 and PIV4. In addition, the initial slope of PIV4 and PI4 is approximately the same, and much less than the N samples, which could, again, be due to the smaller void and the obstructed vascular system inside the specimens.

5.10 SEM Micrograph of the Surface of the Wood Samples

In order to study the morphological modification of the sample's surface before and after the impregnating process, SEM at 10 kV was employed. In this section, the sample with the lowest amount of water uptake (PIV4) and the N sample, according to Figure 5.16, were compared in two magnifications using the SEM technique. As shown in Figure 5.17, agglomerated particles were observed on the outer surface of the PIV4 sample, while such particles were not observed on the N sample. This confirms that the presence of particles on the PIV4 samples is due to the impregnation process.

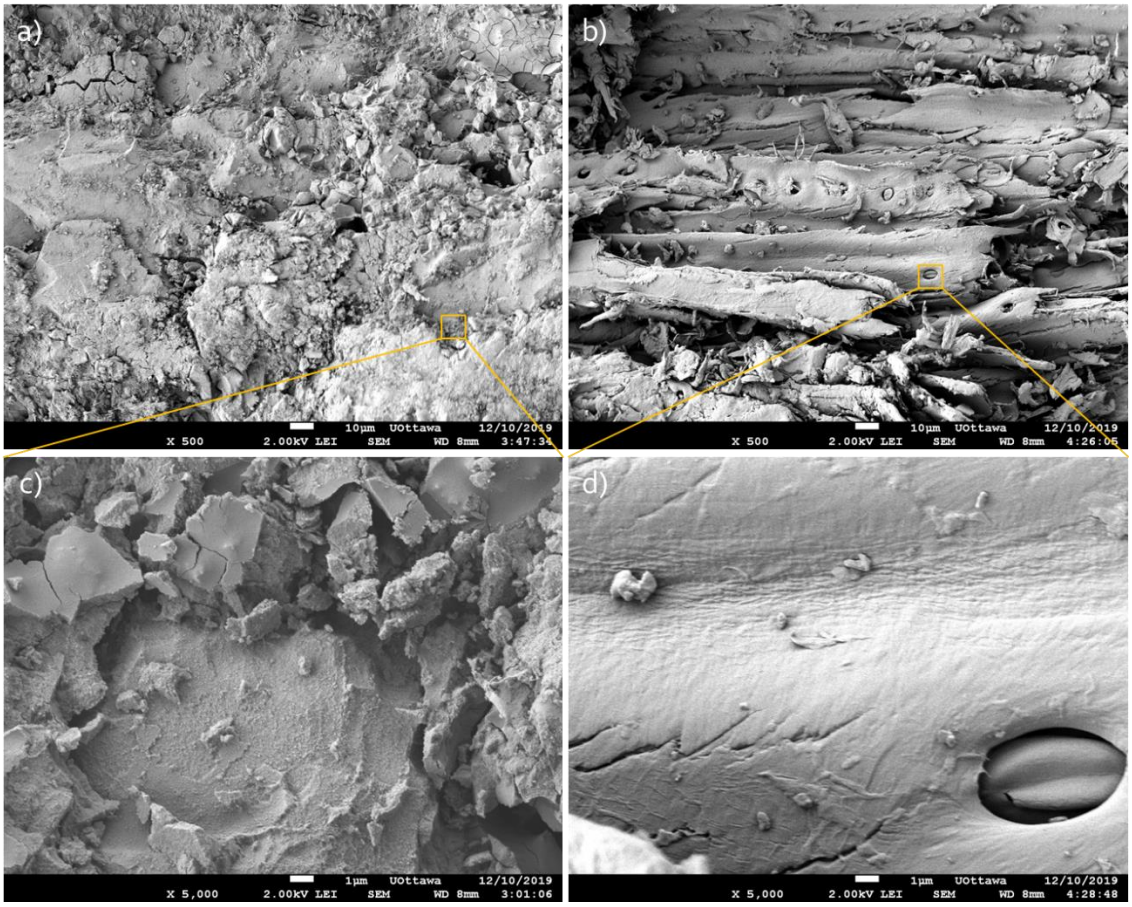

Figure 5.17: Scanning Electron Microscope (SEM) micrograph of outer surface view (a) wood surface treated with SiO_2 colloidal solution and (b) non-treated wood in the scale of 10µm. The high-magnification images of the surface of (c) The pre-treated impregnated vacuumed samples and (d) the N in the scale of 1µm.

5.11 EDX Micro-Analysis Obtained from the Outer surface of PIV4 Sample

The SEM micrograph of wood samples before and after impregnation with silica nanoparticles is shown in Figure 5.17. The chemical composition of the impregnated and the N samples were characterized by EDX micro-analysis (Figure 5.18). The signal produced from the conductive layer on the surface of the sample, with the larger peak related to gold (i.e., as the conductive layer of metal on the specimen to prevent charging), being eliminated. According to the Figure 5.18 (a), silicon and oxygen, which are the main elements of the silica nanoparticles, were found in the PIV4 sample, while the N sample consisted of carbon and oxygen elements (Figure 5.18 b). Thus, the

presence of abundant amounts of silicon within the pre-treated impregnated vacuumed sample, indicates the creation of the agglomerated particles on the surface of the sample during the impregnation process.

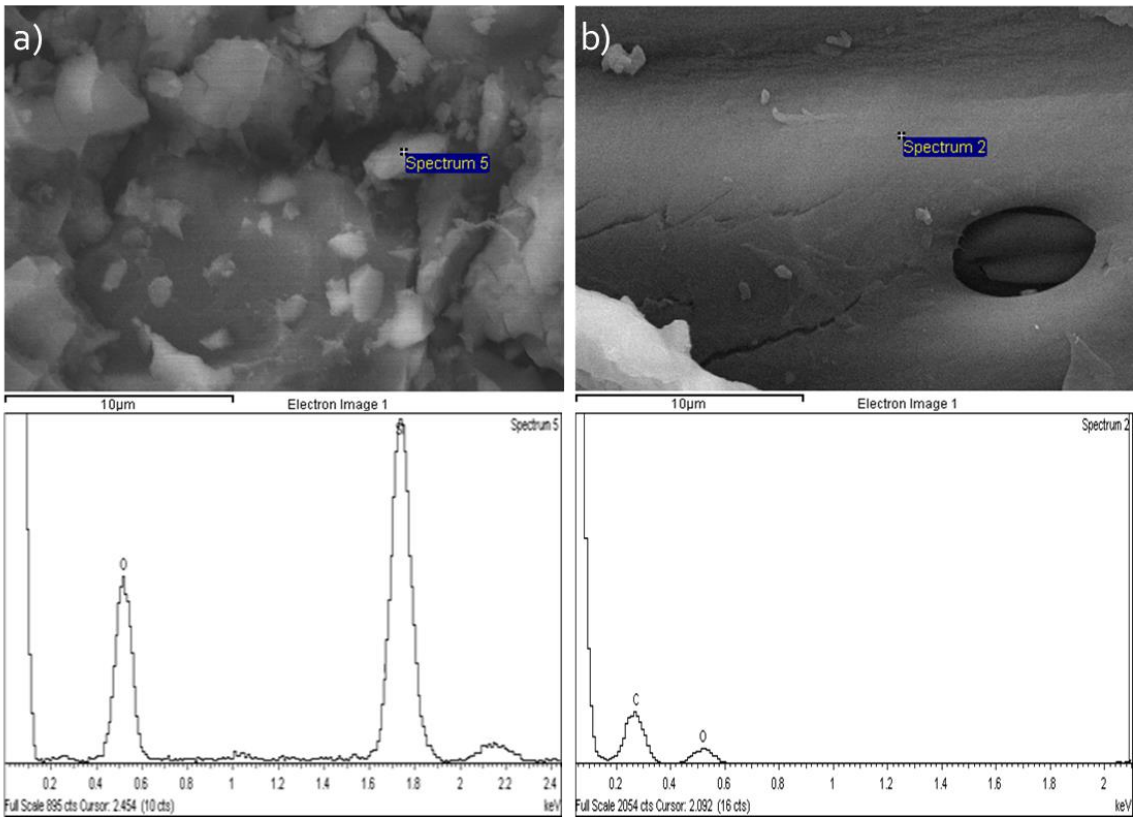

Figure 5.18: EDX micro-analysis of the outer surface of (a) PIV4 , and (b) N, corresponding energy dispersive X-ray spectra.

5.12 SEM Micrograph of the Inside Cross-section of the Wood Samples

SEM was used to investigate the morphological change and composition of the specimens, at the cross-section (i. e., a cut parallel to the outer surface between the two-half section), before and after the impregnation process. The sample with the lowest amount of water uptake (PIV4), and the reference (N) were compared in three magnifications using the SEM technique. As shown in Figure 5.19, agglomerated silica nanoparticles were present inside the Lumina in the PIV4 sample but absent inside the N sample. Based on the micrograph, it is perceived that the PIV4 sample contained less

porosity since the voids and vascular system in its microstructure were filled with particles. Consequently, this reduction in the amount of porosity led to the reduction in the level of water uptake of the specimens.

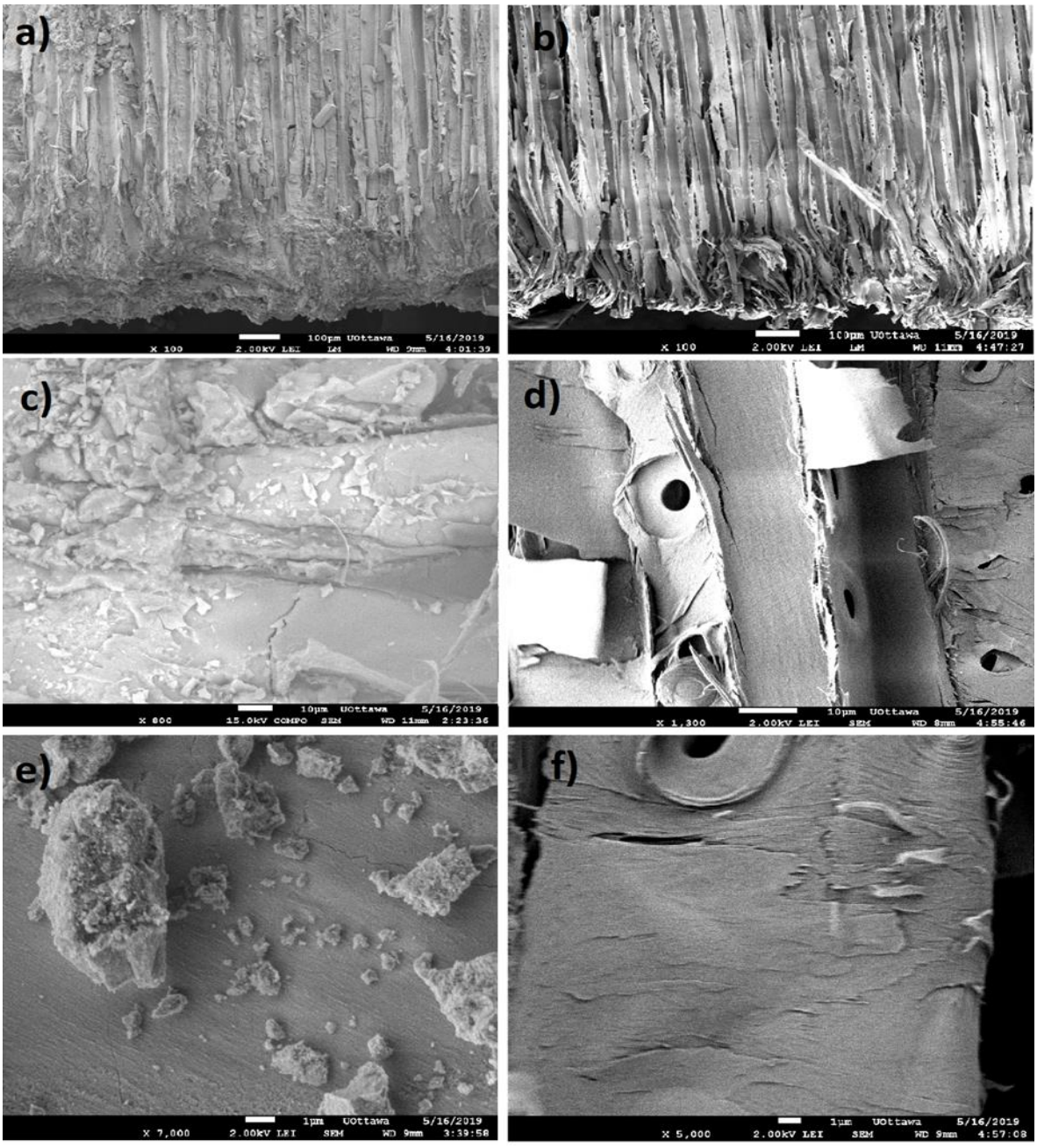

Figure 5.19: Scanning Electron Microscope (SEM) micrograph of cross-section view (a) wood surface treated with SiO_2 colloidal solution and (b) non-treated wood in the scale of 100µm. The high-magnification images show changes in the lumina surface (c) The pre-treated impregnated vacuumed samples and (d) the N sample in the scale of 10µm. Corresponding the particles and the N sample texture are shown in (e) and (f) in scale 1µm.

5.13 EDX Micro-Analysis Obtained from the Inside Cross-section of PIV4 Sample

The EDX micro-analysis of the PIV4 and the N samples at the cross-section are shown in Figure 5.20. The PIV4 and the N samples were characterized by EDX micro-analysis. The signal produced from the conductive coating layer on the surface of the sample was eliminated. According to the spectra, the abundance of silicon and oxygen are detected in the PIV4 sample (Figure 5.20 a). In contrast, based on Figure 5.20 (b), there is no silica inside the N sample (i.e., carbon and oxygen elements). Therefore, the presence of silica agglomerate inside the PIV4 is due to the penetration of the silica nanoparticles during the impregnation process.

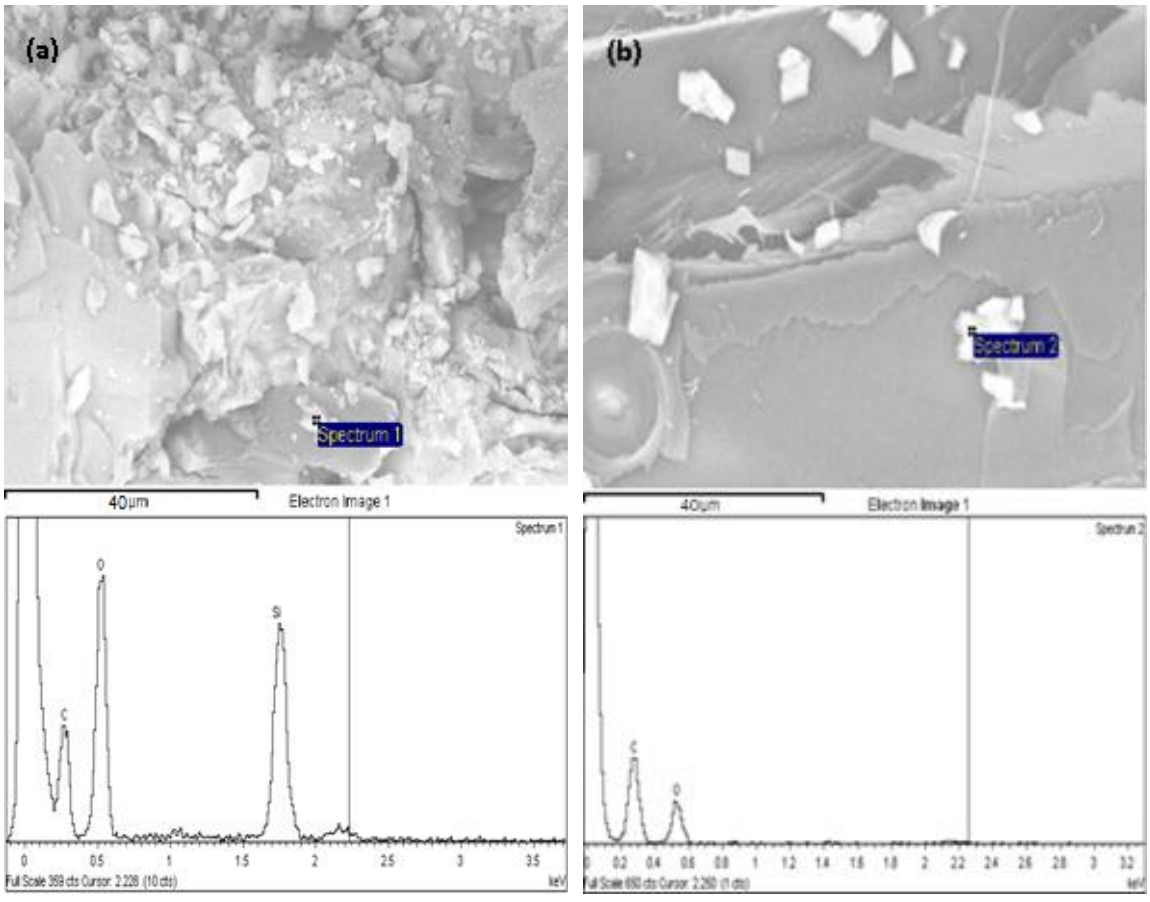

Figure 5.20: EDM micro-analysis of the Inside Cross-section of (a) PIV4 , and (b) N, corresponding energy dispersive X-ray spectra.

5.14 Comparison of SEM micrographs of the Nanocomposite PIV4 to the Extracted Powder from the Colloidal Solution

The surface morphology of the nanocomposite PIV4 and extracted powder from the colloidal solution are shown in Figure 5.21. SEM micrographs indicate formation of a heterogeneous mixture of agglomerate particles with irregular shapes and sizes. The morphology and the topography of the powder samples, Figure 5.21 (b), were similar (i. e., the morphology and size are not exactly same due to the different rate of evaporation), to the agglomerates of the SiO_2 nanoparticles inside the wood samples (Figure 5.21 (a)). Therefore, there are abundant silica agglomerated particles inside the PIV4 samples. The agglomerates decrease the level of water uptake by blocking the Lumina and filling the voids inside the wood samples.

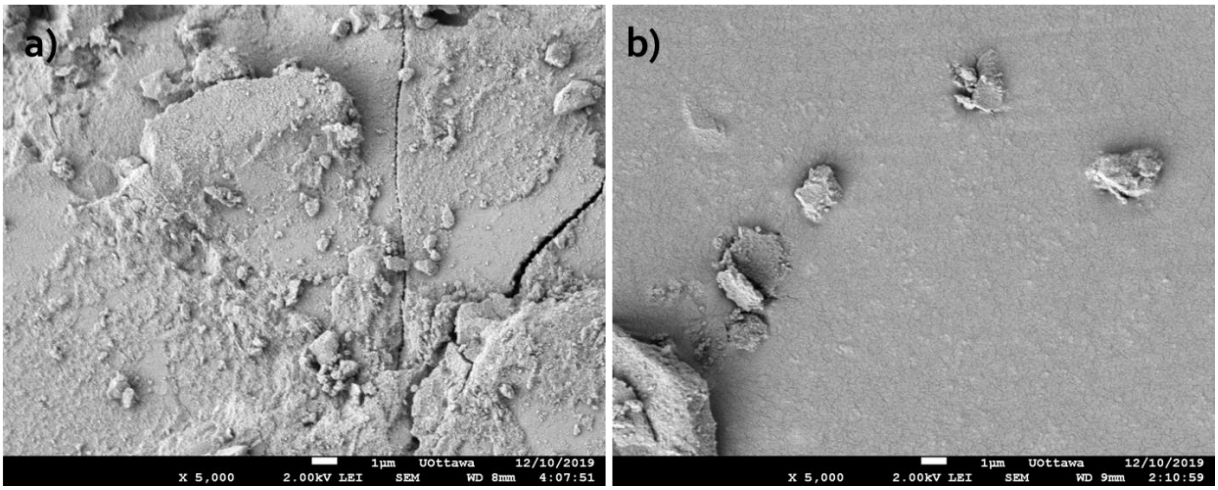

Figure 5.21: The morphology juxtaposition; a) the agglomerate particles within wood samples, b) the powder sample

5.15 Comparison of Wide-Angle X-ray Diffraction (WAXD) of the Nanocomposites

Figure 5.18 illustrates the WAXD diffraction patterns of the PIV4, PI4, P and N samples.

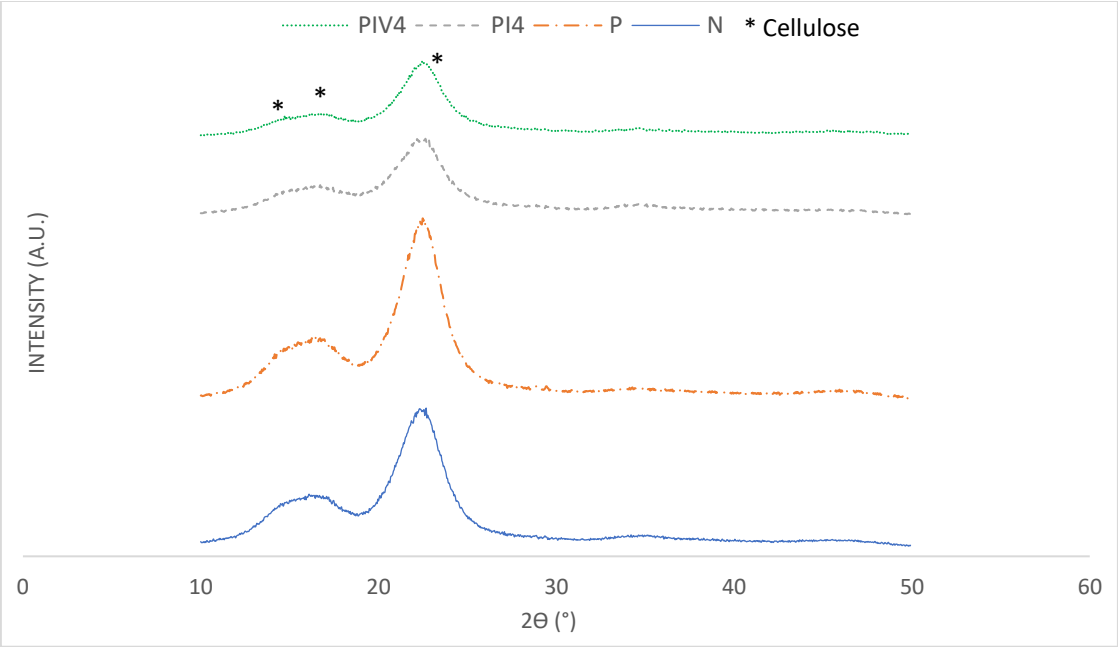

Figure 5.22: Wide-Angle X-ray Diffraction (WAXD) spectra of N, P, PI4, and PIV4 samples in a meridional reflections.

According to figure 5.22, for the N samples the peaks were at 2θ = 16.68°, and 22.68°. The major characteristic peaks for P samples were at 2θ = 16.88°, and 22.48° (Figure 5.23). On the other hand, the PI4 and PIV4 samples showed an almost similar graph that matched the typical cellulose pattern crystalline structure at 2θ =16.64 and 22.44° (the difference was less than 5% and can be considered negligible) (Figure 5.24).

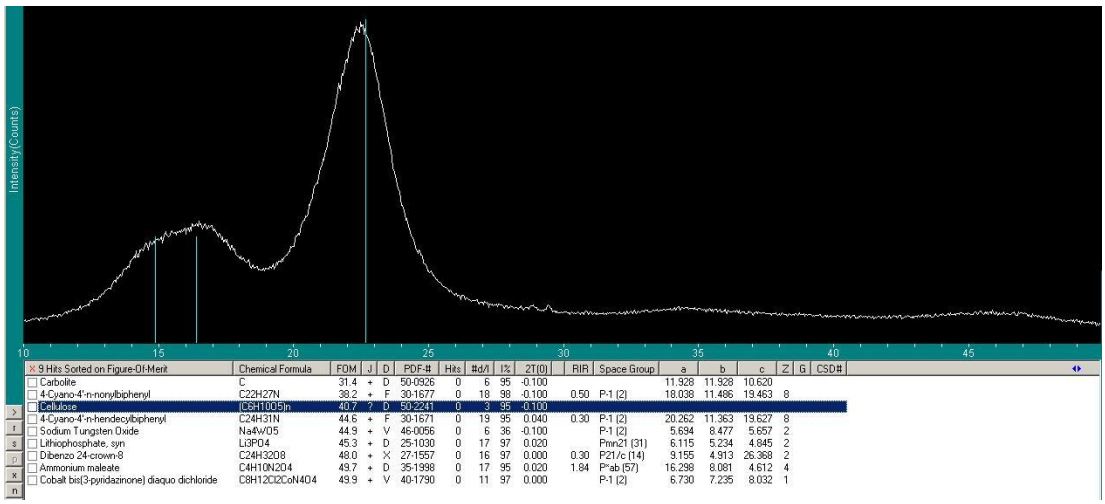

Figure 5.23: WAXD spectra of pre-treated (P) wood sample.

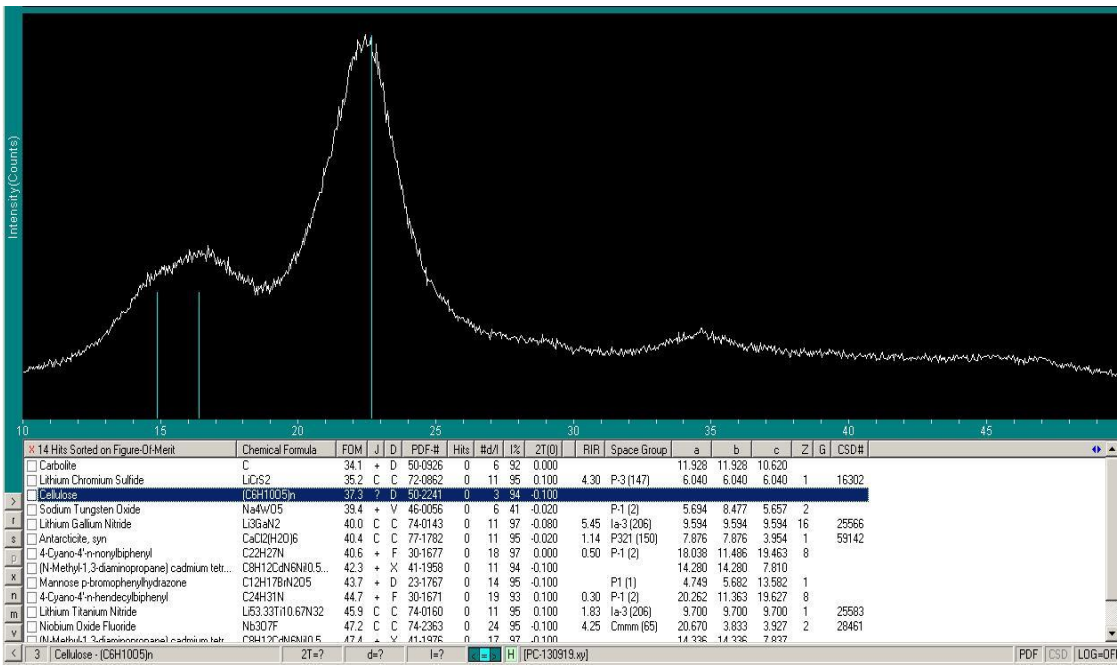

Figure 5.24: WAXD spectra of pre-treated impregnated (PI) wood sample.

These graphs clearly show that a thin layer of silica was formed on the surface of the samples and small particles penetrated inside the Lumina. Moreover, the intensity of the peaks was not weak which is typical for a thin film.

The characteristic distance (d) between the crystal planes of the sample in table 5.1 can be obtained from Bragg's law. According to this law, the size of the distance between the crystal planes of the specimen can be obtained by equation (3.2). In addition, the X-ray machine used sealed tube Cu Kα source, with a wavelength of 1.54 Angstroms[1] (Å), and the order of reflection was considered equal to unity (n = 1). The obtained values of d for each group based on the cellulose nano-crystals are presented in Table 5.1.

[1] Angstrom (Å), length unit for measuring wavelengths of light, equal to 10^{-10} m.

Table 5.1: The distance between the crystal planes of the sample (d).

Group	2θ (°)	Intensity (a.u.)	d(Å)
N	22.68	**8000**	3.92
P	22.48	**10272**	3.95
PI_4	22.44	**4617**	3.96
PIV_4	22.44	**4352**	3.96

According to the table, the intensity value in the P sample is more than the N sample, which is due to higher percentage of cellulose in the P sample after the alkaline treatment. During the impregnation process, incorporation of amorphous silica causes a decrease in the intensity of the major peak of cellulose, such that the highest the amount of SiO_2 leads to the lowest the intensity of the major peak of cellulose. Therefore, the intensity of the PIV4 sample is the lowest in comparison with P, N, and PI4, owing to the presence of the highest value of amorphous silica inside it.

6 Summary, Conclusions and Future Recommendations

6.1 Summary

The present dissertation has proposed a novel method for reducing the level of water uptake of spruce wood, using impregnation of wood samples with colloidal solution. More than 125 wood samples treated under various conditions were studied in terms of water uptake properties before and after impregnation. The samples were prepared from spruce wood, which is common in Ontario.

To obtain the optimum pre-treatment and impregnation conditions to reach the minimum level of water uptake, several experiments were designed and conducted. Parameters were changed in each experiment to evaluate their effects on the amount of water absorption in terms of water uptake. Testing was performed on the best performing sample to evaluate the effect of pre-treating with sodium hydroxide (caustic soda), the influence of submersion time, the effect of the number of impregnations, and the impregnation in vacuum condition. In general, the level of water uptake for the non-treated, pre-treated, and pretreated impregnated samples was studied by measuring the weight changes of each sample after submersion in water. Variations in the weight were measured by two different techniques, namely using a high-precision balance over specific periods of time and using a tensiometer. The outputs were discussed by comparing the percentage of water uptake against the square root of time on the length of the samples. In order to investigate the structural and compositional properties of the samples, they were characterized by WCA, SEM, XRD, EDX, and WAXD

6.2 Conclusions

The following conclusions can be drawn from the current study:

- The significant parameters which affect the water absorption in the wood samples were identified as pre-treatment, submersion time, number of impregnations, and vacuum condition.
- Alkaline treatment creates the cellulose-rich outer wood surface by removing the structural (i.e. hemicellulos, lignin) and nonstructural cell wall components of the wood

samples (i.e. pectin). This would make the cellulose to be more exposed to the solution and enable colloidal particles to bind to the wood samples.

- It was confirmed that the level of water up take was lower in the samples which were submerged in the colloidal solution for a long time.

- Water molecules can disrupt the impregnated samples by relocating the particles inside the samples in the way that obstruct the vascular system of wood.

- Although the silica colloidal solution is not a hydrophobic compound, it can reduce the percentage of water uptake of the samples due to creation of abundance agglomerated silica particles.

- By repeating the impregnation cycles much more amounts of nanoparticles penetrate the Lumina, block them, and prevent water from penetrating inside the porous matrix.

- Even though in most of the tests, the initial rate of water uptake was high, with the repetition of impregnation cycles and creation of more agglomerates inside the Lumina, the rate decreased over time and eventually reached a plateau.

- The most obvious finding to emerge from this study is that submersing the samples in vacuum condition decreases capacity of water uptake as well as, the number of impregnation cycle. This is due to the creation of negative pressure inside the vascular system, which leads to the removal trapped air bubble inside the Lumina and let more solution penetrate through the specimens.

6.3 Recommendations for Future Research

Further studies can be conducted to address the effect of some other parameters on the capacity of water absorption in wood samples. The following suggestions for the future research are proposed:

- More research using randomized controlled trials is needed to find the optimum time for the impregnation duration, as well as the number of submergences to obtain the minimum level of water uptake.

- Studying the effect of concentration of colloidal silica solution on water absorption of the wood samples.

- Studying the long-term water uptake properties of pretreated coated wood samples showing the durability of the deposited nanoparticles.

- Studying durability of the deposited nanoparticles against harsh environmental conditions such as high-pressure water, sonication, etc., and the changes in water uptake properties after subjecting the samples to harsh conditions.

- Mechanical characterizations to evaluate if the coating process affects the mechanical properties of wood.

REFERENCES

Alghunaim, Abdullah, Suchata Kirdponpattara, and Bi-min Zhang Newby. 2016. “Techniques for Determining Contact Angle and Wettability of Powders.” *Powder Technology* 287:201–15.

Ali, Majid. 2012. “Natural Fibres as Construction Materials.” *Journal of Civil Engineering and Construction Technology* 3(3):80–89.

Anon. n.d. “Accoya - Perennial Wood - Lemn Tratat Prin Acetilare – StejarMasiv.” Retrieved December 11, 2019 (https://www.stejarmasiv.ro/accoya-perennial-wood-lemn-tratat-prin-acetilare/).

Ashori, Alireza, Mehran Babaee, Mehdi Jonoobi, and Yahya Hamzeh. 2014. “Solvent-Free Acetylation of Cellulose Nanofibers for Improving Compatibility and Dispersion.” *Carbohydrate Polymers* 102:369–75.

Avramidis, Georg, Gunthard Scholz, Evelyn Nothnick, Holger Militz, Wolfgang Viöl, and Arndt Wolkenhauer. 2011. “Improved Bondability of Wax-Treated Wood Following Plasma Treatment.” *Wood Science and Technology* 45(2):359–68.

Back, E. L. 2000. “The Locations and Morphology of Resin Com-Ponents in the Wood.” *Pitch Control, Wood Resin and Deresination*.

Barnett, John R. and Victoria A. Bonham. 2004. “Cellulose Microfibril Angle in the Cell Wall of Wood Fibres.” *Biological Reviews* 79(2):461–72.

Bayart, Marie, Florent Gauvin, M. Reza Foruzanmehr, Saïd Elkoun, Mathieu Robert, Nano-coated Flax Fibers, Marie Bayart, Florent Gauvin, M. Reza Foruzanmehr, Saïd Elkoun, and Mathieu Robert. 2017. “Mechanical and Moisture Absorption Characterization of PLA Composites Reinforced with Nano-Coated Flax Fibers.” *Fibers and Polymers* 18(7):1288–95.

Bente, M., G. Avramidis, S. Förster, E. G. Rohwer, and W. Viöl. 2004. “Wood Surface Modification in Dielectric Barrier Discharges at Atmospheric Pressure for Creating Water Repellent Characteristics.” *Holz Als Roh-Und Werkstoff* 62(3):157–63.

Di Blasi, Colomba, Antonio Galgano, and Carmen Branca. 2009. “Influences of the Chemical State of Alkaline Compounds and the Nature of Alkali Metal on Wood Pyrolysis.” *Industrial & Engineering Chemistry Research* 48(7):3359–69.

Boulos, Lina, M. Reza Foruzanmehr, Arezki Tagnit-Hamou, Saïd Elkoun, and Mathieu

Robert. 2017. “Wetting Analysis and Surface Characterization of Flax Fibers Modified with Zirconia by Sol-Gel Method.” *Surface and Coatings Technology* 313:407–16.

Brunner, Maurice. 2000. “On the Plastic Design of Timber Beams with a Complex Cross-Section.” *Proceedings of WCTE*.

Burgert, I., J. Keckes, K. Frühmann, P. Fratzl, and S. E. Tschegg. 2002. “A Comparison of Two Techniques for Wood Fibre Isolation-Evaluation by Tensile Tests on Single Fibres with Different Microfibril Angle.” *Plant Biology* 4(1):9–12.

Burgert, Ingo, Michaela Eder, Notburga Gierlinger, and Peter Fratzl. 2007. “Tensile and Compressive Stresses in Tracheids Are Induced by Swelling Based on Geometrical Constraints of the Wood Cell.” *Planta* 226(4):981–87.

Choong, E. T. and F. O. Tesoro. 1989. “Relationship of Capillary Pressure and Water Saturation in Wood.” *Wood Science and Technology* 23(2):139–50.

Denes, Agnes R., Mandla A. Tshabalala, Roger Rowell, Ferencz Denes, and Raymond A. Young. 1999. “Hexamethyldisiloxane-Plasma Coating of Wood Surfaces for Creating Water Repellent Characteristics.” *Holzforschung* 53(3):318–26.

Dumitriu, Severian. 2004. *Polysaccharides: Structural Diversity and Functional Versatility*. CRC press.

Ek, Monica, Göran Gellerstedt, and Gunnar Henriksson. 2009. *Wood Chemistry and Biotechnology*. Vol. 1. Walter de Gruyter.

Epp, J. 2016. “X-Ray Diffraction (XRD) Techniques for Materials Characterization.” Pp. 81–124 in *Materials characterization using Nondestructive Evaluation (NDE) methods*. Elsevier.

Espert, Ana, Francisco Vilaplana, and Sigbritt Karlsson. 2004. “Comparison of Water Absorption in Natural Cellulosic Fibres from Wood and One-Year Crops in Polypropylene Composites and Its Influence on Their Mechanical Properties.” *Composites Part A: Applied Science and Manufacturing* 35(11):1267–76.

Evans, Philip D., Robin Wingate-Hill, and Ross B. Cunningham. 2009. “Wax and Oil Emulsion Additives: How Effective Are They at Improving the Performance of Preservative-Treated Wood?” *Forest Products Journal* 59(1/2):66.

Fengel, D and G. Wegener. 1984. “Wood Chemistry.” *Ultrastructure, Reactions* 227–39.

Fengel, Dietrich and Gerd Wegener. 1984. “Wood: Chemistry, Ultrastructure.” *Reactions* 613:1960–82.

Fick, Adolph. 1855. “V. On Liquid Diffusion.” *The London, Edinburgh, and Dublin Philosophical Magazine and Journal of Science* 10(63):30–39.

Foruzanmehr, MReza, Pascal Y. Vuillaume, Mathieu Robert, and Saïd Elkoun. 2015. “The Effect of Grafting a Nano-TiO2 Thin Film on Physical and Mechanical Properties of Cellulosic Natural Fibers.” *Materials & Design* 85:671–78.

Fujino, Takeshi and Takao Itoh. 1998. “Changes in the Three Dimensional Architecture of the Cell Wall during Lignification of Xylem Cells in Eucalyptus Tereticornis.” *Holzforschung-International Journal of the Biology, Chemistry, Physics and Technology of Wood* 52(2):111–16.

Gao, Zhengxin, Xianglin Zhai, and Chengyu Wang. 2015. “Facile Transformation of Superhydrophobicity to Hydrophilicity by Silica/Poly (ε-Caprolactone) Composite Film.” *Applied Surface Science* 359:209–14.

Gerhards, Charles C. 2007. “Effect of Moisture Content and Temperature on the Mechanical Properties of Wood: An Analysis of Immediate Effects.” *Wood and Fiber Science* 14(1):4–36.

Gibson, Lorna J. 2012. “The Hierarchical Structure and Mechanics of Plant Materials.” *Journal of the Royal Society Interface* 9(76):2749–66.

Goethals, P. and M. Stevens. 1994. “Dimensional Stability and Decay Resistance of Wood upon Modification with Some New Type Chemical Reactants.” *Document-the International Research Group on Wood Preservation (Sweden)*.

Hager, R. 1995. “Waterborne Silicones as Wood Preservatives.” *Document-the International Research Group on Wood Preservation (Sweden)*.

Hager, R. and B. Berglund. 1995. “Waterborne Silicone-Based Coatings Aid Wood Protection.” *Paint & Coatings Industry* 11(9):58–61.

Hill, C. A. S. 2011. “Acetylated Wood–The Science behind the Material.” *Accoya Accsys Group Online*.

Hill, C. A. S., S. C. Forster, M. R. M. Farahani, M. D. C. Hale, G. A. Ormondroyd, and G. R. Williams. 2005. “An Investigation of Cell Wall Micropore Blocking as a Possible Mechanism for the Decay Resistance of Anhydride Modified Wood.” *International*

Biodeterioration & Biodegradation 55(1):69–76.

Hill, Callum A. S. 2007. *Wood Modification: Chemical, Thermal and Other Processes*. Vol. 5. John Wiley & Sons.

Homan, Waldemar, Boke Tjeerdsma, Erwin Beckers, and André Jorissen. 2000. "Structural and Other Properties of Modified Wood." Pp. 3511–18 in *World Conference on Timber Engineering*. Vol. 1. World Conference Timber Enginnering British Columbia.

Hon, David N. S. and Nobuo Shiraishi. 2000. *Wood and Cellulosic Chemistry, Revised, and Expanded*. CRC press.

Humar, Miha, Davor Kržišnik, Boštjan Lesar, Nejc Thaler, Aleš Ugovšek, Klemen Zupančič, and Mojca Žlahtič. 2017. "Thermal Modification of Wax-Impregnated Wood to Enhance Its Physical, Mechanical, and Biological Properties." *Holzforschung* 71(1):57–64.

Icc, Earn, Continuing Education, and Unit Ceu. 2015. "Mid-Rise Light Wood Frame."

Janzen, Gerd. 1992. *Plasmatechnik: Grundlagen, Anwendungen, Diagnostik*. Hüthig.

Kesten, Christopher, Alexandra Menna, and Clara Sanchez-Rodriguez. 2017. "Regulation of Cellulose Synthesis in Response to Stress." *Current Opinion in Plant Biology* 40:106–13.

Khazaei, J. 2008. "Water Absorption Characteristics of Three Wood Varieties." *Cercetări Agronomice În Moldova* 41(2):134.

Kitir, Nurgul, Ertan Yildirim, Üstün Şahin, Metin Turan, Melek Ekinci, Selda Ors, Raziye Kul, Hüsnü Ünlü, and Halime Ünlü. 2018. "Peat Use in Horticulture." *Peat* 75.

Kojiro, Keisuke, Tsunehisa Miki, Hiroyuki Sugimoto, Masamitsu Nakajima, and Kozo Kanayama. 2010. "Micropores and Mesopores in the Cell Wall of Dry Wood." *Journal of Wood Science* 56(2):107–11.

Kolleman, F. F. P. and W. A. Cote. 1984. "Principles of Wood Science and Technology, Vol. I. Solid Wood."

Kollmann, Franz F. P., Edward W. Kuenzi, and Alfred J. Stamm. 2012. *Principles of Wood Science and Technology: II Wood Based Materials*. Springer Science & Business Media.

KOZARIĆ, L. J., D. Kukaras, M. Bešević, A. Prokić, and N. Đurić. 2016. "ACETYLATED WOOD IN CONSTRUCTIONS." *Bulletin of the Transilvania University of Brasov,*

Series I: Engineering Sciences 9.

Lee, Jonggeon, Sungho Tae, and Rakhyun Kim. 2018. "A Study on the Analysis of CO2 Emissions of Apartment Housing in the Construction Process." *Sustainability* 10(2):365.

Lesar, B., M. Zupancic, and M. Humar. 2008. "Microscopic Analysis of Wood Impregnated with Aqueous Montan Wax Emulsion." *Les Wood* 60(9):320–26.

Lesar, Boštjan and Miha Humar. 2011. "Use of Wax Emulsions for Improvement of Wood Durability and Sorption Properties." *European Journal of Wood and Wood Products* 69(2):231–38.

Li, Xiaoyu, Xin Du, and Junhui He. 2010. "Self-Cleaning Antireflective Coatings Assembled from Peculiar Mesoporous Silica Nanoparticles." *Langmuir* 26(16):13528–34.

Livingston, Edward H. 2004. "Who Was Student and Why Do We Care so Much about His T-Test? 1." *Journal of Surgical Research* 118(1):58–65.

Lozhechnikova, Alina, Katja Vahtikari, Mark Hughes, and Monika Österberg. 2015. "Toward Energy Efficiency through an Optimized Use of Wood: The Development of Natural Hydrophobic Coatings That Retain Moisture-Buffering Ability." *Energy and Buildings* 105:37–42.

Lukowsky, D., R. D. Peek, and A. O. Rapp. 1997. "Water-Based Silicones on Wood." *International Research Group on Wood Protection, IRG/Wp* 97–30144.

Mai, Carsten and Holger Militz. 2004. "Modification of Wood with Silicon Compounds. Treatment Systems Based on Organic Silicon Compounds—a Review." *Wood Science and Technology* 37(6):453–61.

Malkov, S., V. Kuzmin, V. Baltakhinov, and P. Tikka. 2003. "Modelling the Process of Water Penetration into Softwood Chips." *Journal of Pulp and Paper Science* 29(4):137.

Mark, Richard E. 1967. "Cell Wall Mechanics of Tracheids." *Cell Wall Mechanics of Tracheids.*

Miyafuji, Hisashi, Hideki Kokaji, and Shiro Saka. 2004. "Photostable Wood–Inorganic Composites Prepared by the Sol-Gel Process with UV Absorbent." *Journal of Wood Science* 50(2):130–35.

Miyafuji, Hisashi and Shiro Saka. 2001. "Na 2 O-SiO 2 Wood-Inorganic Composites Prepared by the Sol-Gel Process and Their Fire-Resistant Properties." *Journal of Wood Science*

47(6):483–89.

Mrad, Hatem, Sébastien Alix, Sebastien Migneault, Ahmed Koubaa, and Patrick Perre. 2018. "Numerical and Experimental Assessment of Water Absorption of Wood-Polymer Composites." *Measurement* 115:197–203.

Nuopponen, M., S. Willför, A. S. Jääskeläinen, and T. Vuorinen. 2004. "A UV Resonance Raman (UVRR) Spectroscopic Study on the Extractable Compounds in Scots Pine (Pinus Sylvestris) Wood: Part II. Hydrophilic Compounds." *Spectrochimica Acta Part A: Molecular and Biomolecular Spectroscopy* 60(13):2963–68.

Papadopoulos, Antonios N., Dimitrios N. Bikiaris, Athanasios C. Mitropoulos, and George Z. Kyzas. 2019. "Nanomaterials and Chemical Modifications for Enhanced Key Wood Properties: A Review." *Nanomaterials* 9(4):607.

Petrič, Marko. 2013. "Surface Modification of Wood." *Reviews of Adhesion and Adhesives* 1(2):216–47.

Petrič, Marko and Primož Oven. 2015. "Determination of Wettability of Wood and Its Significance in Wood Science and Technology: A Critical Review." *Reviews of Adhesion and Adhesives* 3(2):121–87.

Philipse, Albert P. 2018. "Continuity, Gradients and Fick's Diffusion Laws." Pp. 61–70 in *Brownian Motion*. Springer.

Piquero, Alexis Russell and David Weisburd. 2010. *Handbook of Quantitative Criminology*. Springer.

Podgorski, L., C. Bousta, F. Schambourg, J. Maguin, and B. Chevet. 2002. "Surface Modification of Wood by Plasma Polymerisation." *Pigment & Resin Technology* 31(1):33–40.

Poirier, D. R. and G. H. Geiger. 2016. "Fick's Law and Diffusivity of Materials." Pp. 419–61 in *Transport Phenomena in Materials Processing*. Springer.

Pries, Malte. 2014. "Treatment of Solid Wood with Silanes, Polydimethylsiloxanes and Silica Sols."

Pucci, Monica Francesca, Pierre-Jacques Liotier, and Sylvain Drapier. 2016. "Capillary Wicking in Flax Fabrics–Effects of Swelling in Water." *Colloids and Surfaces A: Physicochemical and Engineering Aspects* 498:176–84.

Rapp, A. O., C. Beringhausen, S. Bollmus, C. Brischke, T. Frick, T. Haas, M. Sailer, and C. R. Welzbacher. 2005. "Hydrophobierung von Holz-Erfahrungen Nach 7 Jahren Freilandtest." *24th Holzschutztagung Der DGFH, Leipzig* 157–70.

Robert, J. 2011. *ChemInform Abstract : Cellulose Nanomaterials Review : Structure , Properties Chem Soc Rev*.

Rowell, Roger M. 2005. "14 Chemical Modification of Wood." *Handbook of Wood Chemistry and Wood Composites* 381.

Rowell, Roger M. 2012. *Handbook of Wood Chemistry and Wood Composites*. CRC press.

Salmén, Lennart and Ingo Burgert. 2009. "Cell Wall Features with Regard to Mechanical Performance. A Review COST Action E35 2004–2008: Wood Machining–Micromechanics and Fracture." *Holzforschung* 63(2):121–29.

Scheller, Henrik Vibe and Peter Ulvskov. 2010. "Hemicelluloses." *Annual Review of Plant Biology* 61.

Schuster, Jonathan M., Carlos E. Schvezov, and Mario R. Rosenberger. 2015. "Influence of Experimental Variables on the Measure of Contact Angle in Metals Using the Sessile Drop Method." *Procedia Materials Science* 8(2009):742–51.

Schweingruber, Fritz Hans. 2007. *Wood Structure and Environment*. Springer Science & Business Media.

Segal, LGJMA, J. J. Creely, A. E. Martin Jr, and C. M. Conrad. 1959. "An Empirical Method for Estimating the Degree of Crystallinity of Native Cellulose Using the X-Ray Diffractometer." *Textile Research Journal* 29(10):786–94.

Shi, Sheldon Q. 2007. "Diffusion Model Based on Fick's Second Law for the Moisture Absorption Process in Wood Fiber-Based Composites: Is It Suitable or Not?" *Wood Science and Technology* 41(8):645–58.

Shi, Xianglin, N. S. Dalai, Xiang N. Hu, and V. Vallyathan. 1989. "The Chemical Properties of Silica Particle Surface in Relation to Silica-cell Interactions." *Journal of Toxicology and Environmental Health, Part A Current Issues* 27(4):435–54.

Shmulsky, Rubin and P. David Jones. 2019. *Forest Products and Wood Science: An Introduction*. John Wiley & Sons.

Shupe, Todd, Cheng Piao, and Cran Lucas. 2012. "The Termiticidal Properties of

Superhydrophobic Wood Surfaces Treated with ZnO Nanorods." *European Journal of Wood and Wood Products* 70(4):531–35.

da Silva, Meire R., Bruno H. Fumes, Carlos E. D. Nazario, and Fernando M. Lancas. 2017. "New Materials for Green Sample Preparation: Recent Advances and Future Trends." Pp. 575–99 in *Comprehensive Analytical Chemistry*. Vol. 76. Elsevier.

Sjöström, E. and U. Westermark. 1999. "Chemical Composition of Wood and Pulps: Basic Constituents and Their Distribution." Pp. 1–19 in *Analytical methods in wood chemistry, pulping, and papermaking*. Springer.

Sjöström, Eero and Raimo Alén. 2013. *Analytical Methods in Wood Chemistry, Pulping, and Papermaking*. Springer Science & Business Media.

Sticklen, Mariam B. 2008. "Plant Genetic Engineering for Biofuel Production: Towards Affordable Cellulosic Ethanol." *Nature Reviews Genetics* 9:433.

Taylor, John R., Michael A. Dubson, and Chris D. Zafiratos. 2004. *Modern Physics for Scientists and Engineers*. Prentice-Hall.

Teipel, Ulrich and Irma Mikonsaari. 2004. "Determining Contact Angles of Powders by Liquid Penetration." *Particle & Particle Systems Characterization: Measurement and Description of Particle Properties and Behavior in Powders and Other Disperse Systems* 21(4):255–60.

Tjeerdsma, B., M. Boonstra, and H. Militz. 1998. "Thermal Modification of Non-Durable Wood Species. 2. Improved Wood Properties of Thermal Treated Wood. The International Research Group On Wood Preservation, Section 4-Processes." in *29 Annual Meeting, Maastricht*.

Used, Commonly. 2000. "Cba03E.Pdf." 2–3.

Wadsö, Lars. 1993. "Studies of Water Vapor Transport and Sorption in Wood."

Walker, John C. F. 2006. *Primary Wood Processing: Principles and Practice*. Springer Science & Business Media.

Wang, Dongjun, Toyoko Imae, and Masao Miki. 2007. "Reprint of "Fluorescence Emission from PAMAM and PPI Dendrimers [J. Colloid Interface Sci. 306 (2007) 222–227]." *Journal of Colloid and Interface Science* 312(1):8–13.

Wang, Xiaodong, Zeen Huang, Paul Cooper, Xiang-Ming Wang, Yaolin Zhang, and Romulo

Casilla. 2010. “The Ability of Wood to Buffer Highly Acidic and Alkaline Adhesives.” *Wood and Fiber Science* 42(3):398–405.

Wang, Xiaoqing, Junliang Liu, Sichen Liu, and Huanjun Chang. 2014. “Sol-Gel Deposition of TIO2 Nanocoatings on Wood Surfaces with Enhanced Hydrophobicity and Photostability.” *Wood and Fiber Science* 46(1):109–17.

Wolkenhauer, Arndt, Georg Avramidis, Evelyn Hauswald, Holger Militz, and Wolfgang Viöl. 2008. “Plasma Treatment of Wood–Plastic Composites to Enhance Their Adhesion Properties.” *Journal of Adhesion Science and Technology* 22(16):2025–37.

Wong, T. C. and L. J. Broutman. 1985. “Moisture Diffusion in Epoxy Resins Part I. Non-Fickian Sorption Processes.” *Polymer Engineering & Science* 25(9):521–28.

Żenkiewicz, M. 2007. “Methods for the Calculation of Surface Free Energy of Solids.” *Journal of Achievements in Materials and Manufacturing Engineering* 24(1):137–45.

Zhang, Xiaolei, Weihong Yang, and Wlodzimierz Blasiak. 2011. “Modeling Study of Woody Biomass: Interactions of Cellulose, Hemicellulose, and Lignin.” *Energy and Fuels* 25(10):4786–95.

Zhi, Danfeng, Yao Lu, Sanjayan Sathasivam, Ivan P. Parkin, and Xia Zhang. 2017. “Large-Scale Fabrication of Translucent and Repairable Superhydrophobic Spray Coatings with Remarkable Mechanical, Chemical Durability and UV Resistance.” *Journal of Materials Chemistry A* 5(21):10622–31

Appendix A: SEM and XRD

Scanning Electron Microscope (SEM)

The electron microscopes, which are available in two types, are carried out in a vacuum. The first type is the transmission electron microscope (TEM) that needs a so thin solid material as a track detector (ex. mica flake). The resolution is about 1 nm–10 μm, and the voltage is so high. The second type is called the scanning electron microscope (SEM) that uses a focused beam of electrons. In fact, the information about the composition of the specimens and the surface topography can be attained by analyzing the obtained various signals due to the interactions between the electrons and the atoms of the samples. Compared with the TEM, it uses lower voltage, while its resolution is about 2 nm–50 μm. SEMs and optical microscopes both use an illuminating system to emit light on the sample under the microscope. SEMs need detectors to detect the secondary electrons emitted from the sample to form the final image. SEM involves two main parts that the principal elements of each are shown in FigureA.1.

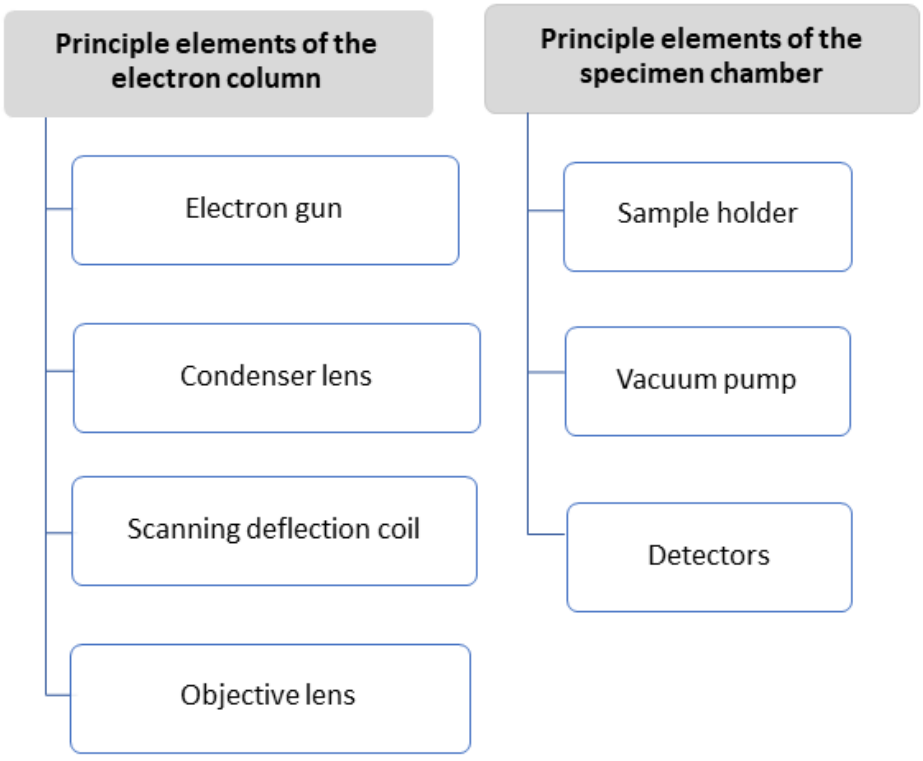

Figure A. 1: The main parts of the SEM

The details are provided in Figure A.2 and Table A.1 (L'Annunziata, 2012).

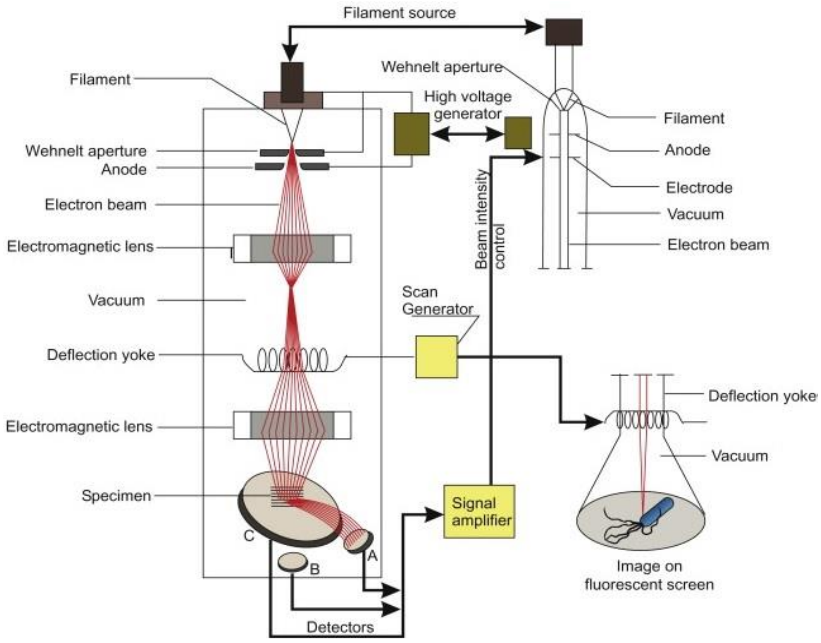

Figure A. 2: Simple schematic of SEM (Roane et al. 2015)

Table A. 1: Comparison of Electron Microscopes vs Optical Microscopes (Roane et al. 2015)

Characteristic	Electron	Optical
Illuminating beam	Electron beam	Light beam
Wavelength	0.086 Å (20 kV)	7500 Å (visible)
2000 Å (ultraviolet)	0.037 Å (100 kV	0.037 Å (100 kV)
Medium	Vacuum	Atmosphere
Lens	Electrostatic lens	Glass lens
Resolving power	3 Å	2000 Å
Magnification	Up to 1,000,000×	Up to 2000×
Focusing	Electrical	Mechanical
Viable specimen	No	Yes
Specimen requires staining or treatment	Always	Yes/no
Colored image produced	No	Yes

X-ray Diffraction (XRD)

X-ray powder diffraction (XRD) is one of the most significant non-destructive rapid analytical techniques, which primarily used for elemental analysis, chemical characterization of a sample, phase identification of a crystalline material and providing information on unit cell dimensions. All crystalline materials consist of atoms, ions or molecules that are arranged in a regular manner.

X-ray diffractometers consist of three basic parts: An X-ray tube, a sample holder, and an X-ray detector. The constrictive or distractive scattered X-ray from the sample was read out by the detector. The peak of intensity of the emitted X-ray from the crystal lattice is observed based on the Bragg's Law conditions. Based on this law, the angle of incidence is equal to the angle of scattering. Moreover, an integer number of wavelengths is equal to the path length difference. The process is schematically shown in the next picture.

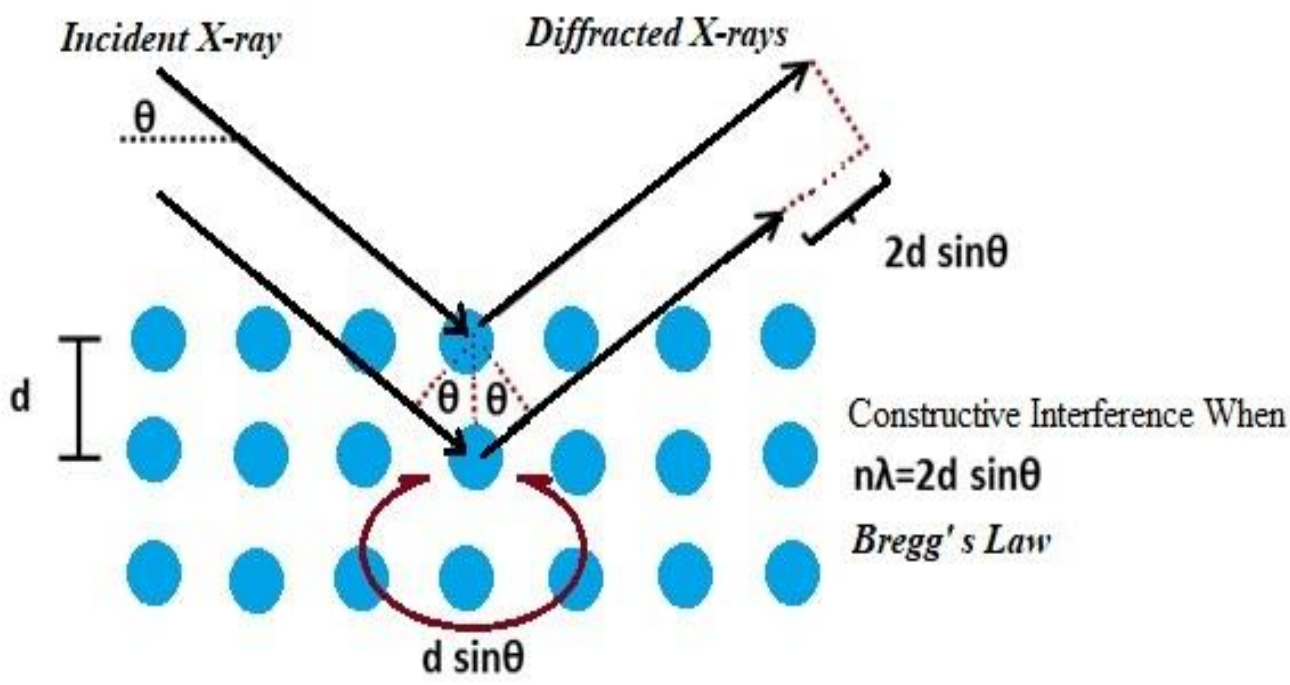

Figure A. 3: Schematic representation of the XRD operation

The wavelength of the incident x-ray beam can be obtained by the following equation known as Bragg's law:

$n\lambda=2d\sin\theta$

(3.1)

Where n is order of reflection that is an integer, λ is the wavelength of x-rays, d is the characteristic distance between the crystal planes of the sample and θ is the angle between the normal beam and the incident to the reflecting lattice plane. In addition, d, which is the inter planer spacing of every single crystallographic phase, can be obtained by calculating the angles, θ, under which the constructive interfering x-rays leave the crystal (Taylor et al. 2004).

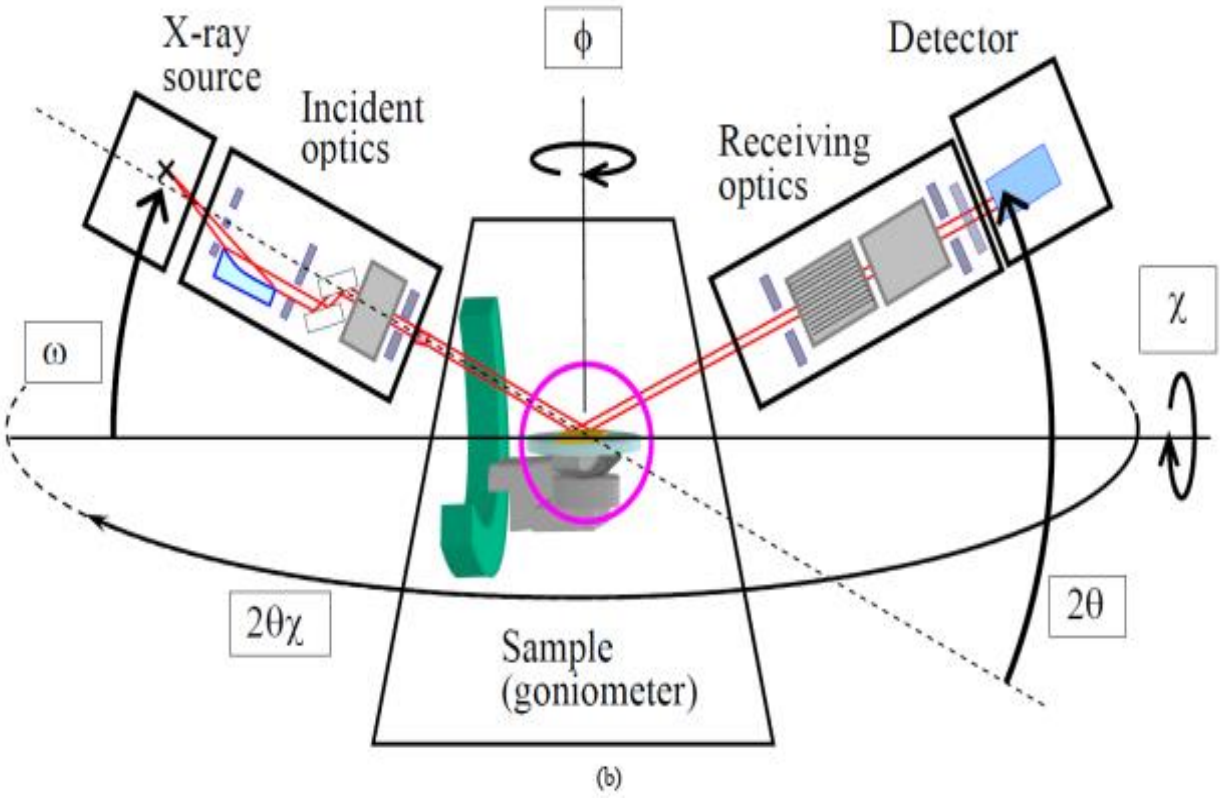

Figure A. 4: Schematic of XRD characterization technique (Inaba et al. 2013)

Appendix B: Water capillary rise graphs

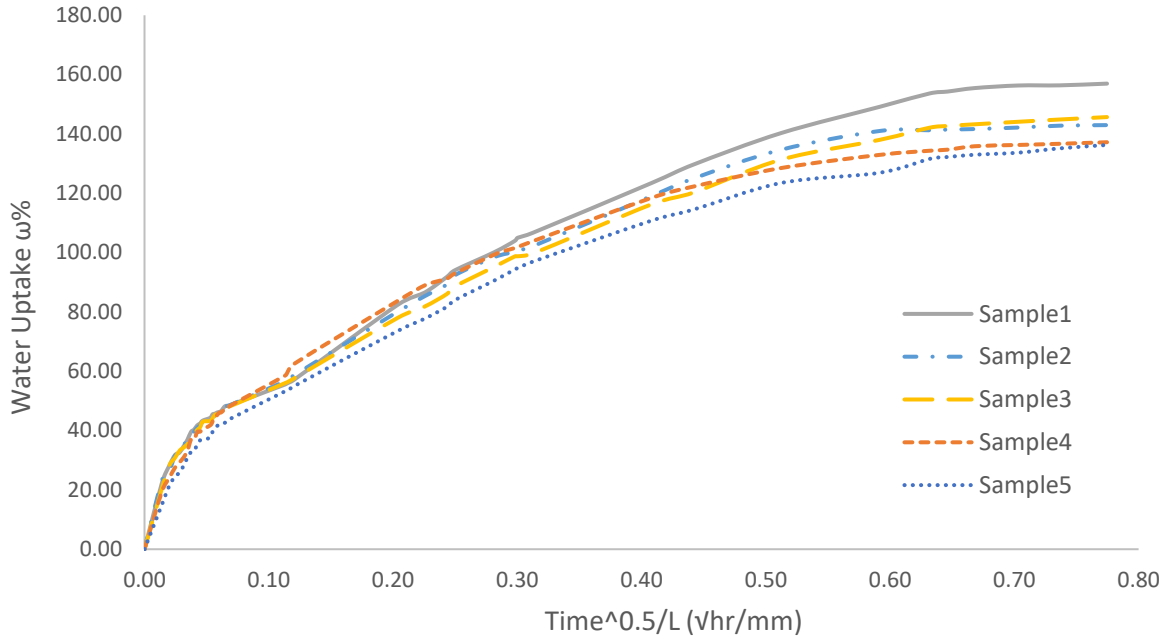

Figure B. 1: Water capillary rise of Non-treated (Reference) wood samples given as a percentage of the weight of absorbed water vs square root of time on the length of samples.

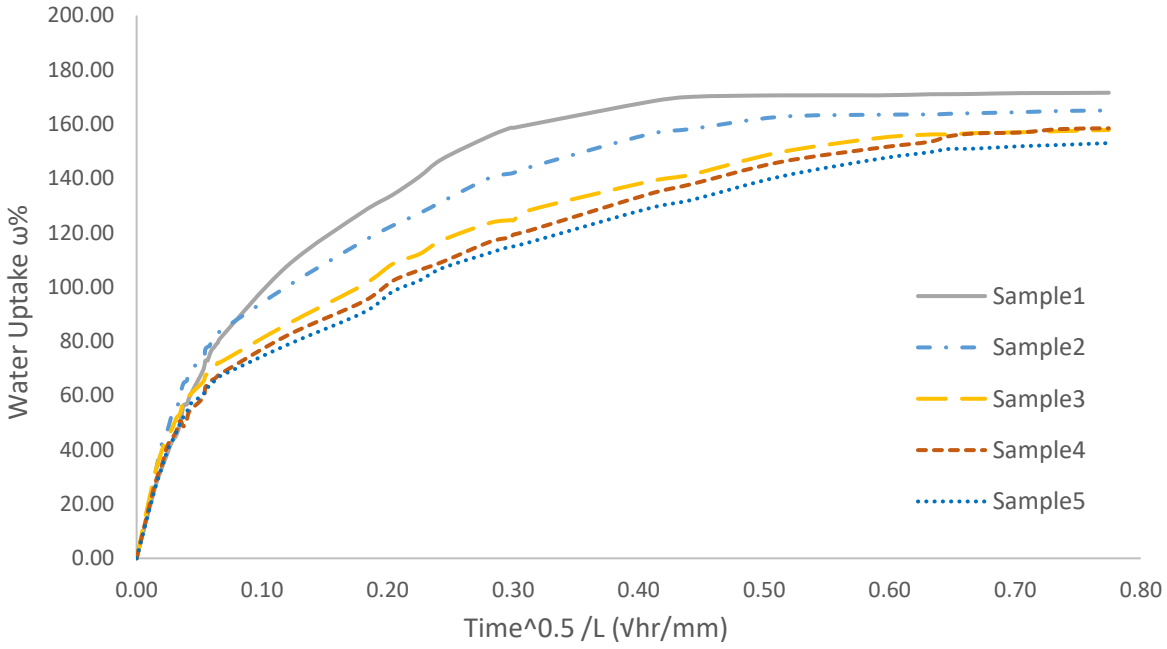

Figure B. 2: Water capillary rise of Pre-treated wood samples given as a percentage of the weight of absorbed water vs square root of time on the length of samples.

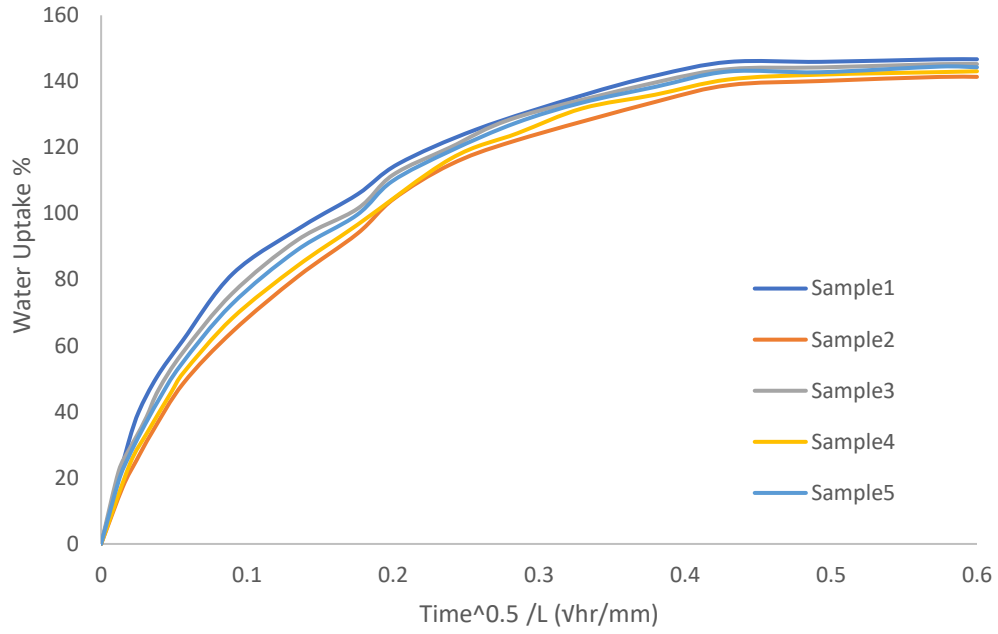

Figure B. 3: Water capillary rise of Pre-treated Impregnated (20 min) wood samples

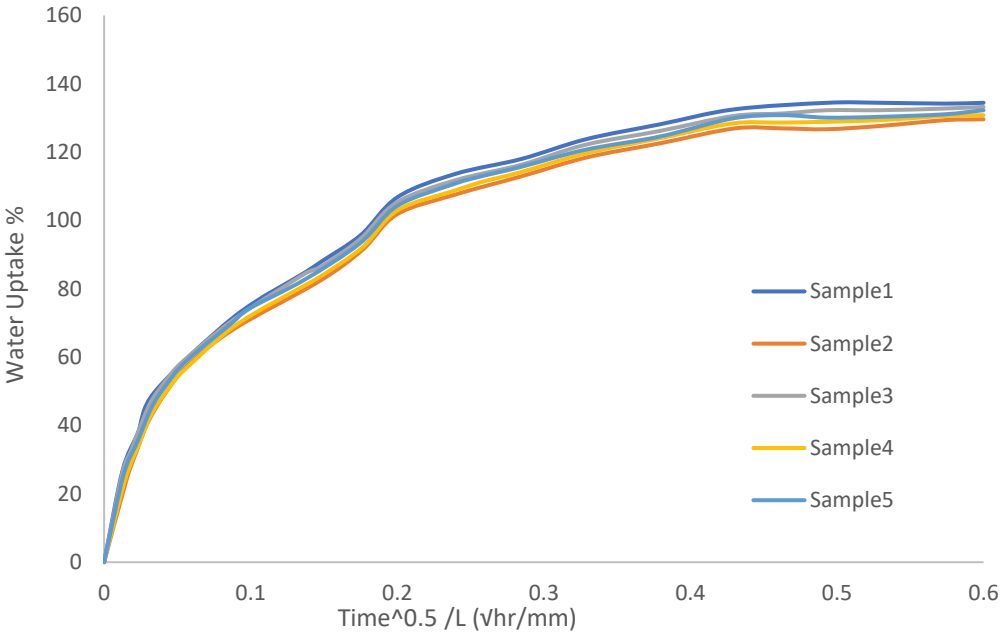

Figure B. 4: Water capillary rise of Pre-treated Impregnated (40 min) wood samples

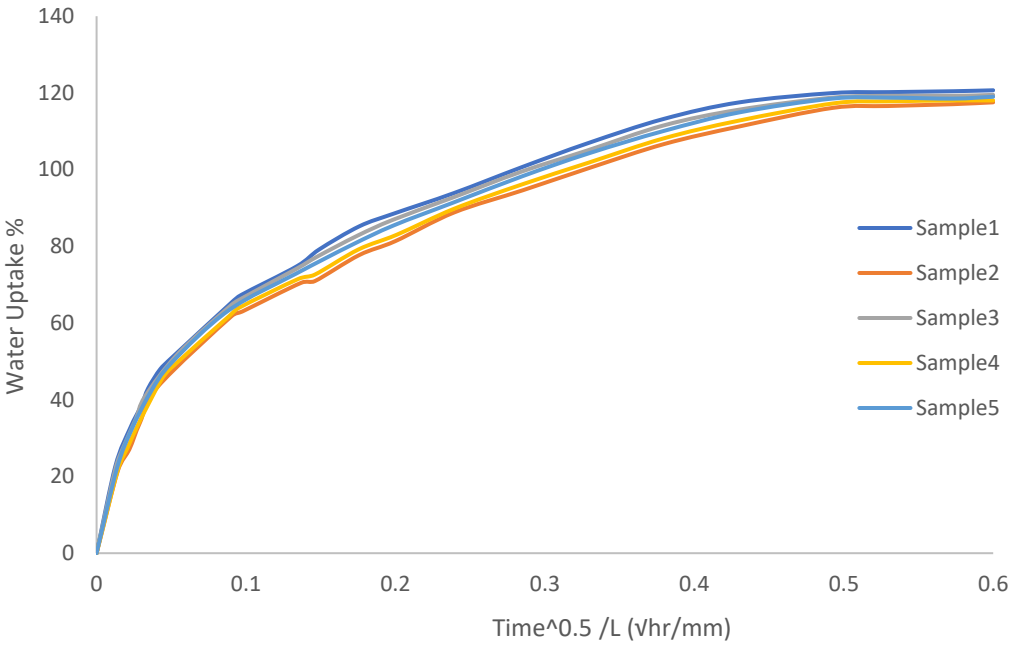

Figure B. 5: Water capillary rise of Pre-treated Impregnated (60 min) wood samples

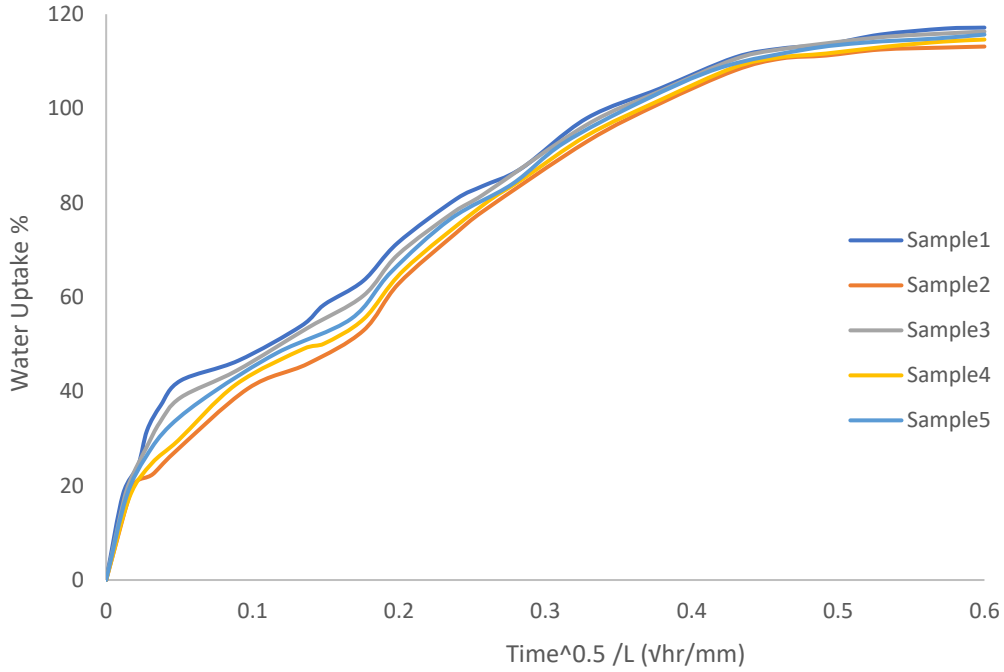

Figure B. 6: Water capillary rise of Non-treated Impregnated (20 min) wood samples

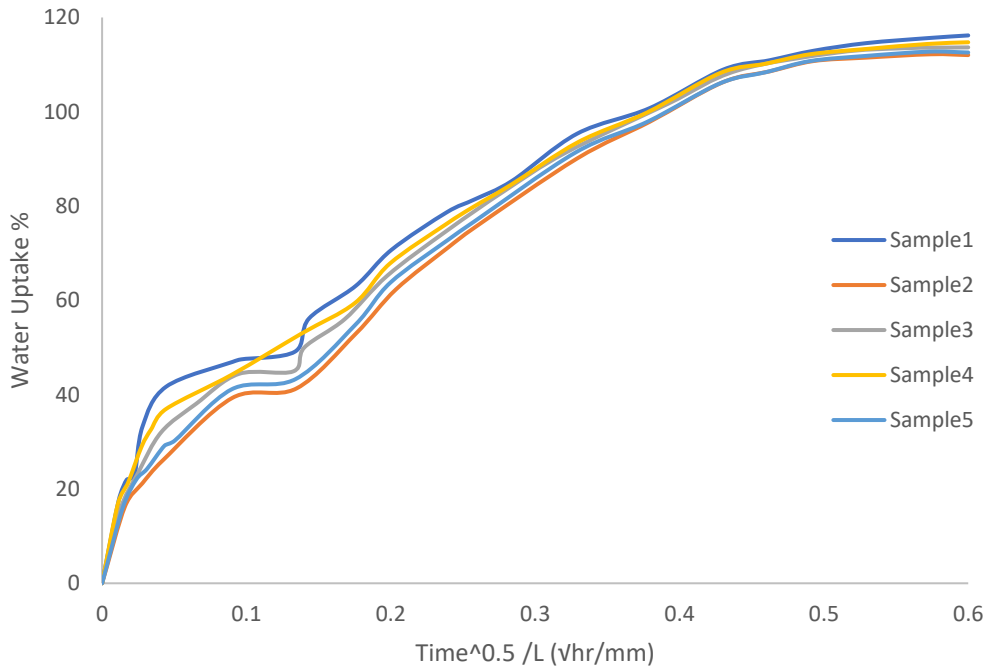

Figure B. 7: Water capillary rise of Non-treated Impregnated (40 min) wood samples

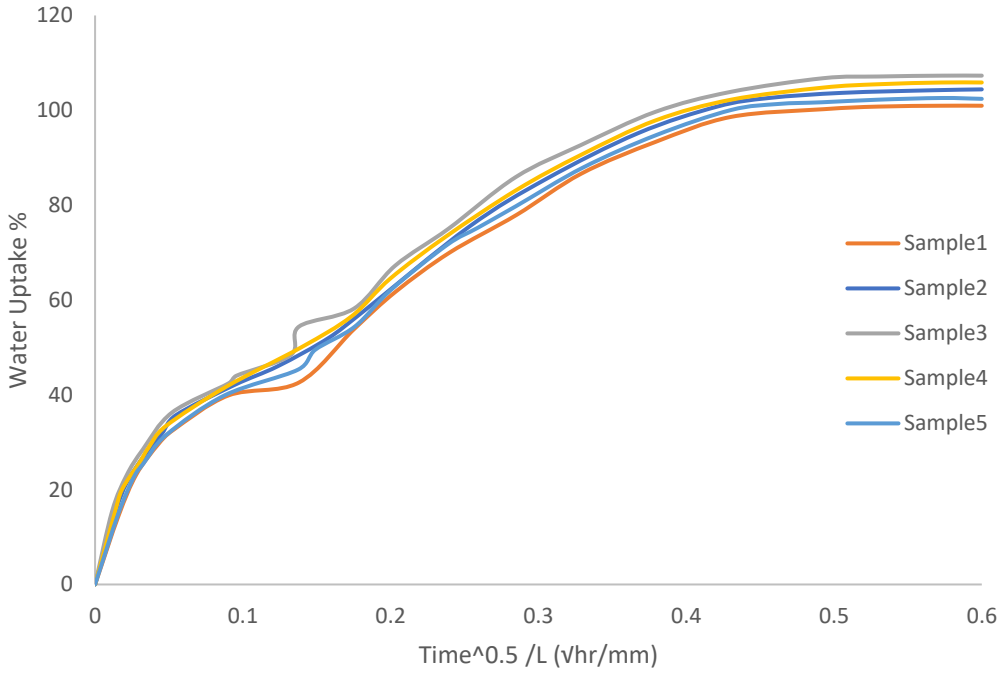

Figure B. 8: Water capillary rise of Non-treated Impregnated (60 min) wood samples

Appendix C: SEM Micrographs of the Samples

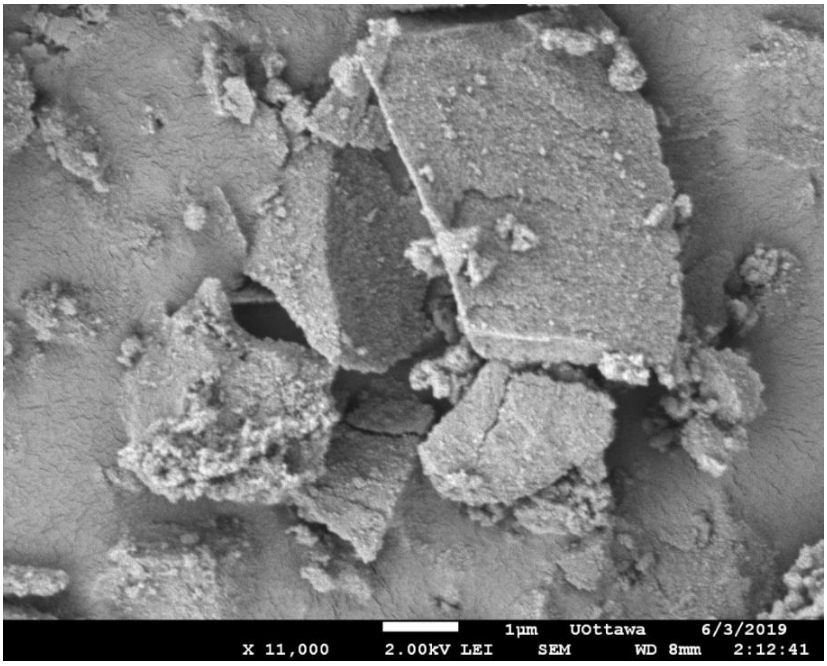

Figure C. 1: Scanning Electron Microscope (SEM) micrograph view from powder

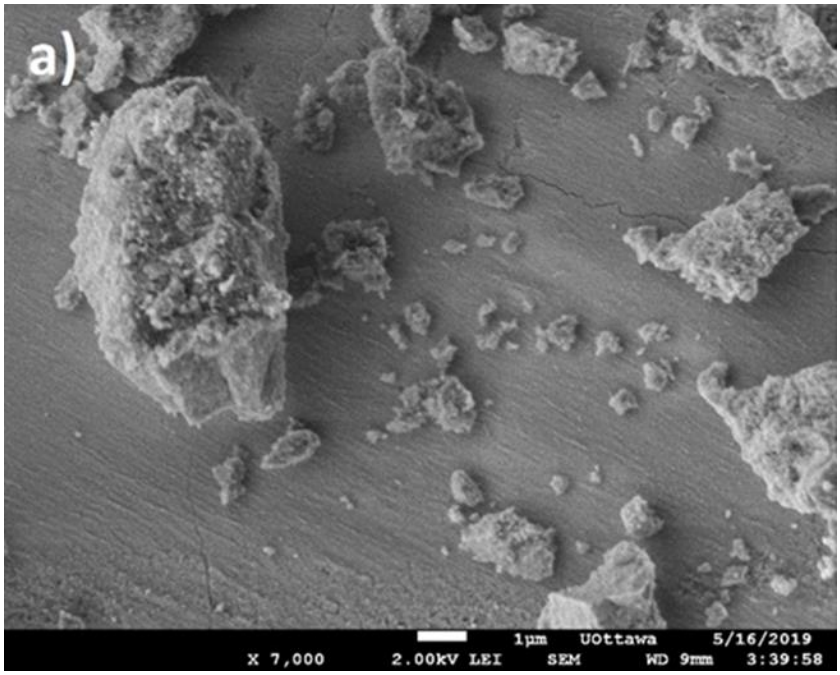

Figure C. 2: Scanning Electron Microscope (SEM) micrograph view from agglomerated particles

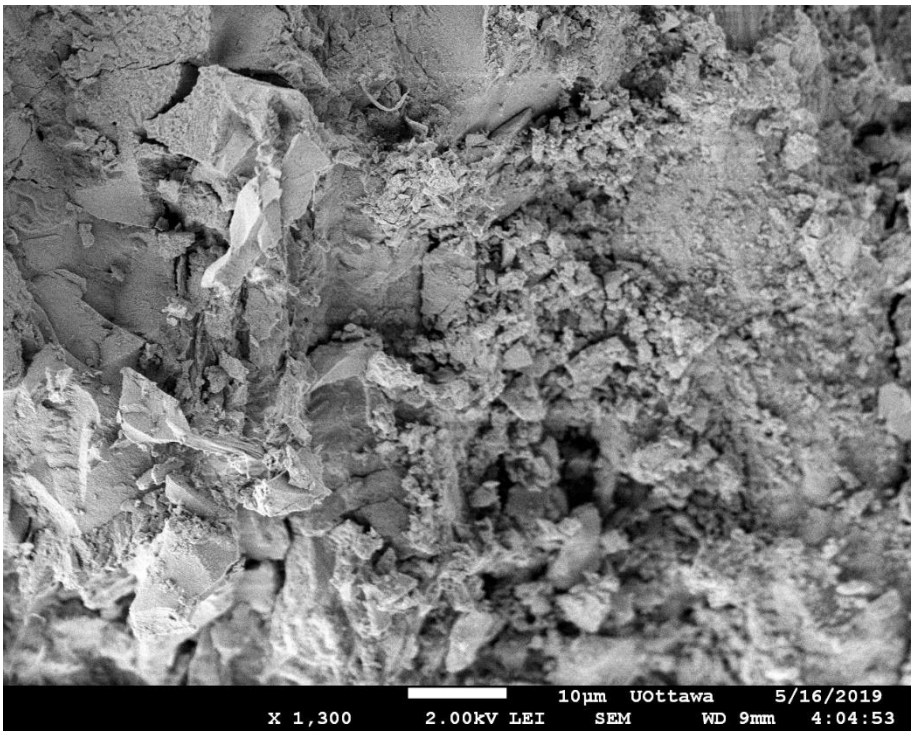

Figure C. 3: SEM micrograph view from PI10

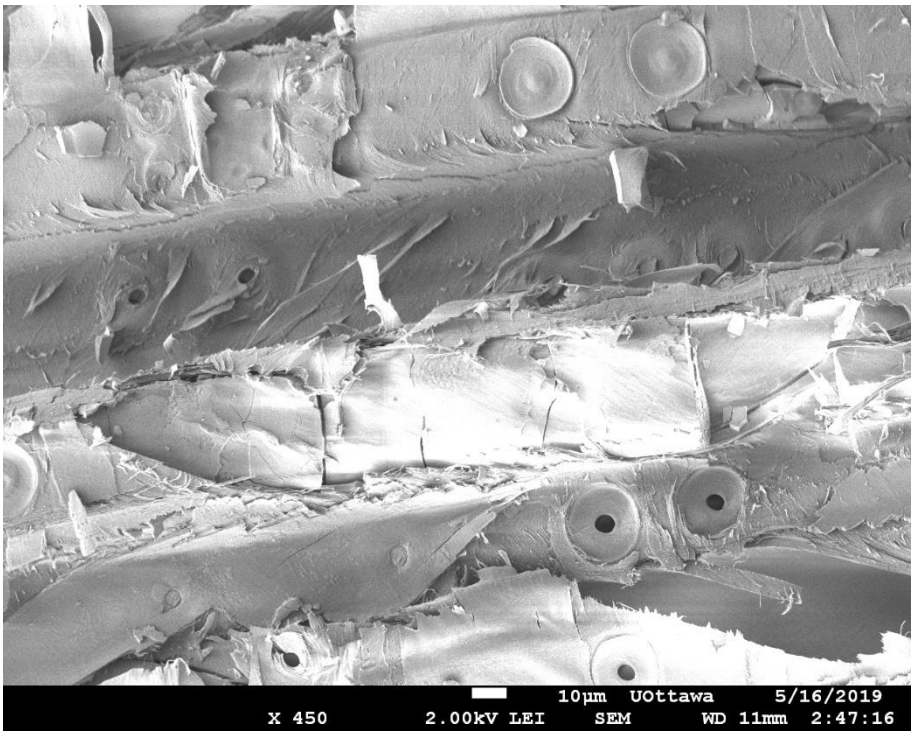

Figure C. 4: SEM micrograph view from N sample

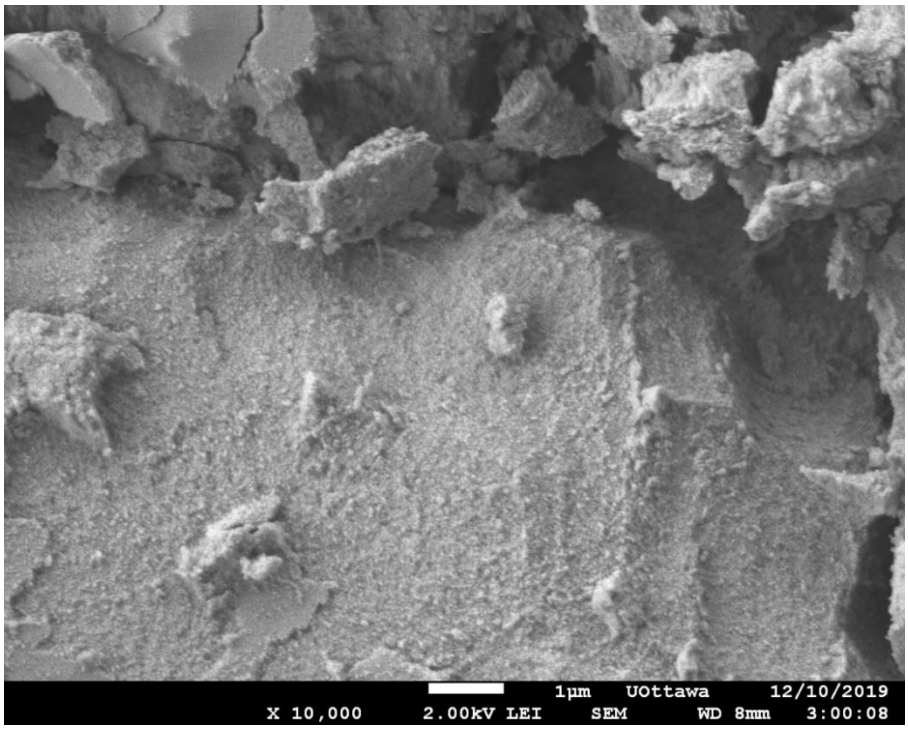

Figure C. 5: SEM micrograph view from PIV

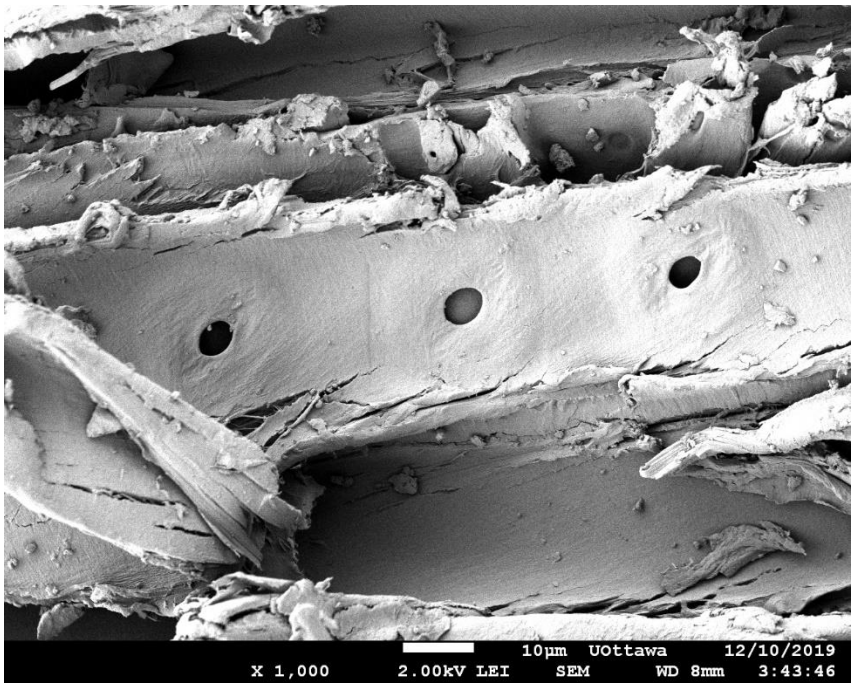

Figure C. 6: SEM micrograph view from P

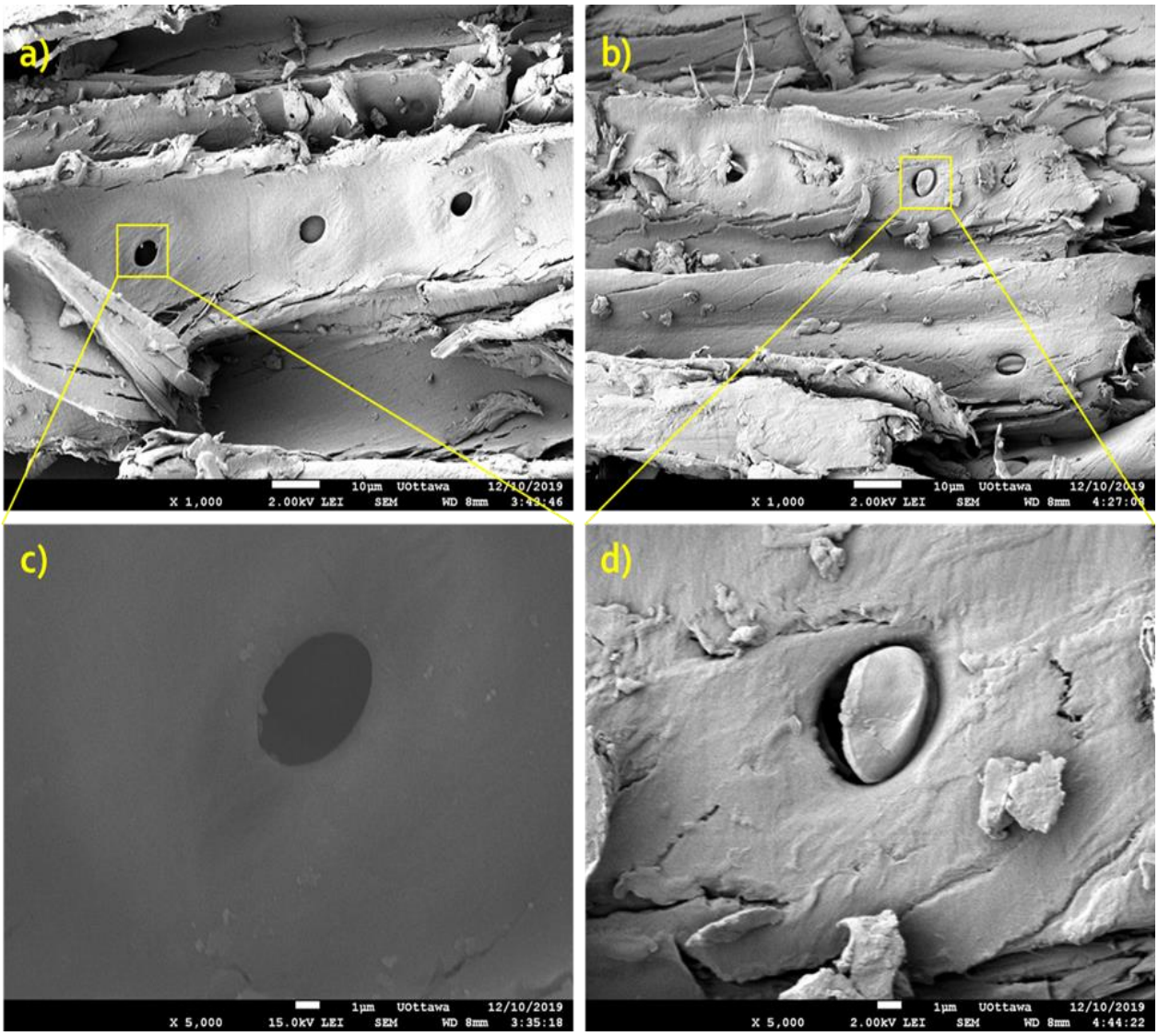

Figure C. 7: Scanning Electron Microscope (SEM) micrograph view from the external surface of (a) Pretreated sample (b) untreated sample in the scale of 10µm. The high-magnification images show changes in the surface (c) The pretreated samples and (d) the reference in the scale of 1µm

Appendix D: EDX Micro-analysis of the Samples

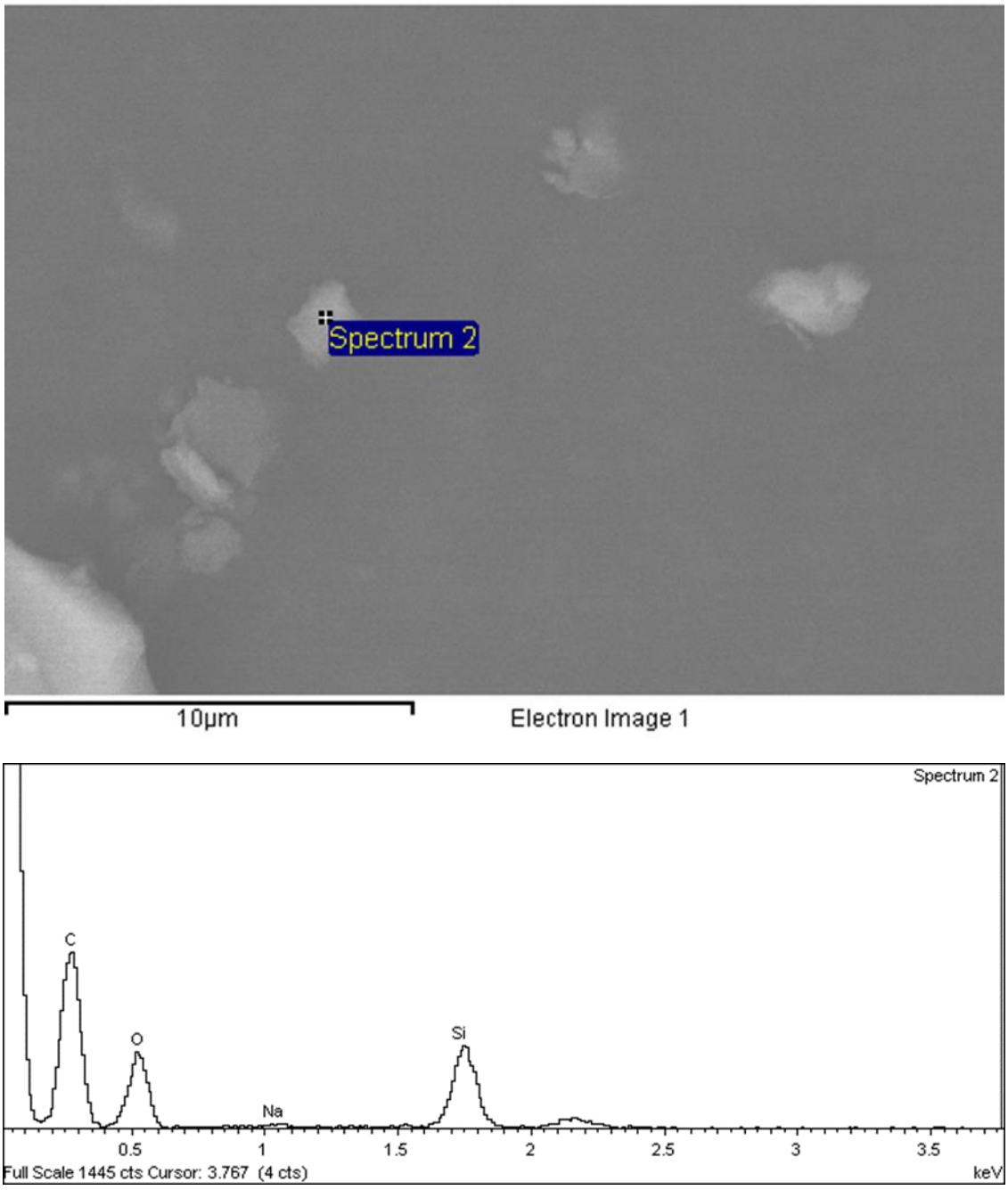

Figure D. 1: EDX micro-analysis of the powder

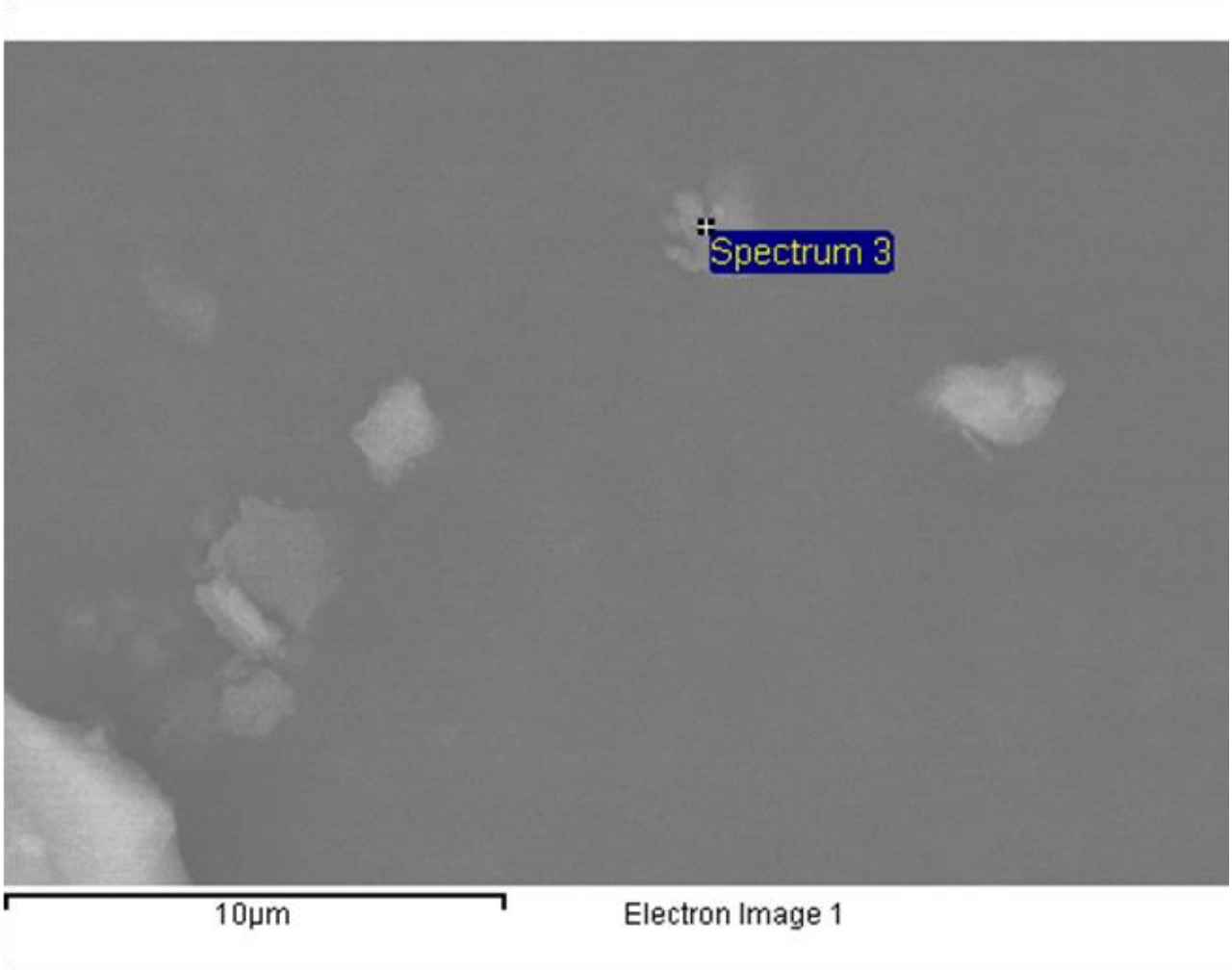

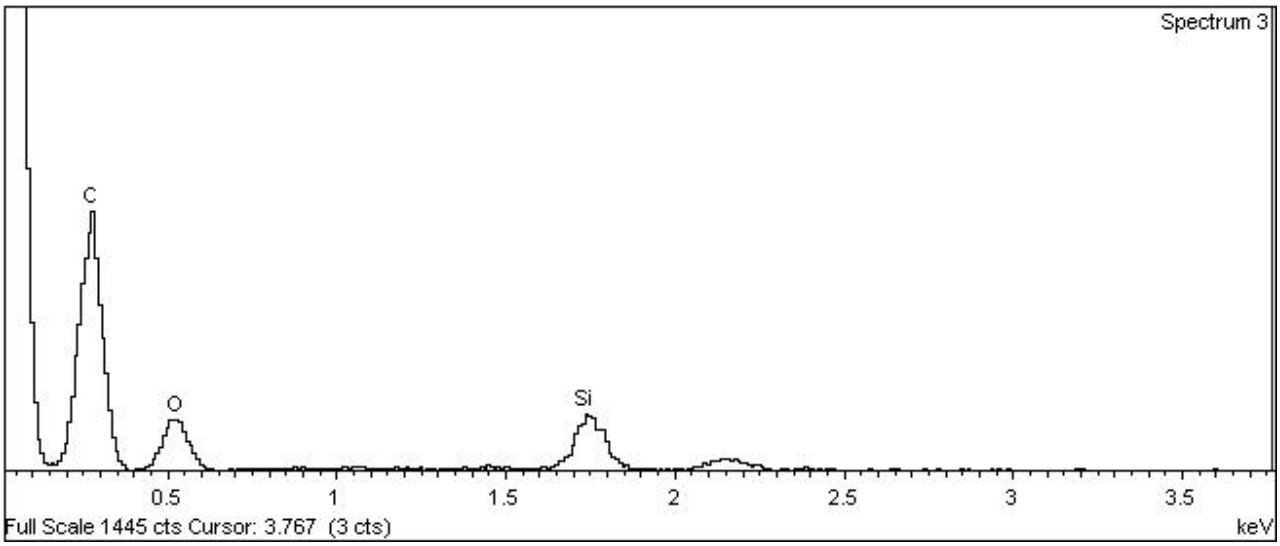

Figure D. 2: EDX micro-analysis of the powder

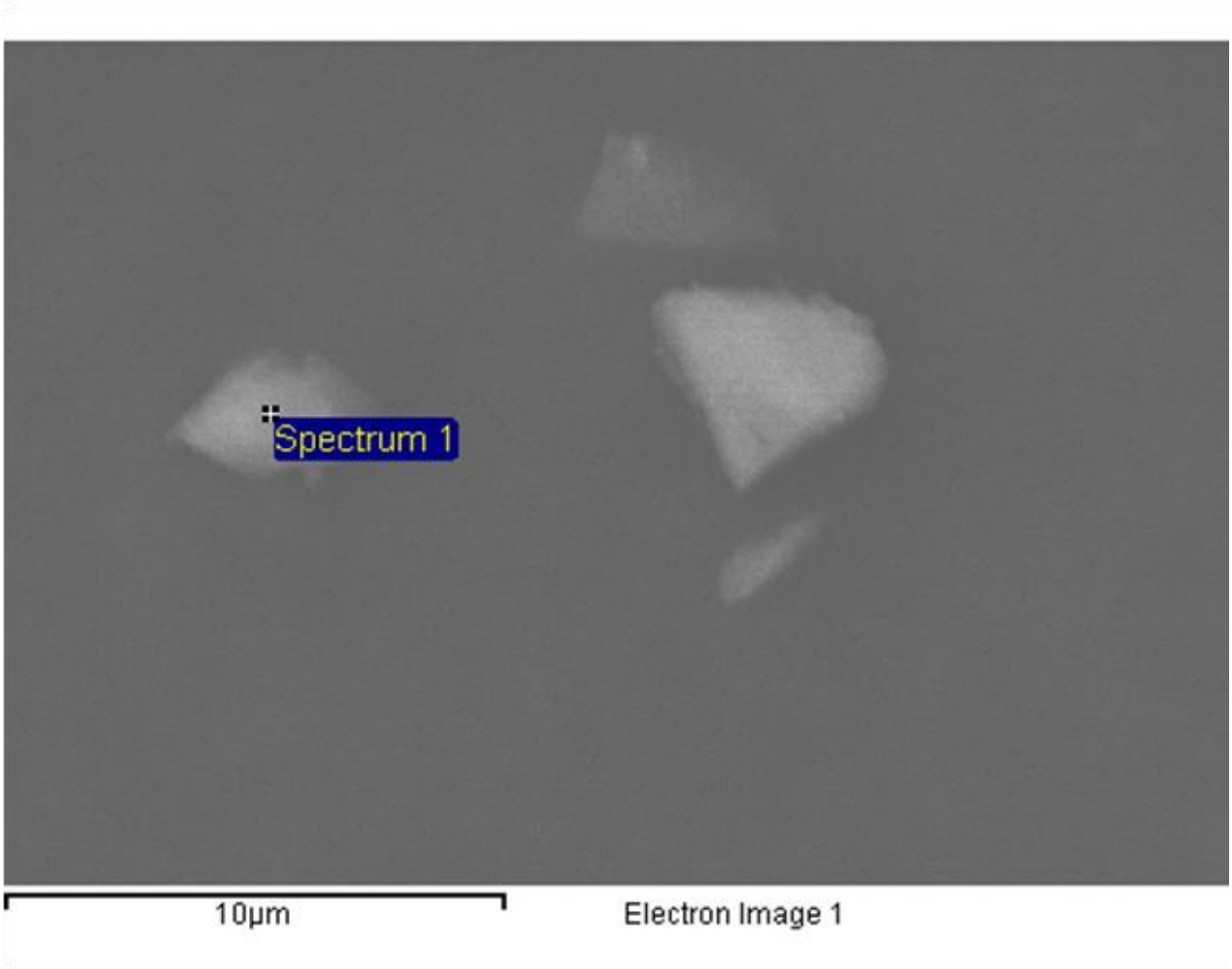

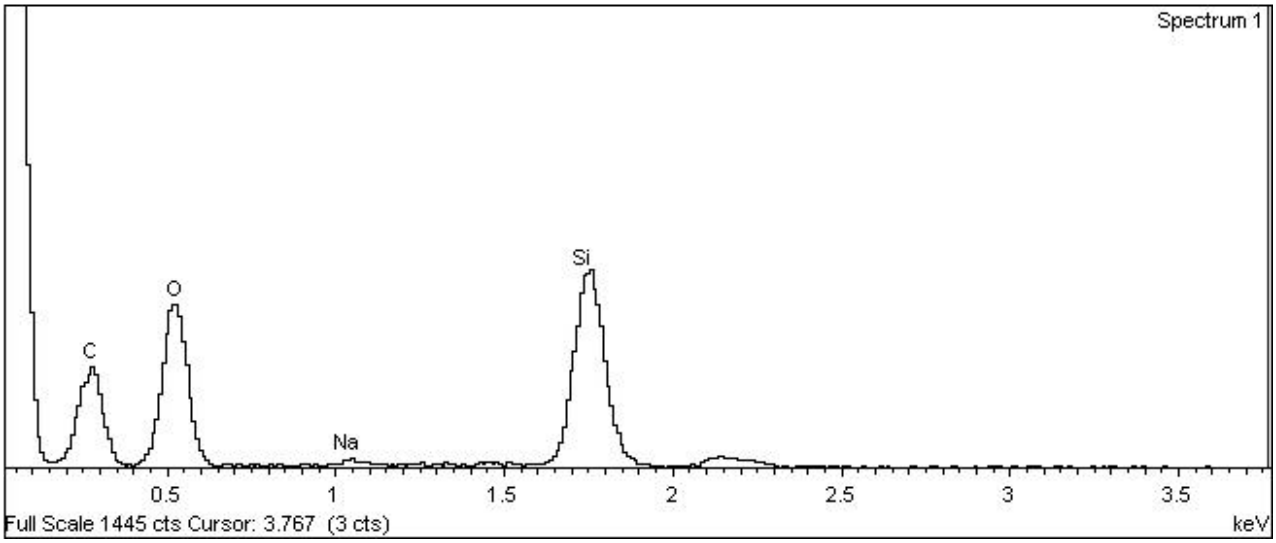

Figure D. 3: EDX micro-analysis of the powder

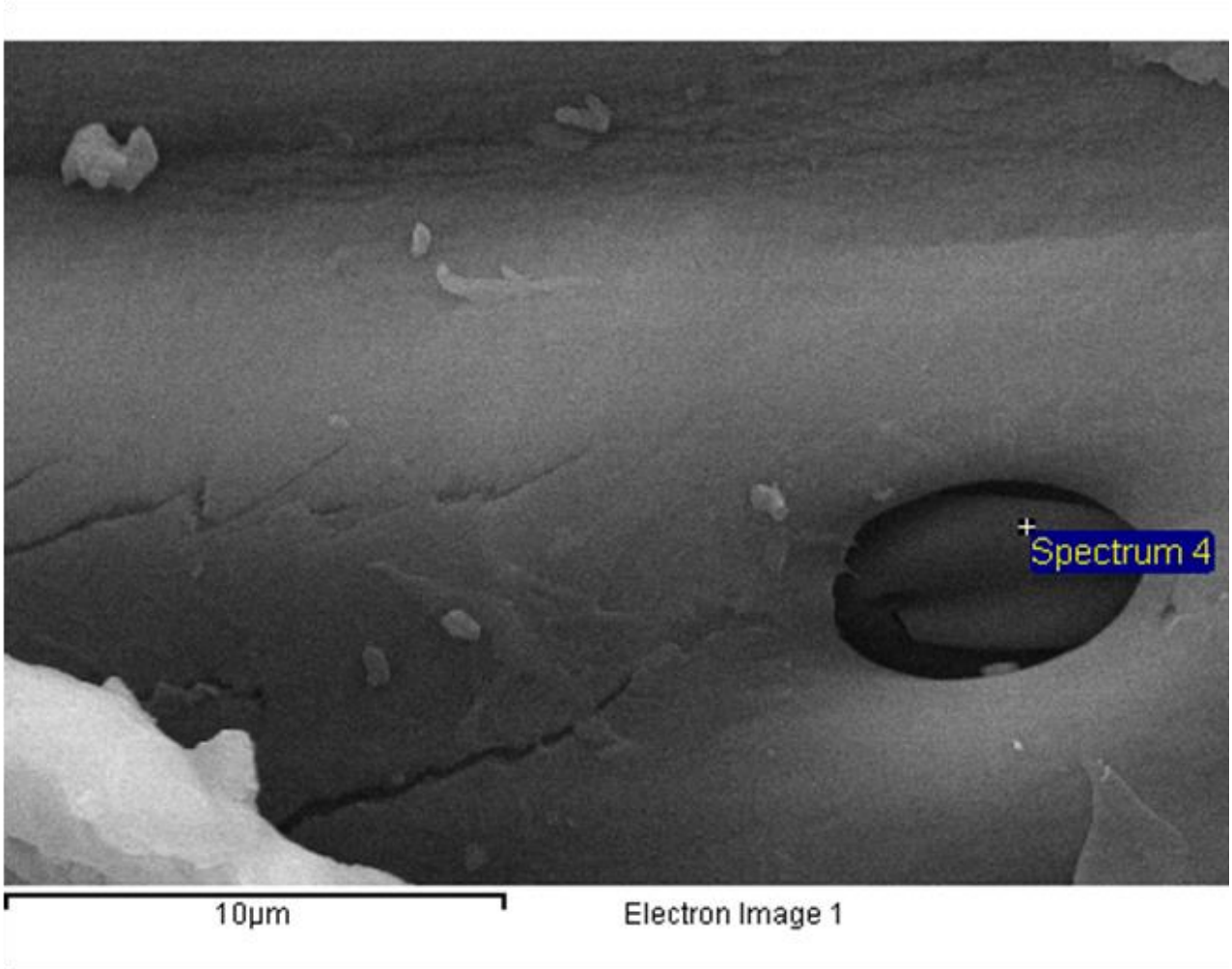

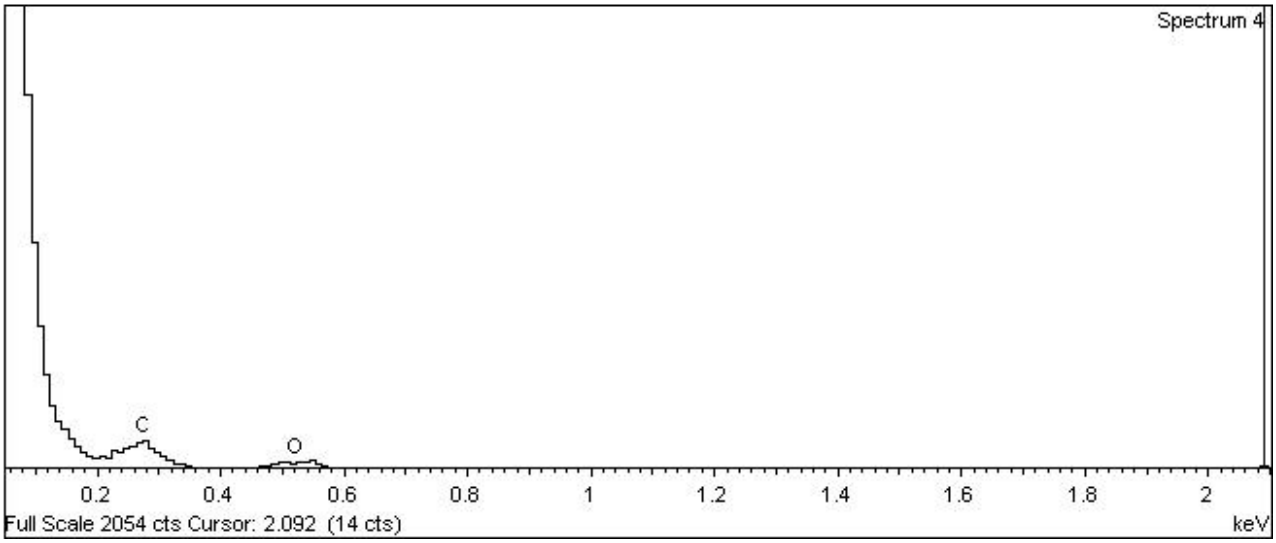

Figure D. 4: EDX micro-analysis of the Non-treated sample

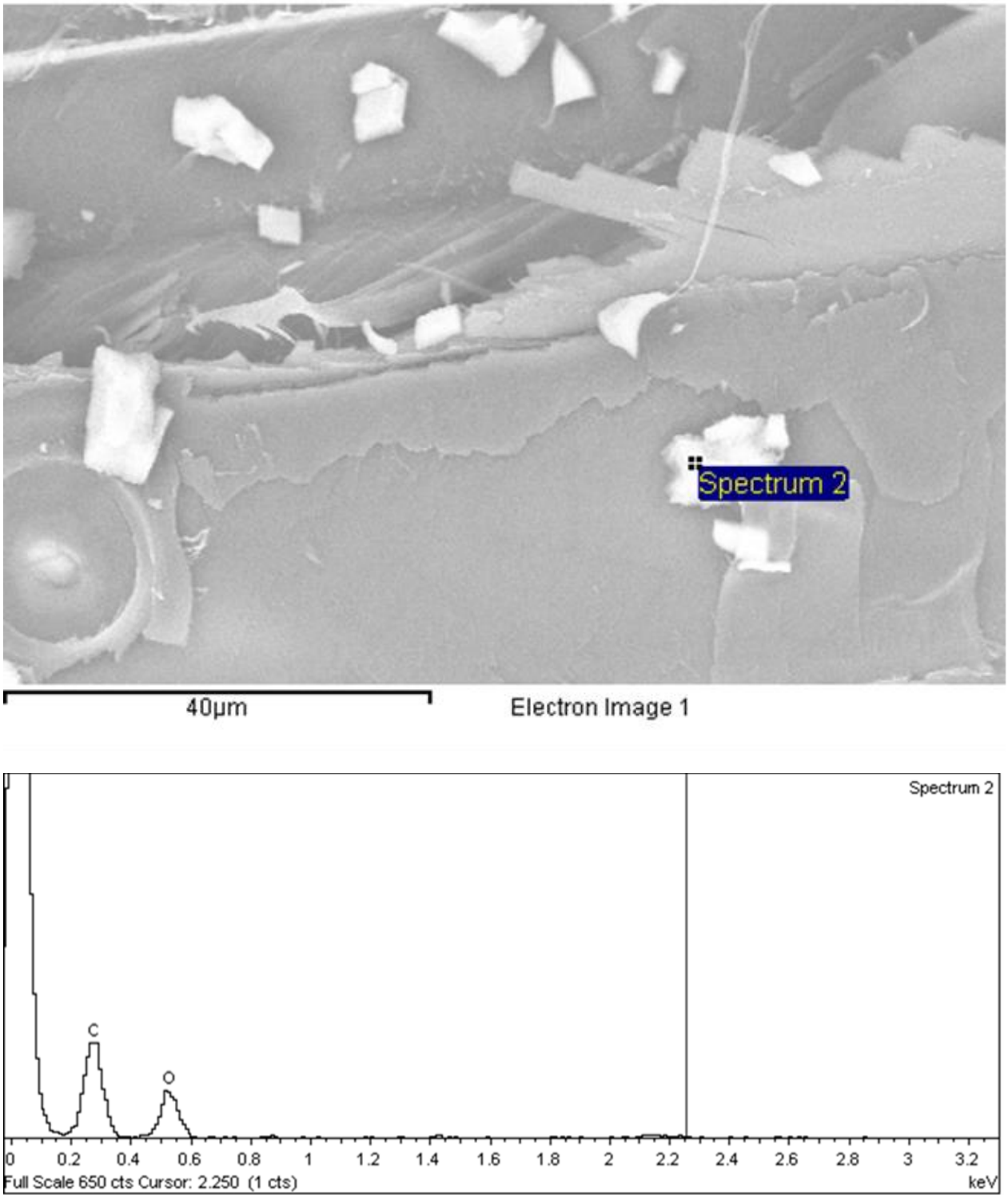

Figure D. 5: EDX micro-analysis of the Non-treated sample

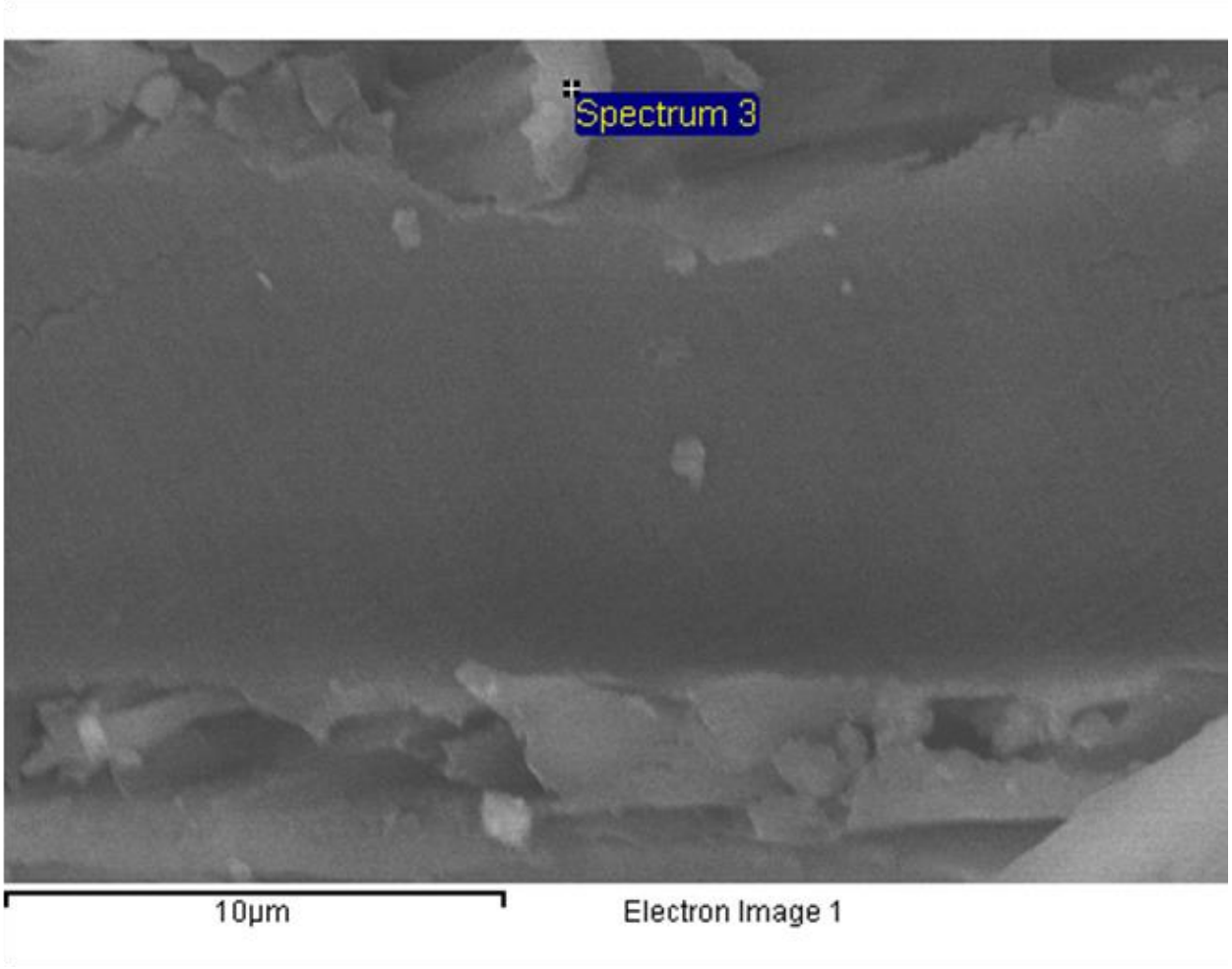

Figure D. 6: EDX micro-analysis of the Pre-treated sample

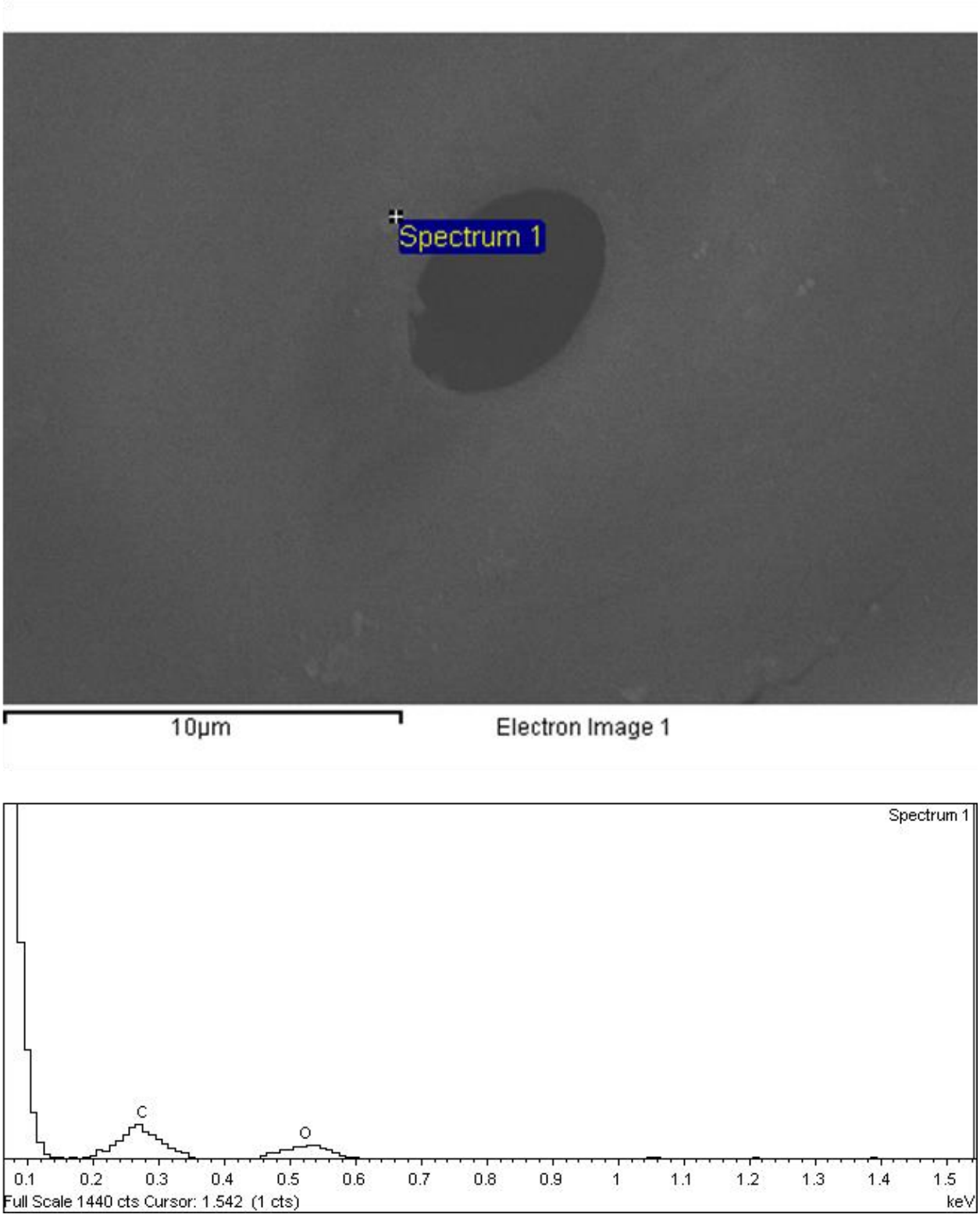

Figure D. 7: EDX micro-analysis of the Pre-treated sample

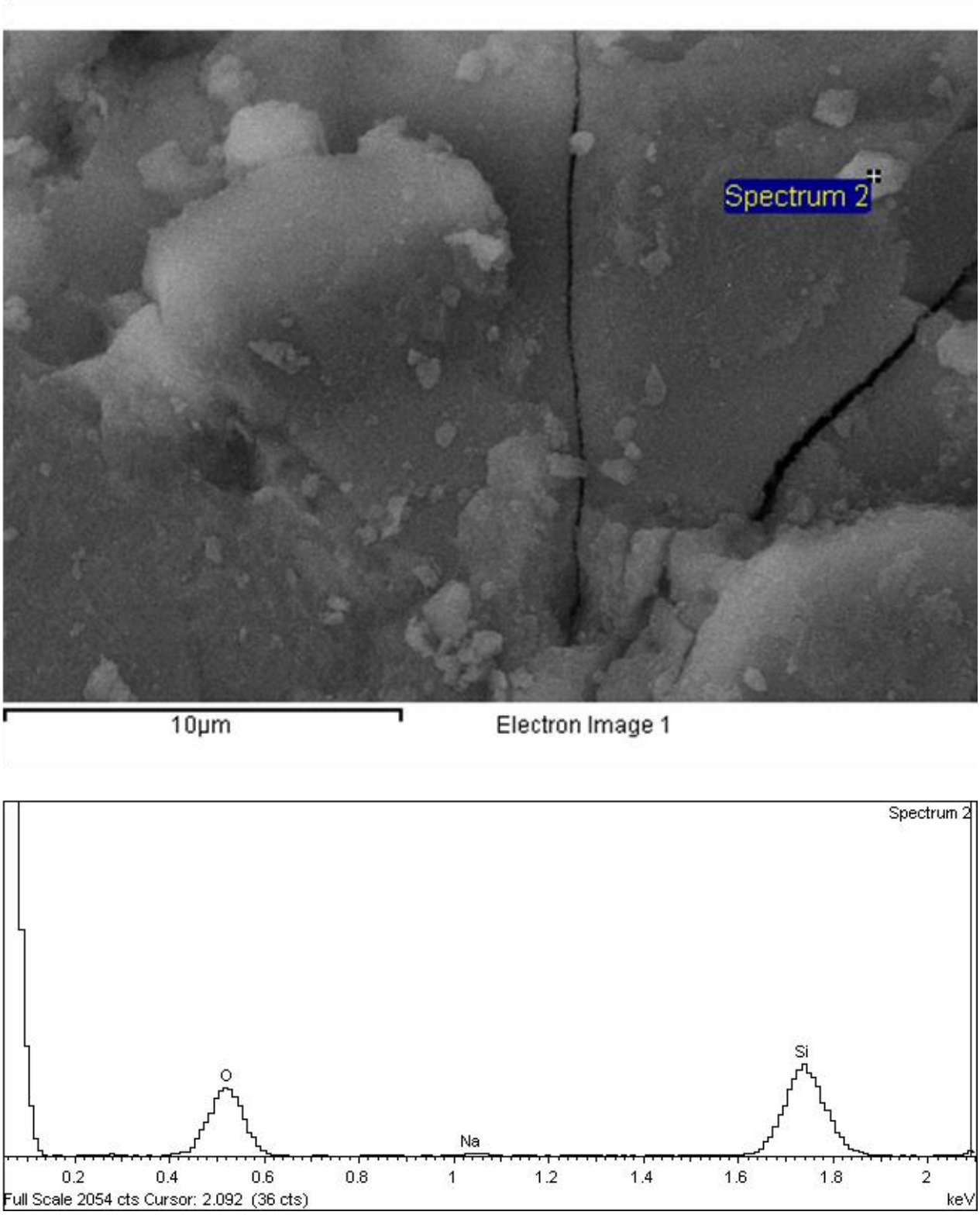

Figure D. 8: EDX micro-analysis of the Pre-treated Impregnated sample

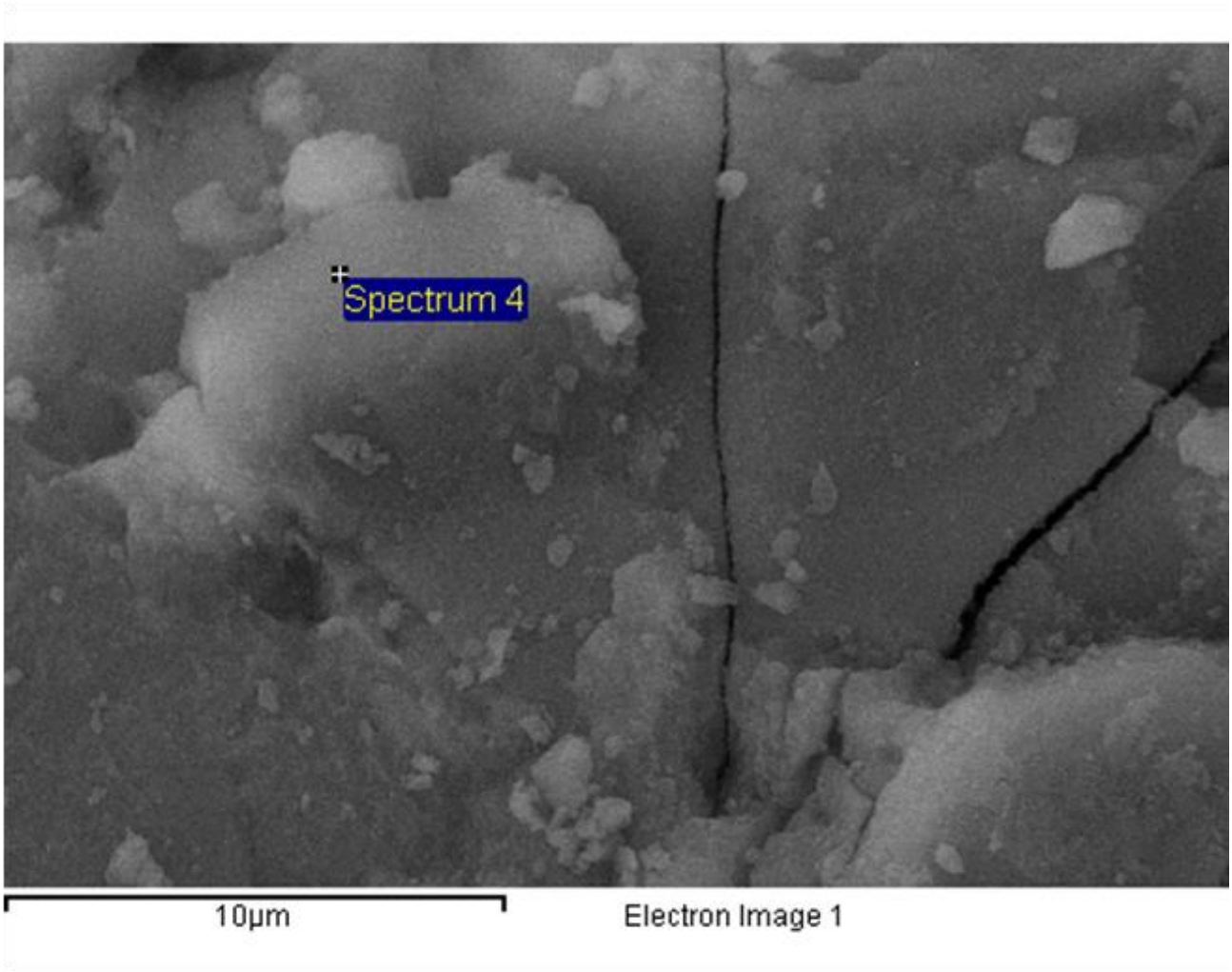

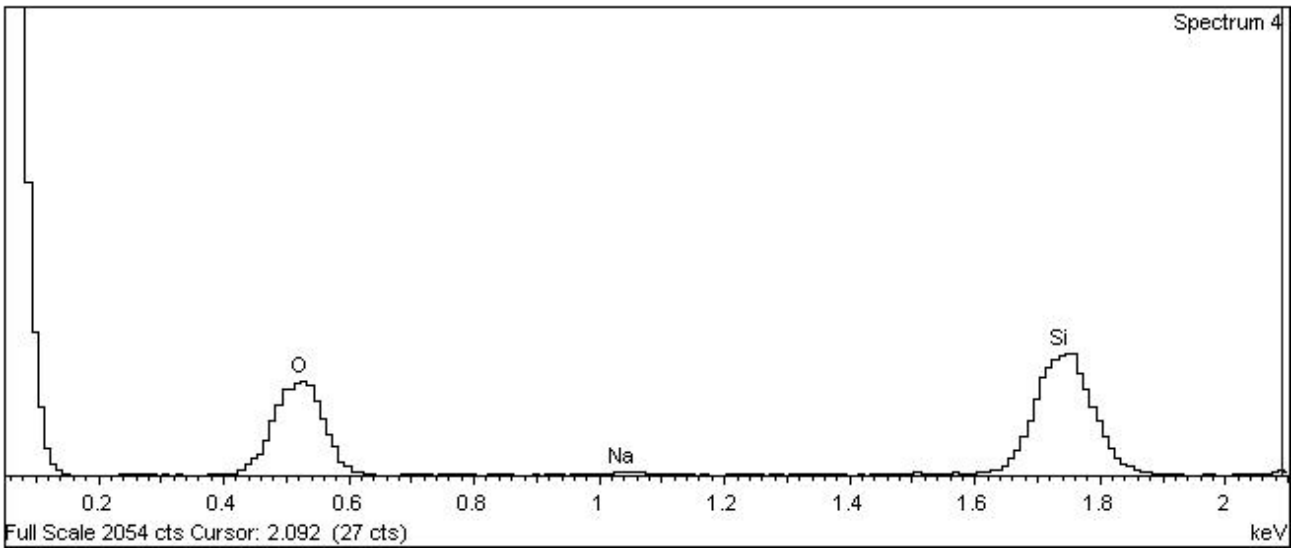

Figure D. 9: EDX micro-analysis of the Pre-treated Impregnated sample

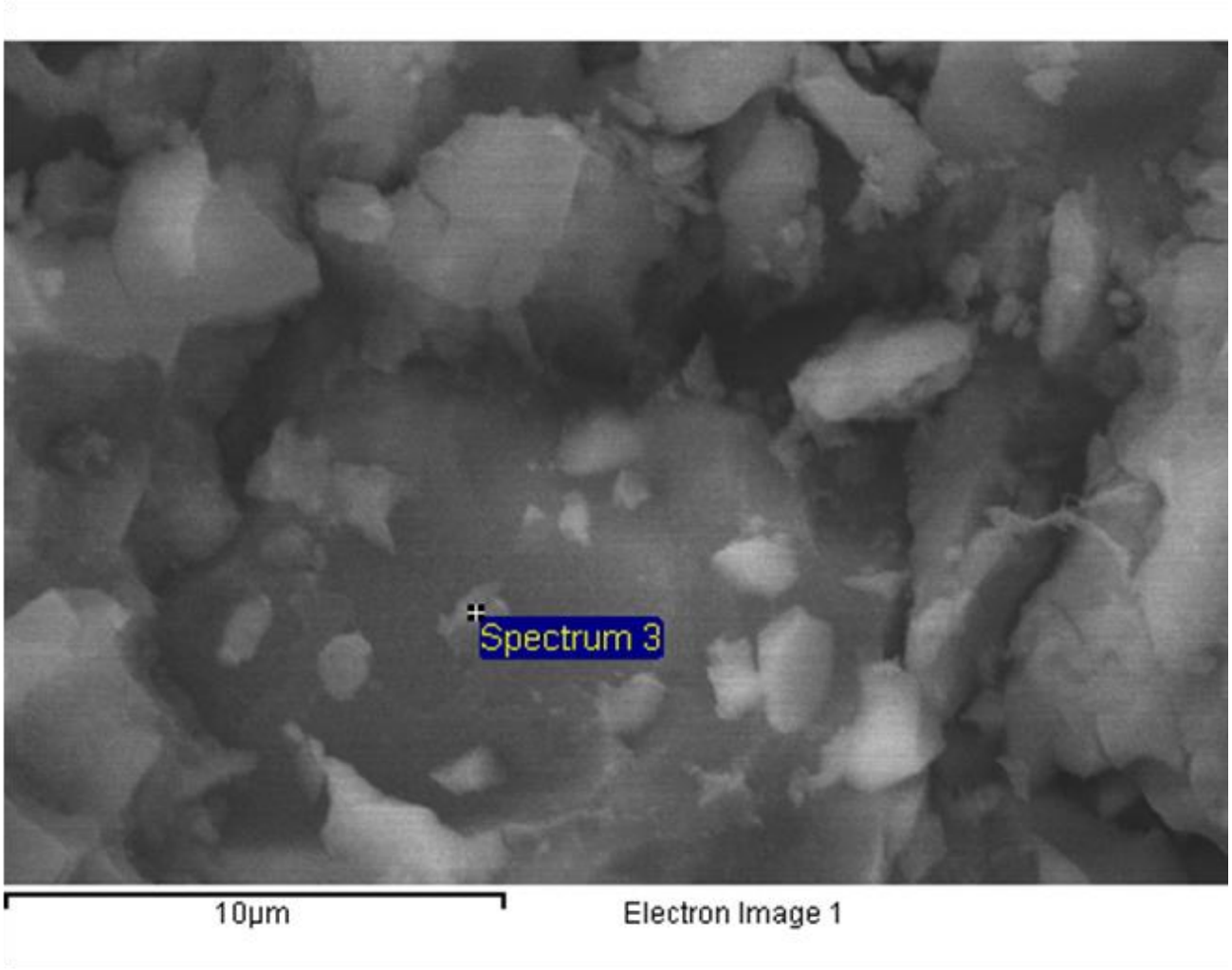

Figure D. 10: EDX micro-analysis of the Pre-treated Impregnated vacuumed sample

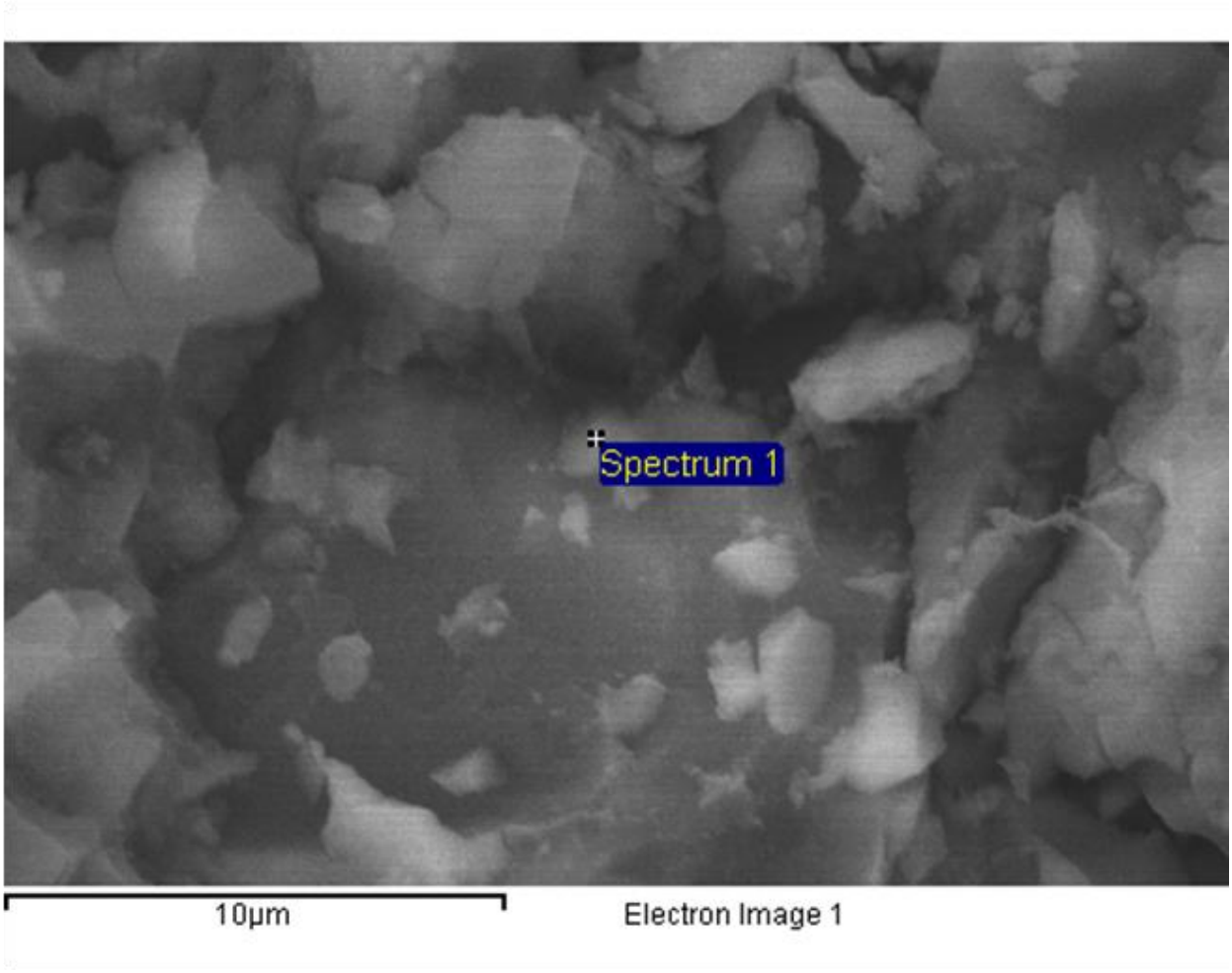

Figure D. 11: EDX micro-analysis of the Pre-treated Impregnated vacuumed sample